

**HANDOVER MANAGEMENT IN DENSE
CELLULAR NETWORKS: A STOCHASTIC
GEOMETRY APPROACH**

BY

RABE ARSHAD

A Thesis Presented to the
DEANSHIP OF GRADUATE STUDIES

KING FAHD UNIVERSITY OF PETROLEUM & MINERALS

DHAHRAN, SAUDI ARABIA

In Partial Fulfillment of the
Requirements for the Degree of

MASTER OF SCIENCE

In

ELECTRICAL ENGINEERING

APRIL 2017

KING FAHD UNIVERSITY OF PETROLEUM & MINERALS
DHAHRAN 31261, SAUDI ARABIA

DEANSHIP OF GRADUATE STUDIES

This thesis, written by **RABE ARSHAD** under the direction of his thesis adviser and approved by his thesis committee, has been presented to and accepted by the Dean of Graduate Studies, in partial fulfillment of the requirements for the degree of **MASTER OF SCIENCE IN ELECTRICAL ENGINEERING**.

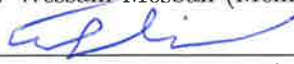
Thesis Committee

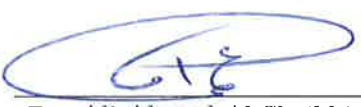

Dr. Ali Ahmad Al-Shaikhi (Adviser)

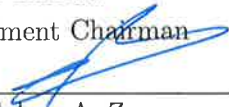

Prof. Mohamed-Slim Alouini (Co-adviser)


Dr. Sameh Sorour (Member)


Dr. Wessam Mesbah (Member)


Dr. Samir Al-Ghadhban (Member)


Dr. Ali Ahmad Al-Shaikhi
Department Chairman


Prof. Salam A. Zummo
Dean of Graduate Studies

1/5/17
Date



©*Rabe Arshad*
2017

Dedicated to the memory of my mother, who always supported me in crossing the milestones, To my father for trusting my capabilities and my wife who encouraged me among all the thick and thins I have passed by.

ACKNOWLEDGMENTS

In the name of Allah, the most merciful and the most beneficent, all praises to Allah for the strengths to complete this thesis. First, I would like to express my deep gratitude to my supervisors, Dr. Ali Ahmad Al-Shaikhi and Prof. Mohamed-Slim Alouini, for their close supervision and the precious time given to review and improve my work. A special thanks to my thesis committee members, Dr. Sameh Sorour, Dr. Wessam Mesbah and Dr. Samir Al-Ghadhban, for their extensive support along this journey.

Finally, I would like to acknowledge Dr. Tareq Y. Al-Naffouri and Dr. Hesham Elsayy from King Abdullah University of Science and Technology (KAUST), Saudi Arabia, for giving me an opportunity to work in an extra-ordinary environment and helping me in building key concepts in this particular area of research. I feel so gratified to be a part of this research group.

TABLE OF CONTENTS

ACKNOWLEDGEMENT	iii
LIST OF TABLES	vii
List of Tables	vii
LIST OF FIGURES	viii
List of Figures	viii
ABSTRACT (ENGLISH)	xi
ABSTRACT (ARABIC)	xiii
CHAPTER 1 INTRODUCTION	3
1.1 Handover Rates	5
1.2 Stochastic Geometry	7
1.3 Objectives	9
CHAPTER 2 LITERATURE REVIEW	11
2.1 Point processes	12
2.2 Stochastic Geometry analysis	13
2.3 Handover Rate	16
2.4 Summary	19

CHAPTER 3	SINGLE-TIER DOWNLINK CELLULAR NETWORK	20
3.1	Introduction	21
3.1.1	System Model	21
3.1.2	Service Distance Distribution	25
3.1.3	Coverage Probability	27
3.2	Single-tier Network with Coordinated Multipoint Transmission	33
3.2.1	Cooperative Distance Distribution	35
3.2.2	Cooperative Coverage Probability	36
3.3	Handover Cost	41
3.4	Average Throughput	43
3.5	Numerical Results	44
3.6	Summary	46
CHAPTER 4	MULTI-TIER CELLULAR NETWORKS	47
4.1	Introduction	48
4.2	System Model	49
4.2.1	User Mobility and Handover Strategies	50
4.2.2	Methodology of Analysis	54
4.3	Distance Analysis and Coverage Probability	55
4.3.1	Best Connected Strategy (BC)	55
4.3.2	Femto Skipping Strategy (FS)	60
4.3.3	Femto Disregard Strategy (FD)	66
4.3.4	Macro Skipping Strategy (MS)	72
4.4	Handover Cost	80
4.5	User Throughput	83
4.5.1	Design Insights	84
4.6	Summary	87

CHAPTER 5	TOPOLOGY AWARE HANDOVER MANAGEMENT	88
5.1	Handover Skipping in Single Tier Networks	92
5.1.1	Coverage Probability	93
5.1.2	Handover Cost	95
5.1.3	Average Throughput	99
5.2	Handover Skipping in Two Tier Networks	101
5.3	Summary	104
CHAPTER 6	TWO TIER UPLINK CELLULAR NETWORKS	106
6.1	Introduction	106
6.2	System Model	108
6.3	Stationary Analysis	110
6.3.1	Coverage Probability	112
6.3.2	Network Throughput	114
6.4	User Mobility Analysis	115
6.5	Design Insights	117
6.6	Summary	118
CHAPTER 7	CONCLUSIONS & FUTURE WORK	119
REFERENCES		129

List of Tables

3.1	Mathematical Notations	23
3.2	Spectral Efficiency for all cases in nats/sec/Hz	44
3.3	Simulation parameters	45
4.1	Mathematical Notations	51
4.2	Achievable rate for all cases in nats/sec/Hz ($T = 6$ dB, $\beta_{12} = 0$ dB)	84
5.1	Simulation parameters for PPP based cellular network	93
5.2	Spectral Efficiency for all cases in nats/sec/Hz	100
5.3	Spectral Efficiency for PCP Network in nats/sec/Hz	104
6.1	Simulation parameters	116

List of Figures

1.1	Network densification objectives	5
1.2	Major blocks in stochastic geometry based analysis	8
2.1	(a) PPP in 20m x 20m area (b) BPP in 20m x 20m area (c) HCPP in 20m x 20m area (d) PCP in 20m x 20m area	14
2.2	Taxonomy of detailed literature review on Stochastic Geometry	17
3.1	(a) represents best connected case. (b) shows the blackout case. In both cases, r_0 represents the distance between test user and its serving BS, r_1 represents the distance between test user and its first interfering BS and blue solid line represents the user trajectory.	22
3.2	Voronoi tessellation of an actual cellular network (Macros only) in urban area with $\lambda=3$ BS per km^2 . Red solid line depicts user trajectory while green dotted and blue solid lines show conventional and skipping HOs respectively. In the conventional (skipping) scheme the test user associates to the BSs $\{A, B, C, D, E, F, G\}$ ($\{A, C, E, G\}$).	24
3.3	Coverage probability plots for the conventional and skipping cases at $\eta = 4$. .	33
3.4	A and B represent best connected and blackout with BS cooperation users, respectively. r_i represents the distance between the user and i^{th} nearest BS. Red and green colors show interference and serving regions with BSs located at the corresponding Voronoi centers, respectively. Brown solid line represents the user trajectory.	35

3.5	Coverage probability plots for best connected and HO skipping cases evaluated at $\eta = 4$	39
3.6	Coverage probability plots for best connected and HO skipping cases with IC evaluated at $\eta = 4$	41
3.7	D_{HO} plots for conventional and HO skipping cases vs. user velocity (Kmph) for $\lambda = 30BS/km^2$	42
3.8	Average Throughput (Mbps) vs. user velocity (Km/h) for $\lambda = 50BS/Km^2$.	45
3.9	Average Throughput (Mbps) vs. user velocity (Km/h) for $\lambda = 70BS/Km^2$.	46
4.1	Weighted Voronoi tessellations of two tier cellular network. Green solid line represents user trajectory while black squares and red circles represent macro and femto BSs, respectively.	50
4.2	Coverage probability plots for all cases at $\eta = 4$, $\beta_{12} = 0$ dB, transmission power $P_1 = 1$ watt, $P_2 = 0.1P_1$ watt and BS intensities $\lambda_1 = 30$ BS/km ² , $\lambda_2 = 70$ BS/km ²	80
4.3	Handover cost vs. User velocity (km/h) with $P_1 = 1$ watt, $P_2 = 0.1P_1$ watt, $\beta_{12} = 0$ dB, $d_m = 0.35$ s, $d_f = 2d_m$	83
4.4	Average Throughput (Mbps) vs. User velocity (km/h) with $W = 10$ MHz, $P_1 = 1$ watt, $P_2 = 0.1P_1$ watt, $\lambda_1 = 30$ BS/km ² , $\lambda_2 = 70$ BS/km ² , $T = 6$ dB.	85
4.5	Average throughput per user vs. BS intensity with $P_1 = 1$ watt, $P_2 = 0.1P_1$ watt, $\lambda_2 = 2\lambda_1$, $\lambda_u = 10$ user/km ² , $T = 6$ dB, $\beta_{21} = 0$ dB, $d_m = 0.7$ s, $d_f = 3d_m$	86
5.1	Voronoi tessellation of a PPP based single tier cellular network with black circles representing the BSs' locations in 30 km x 30 km grid. (a), (b), and (c) represent alternating, user location aware, and cell-size aware HO skipping schemes, respectively. Blue line represents user trajectory while green and red colors denote serving (circles) and skipped (cross) BSs' coverage areas, respectively.	89
5.2	Coverage probability vs. SINR threshold for best connected and HO skipping cases.	96

5.3	Coverage probability vs. SINR threshold for best connected and HO skipping cases with CoMP transmission.	97
5.4	Handover cost for conventional and HO skipping cases.	98
5.5	Average throughput vs. user velocity for conventional and HO skipping cases.	101
5.6	Weighted Voronoi tessellation of two tier PCP based downlink cellular network with $\lambda_p = 0.04$ BS/km ² , $\lambda_c = 1$ BS/km ² , $P_1 = 1$ watt, $P_2 = 0.5P_1$ watt, $r = 2$ km. Black squares represent macro BSs while red circles denote femto BSs. .	103
5.7	Average throughput vs. user velocity for PCP based two tier network with $P_1 = 1$ watt, $P_2 = 0.1$ watt, $\lambda_p = 4$ BS/km ² , $\lambda_c = 12$ BS/km ² , $d = 1$ s, $r = 0.6$ km, $\eta_1 = \eta_2 = 4$	104
6.1	User-to-BS associations for (a) DUDe and (b) RSS based policies modeled via weighted Voronoi tessellation. Macro and femto BSs/users are represented by black and red colors, respectively. Green circles show the disparity in user-to-BS associations in RSS and DUDe architecture.	109
6.2	Achievable rate per unit bandwidth (nats/sec/Hz) and HO cost in RSS and DUDe architectures	115
6.3	Network Throughput (Mbps) per unit area plots with RSS and DUDe associations	115

THESIS ABSTRACT

NAME: Rabe Arshad

TITLE OF STUDY: Handover Management in Dense Cellular Networks: A
Stochastic Geometry Approach

MAJOR FIELD: Electrical Engineering

DATE OF DEGREE: April 2017

Cellular operators are continuously densifying their networks to cope with the ever-increasing capacity demand. Furthermore, an extreme densification phase for cellular networks is foreseen to fulfill the ambitious fifth generation (5G) performance requirements. Network densification improves spectrum utilization and network capacity by shrinking base stations' (BSs) footprints and reusing the same spectrum more frequently over the spatial domain. However, network densification also increases the handover (HO) rate, which may diminish the capacity gains for mobile users due to HO delays. In highly dense 5G cellular networks, HO delays may neutralize or even negate the gains offered by network densification. Hence, user mobility imposes a nontrivial challenge to harvest capacity gains via network densification. In this work, theoretical expressions for the coverage probability and HO cost are derived, based on stochastic geometry, to quantify the effect of HO delay on the average user rate in

cellular networks. Also, flexible handover schemes are proposed to reduce HO delay in case of highly dense cellular networks. These schemes allow skipping the HO procedure with some BSs along users' trajectories. Furthermore, the proposed model is extended to coordinated multi-point (CoMP) transmission based two-tier heterogeneous cellular network with user velocity aware HO skipping. The performance evaluation and testing of the proposed model shows up to 77% gains in the user rate that can be achieved in many practical scenarios.

ملخص الرسالة

الاسم: ربيع ارشد

عنوان الرسالة: ادارة تبادل الأبراج فى الشبكات الخلوية الكثيفة: باستخدام الهندسه العشوائيه

التخصص: الهندسه الكهربائية

تاريخ الحصول على الدرجة: شعبان 1438 هـ

مشغلوا الشبكات الخلوية يقومون بتكثيف الشبكات الخاصة بهم بشكل مستمر وذلك لمواكبة الاحتياج المتصاعد لزيادة سعة الشبكة. بالإضافة الى ذلك من المتوقع أن مرحلة التكثيف الهائل للشبكة ستحقق متطلبات أداء الجيل الخامس. تكثيف الشبكة يساعد في تحسين استغلال الطيف الترددى المتاح و سعة الشبكة من خلال تقليص الأماكن التي يتم تغطيتها من خلال الأبراج بالإضافة الى إعادة استخدام هذه الأطياف بشكل مستمر في المجال المكاني. ومع ذلك فإن تكثيف الشبكة يزيد من معدل التبادل ويقلل من السعة التي يحصل عليها مستخدمى أجهزة الهاتف الخلوي بسبب تأخر التبادل بين الأبراج. لذا فإن هذا التأخر الناتج عن تكثيف الأبراج في شبكات الجيل الخامس قد يؤدي إلى تقليص و ربما إلغاء الفائدة المرجوة من هذا التكثيف. بناء على ما قد سلف , ان حركة المستخدمين تشكل تحديا ليس باليسير لحصد زيادة سعة الشبكة عن طريق تكثيفها. في هذا البحث سوف نقدم معادلات نظرية لمعدل التبادل عن طريق محاكاة مواقع أبراج الإرسال من خلال معالجة نقاط مختلفة وتقديم نموذج تحليلي يركز على الهندسة العشوائية لتحديد تأثير التأخر في تبادل الأبراج على معدلات الأرسال لمستخدمي شبكة الهاتف الخلوي. كما قمنا بتقديم مخطط مرن للتقليل التأخر في تبادل الأبراج في شبكات الهاتف الخليوية الكثيفة. هذا المخطط يسمح بتخطي إجراء التأخير من خلال تتبع مسارات المستخدمين من قبل محطات الإرسال. من ناحية أخرى، قمنا بالتوسع في بحثنا من خلال تغطية تناسقية متعددة الأطراف بالإعتماد على شبكات الخليوية ثنائية التهجين مع اخذ سرعة المستخدم فى الاعتبار عند تخطي التبادل. تقييم الأداء والاختبارات على المخطط الخاص بنا تظهر نتائج ممتازة في العديد من التجارب التي قمنا بها.

Publications

[j1] **Rabe Arshad**, Hesham ElSawy, Sameh Sorour, Tareq Y. Al-Naffouri, and Mohamed-Slim Alouini, “Velocity-aware Handover management in two-tier cellular networks,” *in IEEE Transactions on Wireless Communications*, Jan. 2017.

[j2] **Rabe Arshad**, Hesham ElSawy, Sameh Sorour, Tareq Y. Al-Naffouri, and Mohamed-Slim Alouini, “Handover management in 5G and beyond: A topology aware skipping approach, ” *in IEEE Access*, Dec. 2016.

[j3] **Rabe Arshad**, Hesham ElSawy, Sameh Sorour, Tareq Y. Al-Naffouri, and Mohamed-Slim Alouini, “Mobility-Aware User Association in Uplink Cellular Networks” *submitted in IEEE Communication Letters*, April 2017.

[p1] **Rabe Arshad**, Hesham ElSawy, Sameh Sorour, Tareq Y. Al-Naffouri, and Mohamed-Slim Alouini, “Reducing Handover Signaling in Dense Cellular Networks through Base Station Skipping”, *provisionally filed in US Patent Office*, March 2016.

[c1] **Rabe Arshad**, Hesham ElSawy, Sameh Sorour, Tareq Y. Al-Naffouri, and Mohamed-Slim Alouini, “Handover management in dense cellular networks: A stochastic geometry approach,” *Proc. IEEE International Conference on Communications (ICC)*, Kuala Lumpur, Malaysia, May 2016.

[c2] **Rabe Arshad**, Hesham ElSawy, Sameh Sorour, Tareq Y. Al-Naffouri, and Mohamed-Slim Alouini, “Cooperative handover management in dense cellular networks,” *Proc. IEEE Global Communications Conference (GLOBECOM)*, Dec. 2016.

CHAPTER 1

INTRODUCTION

Network densification is a potential solution to cater the increasing traffic demand and is expected to have a major contribution in fulfilling the ambitious 1000-fold capacity improvements required for next generation 5G cellular networks [1]. This approach is accepted over several cellular generations. For instance, in 4G cellular networks deployed in the dense urban areas, macro BSs are around 200 meters apart in contrast to 500 meters in 2G cellular networks. Network densification is performed to achieve multiple objectives as shown in Figure 1.1, which is achieved by deploying various types of BSs based on the coverage, capacity and quality objectives i.e. micro, macro and pico. Network densification improves the spatial frequency reuse by shrinking the BSs' footprints to increase the delivered data rate per unit area. Hence, each BS serves lesser number of users with higher throughput for each user. However, such improvement comes at the expense of increased handover (HO) rates for mobile users. Mobile users change their BS associations more frequently in denser network environment due to the reduced BSs' footprints, to maintain the best connectivity.

It is to be noted that the best network connectivity may differ according to the network objective. However, in all cases, densifying the network by deploying more BSs, decreases the service region of each BS and increases the handover rate. Such problem will become more prominent in the foreseen ultra-dense cellular networks [2, 3]. To this end, we develop a mathematical model, via stochastic geometry, to quantify the effect of HO delay on the user throughput. Furthermore, we propose a flexible HO scheme, which we refer to as HO skipping, to reduce the overall HO delay in dense cellular networks. This scheme allows skipping the HO procedure with some BSs along users' trajectories.

Network densification improves the coverage probability and average user rate by adding more BSs to the network. But, for the next generation cellular networks, it is very difficult to meet ambitious capacity requirements using BS densification alone. To this end, integration of multiple capacity improvement techniques is required. In the recent years, coordinated multipoint (CoMP) transmission has provoked much attention of people from both industry and academia to help cellular operators maintain their financial growth and provide better services to the subscribers. Here, two or more BSs cooperate with each other to have a simultaneous data transmission for a particular user. The idea of CoMP transmission is to mitigate the effect of additional interference incurred due to the massive BSs deployment. The cooperating BSs communicate with each other over a backhaul link with negligible latency. Thus, we propose our model based on both non-CoMP and CoMP transmission and analyze the average user throughput for both cases.

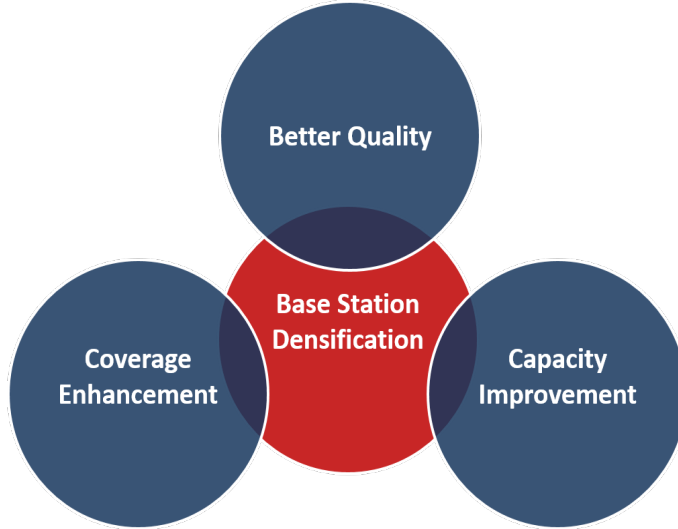


Figure 1.1: Network densification objectives

1.1 Handover Rates

Handover (HO) is the procedure of changing the association of mobile users from one BS to another to maintain their connection to their best serving BS. According to the network objective (e.g., best signal strength, equal BSs' load, low service delay, etc), different association strategies may be defined to determine the best serving BS. In all cases, HO is employed to update users' association with mobility to satisfy the defined network objective along their path. The HO procedure involves signaling overhead between the mobile user, the serving BS, the target BS, and the core network elements, which consumes resources and introduces delay. It is to be noted that the HO rate increases with the intensity of BSs, which imposes higher delays and negatively affects the mobile user's throughput. In the

case of highly dense cellular networks, the HO delay may become a performance limiting parameter that may neutralize or even negate the gains offered by network densification. Therefore, the HO delay should be carefully incorporated into the design of dense cellular networks to visualize and mitigate its effect. In particular, novel HO strategies are required to reduce the HO delay in order to harvest the foreseen network densification gains, which are presented in this work.

In general, HO is performed in three phases: initiation, preparation, and execution. During the initiation phase, the user reports reference signal measurements from neighboring BSs to the serving BS. For instance, the signal measurement report in 4G Long Term Evolution (LTE) includes, but not limited to, reference signal received power (RSRP) and reference signal received quality (RSRQ) (see [4] for the HO procedure in LTE). Also, the HO may be initiated based on downlink and/or uplink signal measurement reports. In the next phase, which is the preparation phase, signaling is exchanged between the serving BS, target BS, and the admission controller. The admission controller makes a decision about the initiation of the HO based on network defined HO criteria. Once the HO criteria are met, the user releases the serving BS and attempts to synchronize and access the target BS using the random access channel (RACH). Upon synchronization with the target BS, the UE sends the confirmation message to notify the network that the HO is executed. The aforementioned HO procedure involves signaling overhead between the user, serving BS, target BS, and core network, which interrupts the data flow and decreases the throughput of mobile user. The frequency at which such interruptions happen

is a function of the relative values of the BS intensity and user velocity. The duration of each interruption, denoted as HO delay, measured from the beginning of initiation phase to the end of execution phase can be significant [5]. Consequently, at high velocities and/or dense cellular environment, it is desirable to decrease the frequency of such HO interruptions, which motivates the HO management schemes that reduce HO rate and its associated delay. It is to be noted that high mobility can exist in dense cellular environments such as riding monorails or driving over elevated highways that go through downtowns.

1.2 Stochastic Geometry

Stochastic geometry has succeeded in providing a systematic analytical paradigm to model and design cellular networks, see [6] for a survey and [7] for a tutorial. In stochastic geometry analysis, the network is abstracted by a convenient point process that maintains a balance between practicality and tractability. The Poisson point process (PPP) is well understood and widely accepted due to its tractability and simplicity. Stochastic geometry with BSs modeled as a PPP has enriched the literature with valuable results that enhanced our understanding of the cellular network behavior. In stochastic geometry analysis, it is very important to characterize the service distance distribution which is further utilized to calculate the coverage probability and average throughput. Figure 1.2 shows the major blocks in stochastic geometry based analysis.

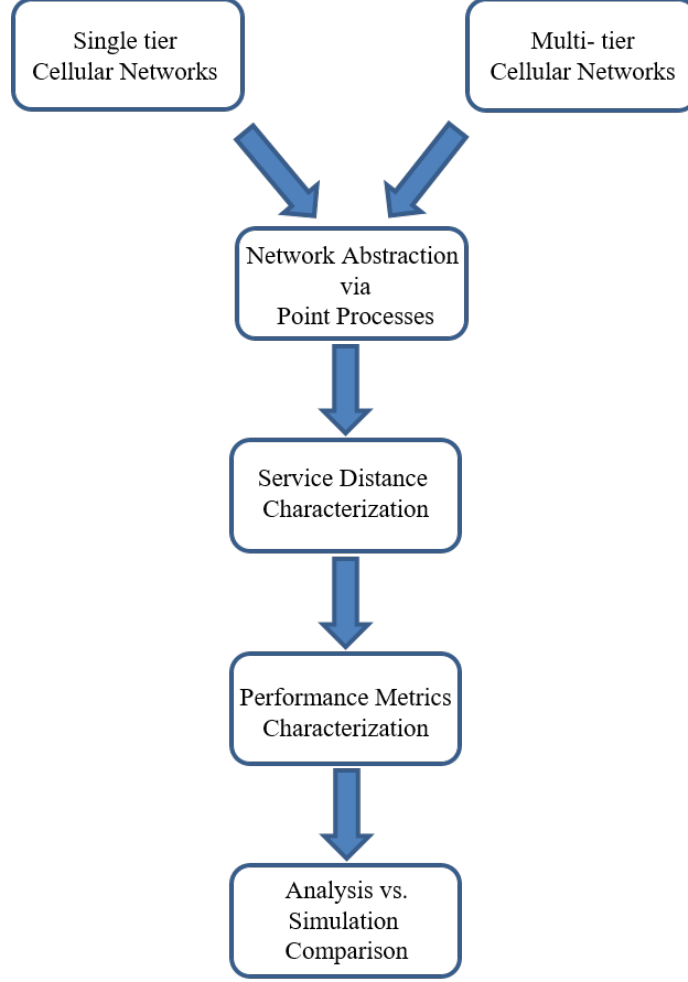


Figure 1.2: Major blocks in stochastic geometry based analysis

Stochastic geometry provides spatial averages averaged over a large number of nodes deployed at random locations. In stochastic geometry analysis, we focus on the performance of a randomly selected user or the average performance of all users encompassing all user locations. In this respect, we are interested in the average performance over all cellular network realizations. We denote such average performance metrics as spatially averaged performance metrics. Here, we define some of the performance metrics, which are extensively

studied in the literature.

Coverage probability: It is defined as the probability that the received SINR is greater than some threshold (T) i.e., $\mathbb{P}[SINR > T]$

Link Spectral efficiency: It is the maximum rate per unit bandwidth that can be reliably transmitted over a channel. It is defined by Shannon's capacity formula given by:
 $C = \log(1 + SINR)$.

Ergodic capacity: It is the long term average achievable rate averaged over all channel states. It can be expressed as $\mathbb{E}[\log(1+SINR)]$.

Handover rate: It is defined as the number of intersections between the user's trajectory and cell boundaries per unit time.

1.3 Objectives

In this work, we focus on single and multi-tier cellular networks and study the effect of the HO delay on average throughput. We derive coverage probability expressions which are further used to obtain the average throughput. We abstract the BSs locations via a homogeneous PPP and evaluate the HO rate and HO cost i.e. time wasted in HO per unit

time. Furthermore, we perform a similar study on user rate by abstracting BSs via poisson cluster process (PCP). The key objectives of this research work are listed below:

- A flexible HO scheme is proposed, which we refer to as HO skipping scheme that allows users to skip some of the BSs along user's trajectory
- Considering CoMP based two-tier cellular network, we propose multiple HO skipping schemes based on user velocity (velocity aware HO skipping)
- Deriving theoretical expressions for performance metrics like coverage probability, HO cost and average throughput
- Validation of theoretical expressions with the simulation results
- Comparison of the proposed HO skipping scheme with the conventional scheme i.e. BS skipping vs. no skipping, cooperative BS skipping vs. BS cooperation only
- Proposing smarter HO skipping techniques and analyzing the performance based on simulations
- Conducting HO analysis and its effect on average user rate in uplink cellular networks with different user-to-BS associations

CHAPTER 2

LITERATURE REVIEW

Stochastic geometry (SG) provides a unified mathematical paradigm to model wireless networks and analyze their performance. The main strength of the analysis based on SG, hereafter denoted as SG analysis, can be attributed to its ability to capture the spatial randomness inherent in wireless networks. Furthermore, SG models can be naturally extended to account for other sources of uncertainties such as fading, shadowing, and power control. In some special cases, SG analysis can lead to closed-form expressions that govern system behavior. These expressions enable the understanding of network operation and provide insightful design guidelines, which are often difficult to get from computationally intensive simulations. In SG analysis, BSs locations are abstracted to a convenient point process which captures the network properties. For every point process Φ , its intensity measure Λ is equal to the average number of points in a set $B \subset \mathbb{R}^d$ i.e.,

$$\Lambda(B) = \mathbb{E}(\Phi(B)) \tag{2.1}$$

If Φ is stationary, then $\Lambda(B) = \lambda|B|$, where λ is the intensity of the stationary point process and $|\cdot|$ denotes the Lebesgue measure.

2.1 Point processes

In this section, we discuss some commonly used point processes used in the literature as mentioned below [6].

Poisson Point Process (PPP): A point process in which the total number of points in any compact set is a poisson random variable and the number of points in any disjoint sets are independent random variables. PPP is the most well-studied point process in the literature, and its acceptance is based on the ease of analysis. The intensity measure of a stationary PPP is represented by $\lambda|B|$. Figure 2.1a shows a PPP in 20m x 20m area with intensity $0.1m^2$.

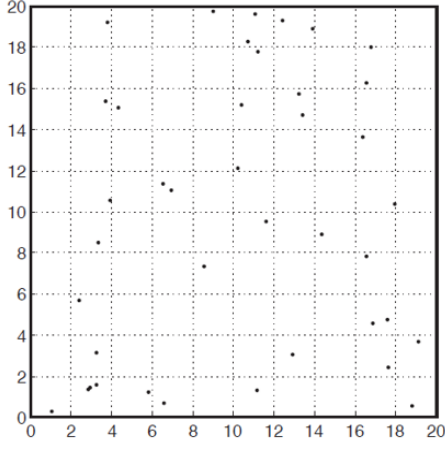
Binomial Point Process (BPP): A point process in which the total number of points in any compact set is a binomial random variable and the number of points in disjoint sets are related via a multinomial distribution. The intensity measure of a BPP is equal to $\frac{n|B \cap A|}{|A|}$, where n is the fixed number of points on the compact set A . The name of the point process comes from the fact that the number of points in a set $B \subset A$ is binomially distributed with the parameter n . Figure 2.1b shows a BPP with $n = 100$.

Hardcore Point Process (HCPP): A repulsive process where no two points of the process coexist within a specified distance r_h . Figure 2.1c shows a HCPP with $r_h = 2m$.

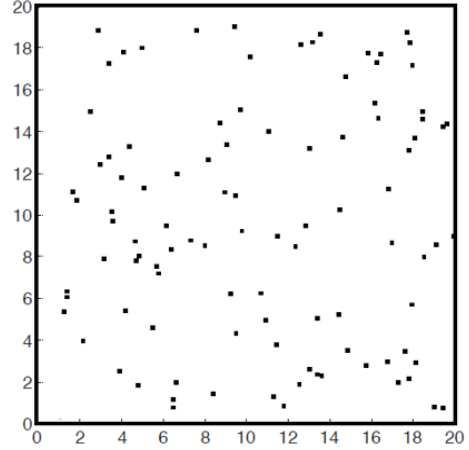
Poisson Cluster Process (PCP): It is constructed from a parent PPP where each point is then replaced by a cluster of points which are independent and identically distributed in the spatial domain. The intensity measure of a PCP is equal to $\lambda_p \bar{c} |B|$. Figure 2.1d shows a PCP with mean 2.

2.2 Stochastic Geometry analysis

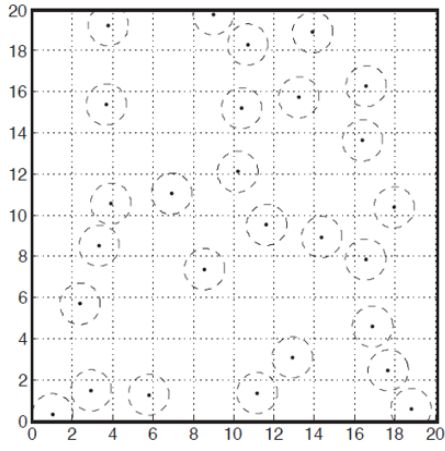
In SG analysis, we use point processes to abstract BSs locations. Then, the Laplace Transform, Characteristic Function and Moment Generating Function are obtained for the aggregate interference. Here, signal-to-noise-plus-interference-ratio (SINR) is characterized first, which is further used to obtain other performance metrics like coverage probability and ergodic capacity but not limited to these only. In SG, a function that involves all points in a point process can be transformed into a simple integral over the point process domain using two techniques, namely, Campbell's theorem and the probability generating functional (PGFL). These techniques are mainly used to characterize the aggregate interference. Campbell's theorem requires expectation over a random sum while PGFL requires expectation over a random product [8].



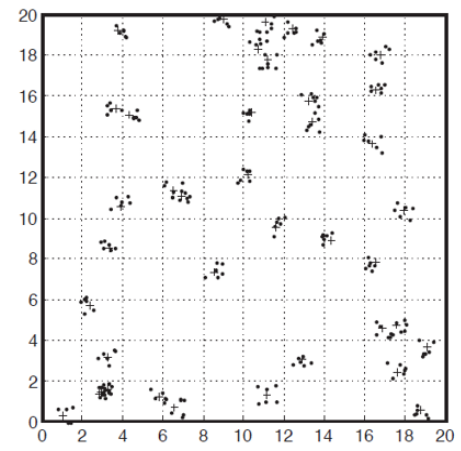
(a)



(b)



(c)



(d)

Figure 2.1: (a) PPP in 20m x 20m area (b) BPP in 20m x 20m area (c) HCPP in 20m x 20m area (d) PCP in 20m x 20m area

Theorem 1 (Campbell's Theorem) *Let $f(x) : \mathbb{R}^d \rightarrow [0, \infty]$ be a measurable function for the point process Φ , then*

$$\mathbb{E}\left(\sum_{x \in \Phi} f(x)\right) = \int_{\mathbb{R}^d} f(x) \Lambda(dx) \quad (2.2)$$

where $\Lambda(dx)$ is the intensity measure of the point process. In case of \mathbb{R}^2 , Campbell's Theorem can be expressed as:

$$\mathbb{E}\left(\sum_{x \in \Phi} f(x)\right) = \int_{\mathbb{R}^2} f(x) \lambda(x) dx \quad (2.3)$$

where $\lambda(x)$ is the two dimensional intensity measure.

If we apply Campbell's Theorem on PPP with intensity λ , we get:

$$\mathbb{E}\left(\sum_{x \in \Phi} f(x)\right) = \lambda \int_{\mathbb{R}^d} f(x) dx \quad (2.4)$$

Theorem 2 (Probability generating functional(PGFL)) Let $\nu(x) : \mathbb{R}^d \rightarrow [0, \infty]$ be a measurable function for the point process Φ , then

$$\mathcal{G}[\nu] = \mathbb{E}\left(\prod_{x \in \Phi} \nu(x)\right) \quad (2.5)$$

The PGFL for PPP is given by:

$$\mathcal{G}[\nu] = \exp\left(-\int_{\mathbb{R}^d} (1 - \nu(x)) \Lambda(dx)\right) \quad (2.6)$$

Figure 2.2 shows the taxonomy of detailed literature review on stochastic geometry according to the target network model, the point process used and the performance metrics studied [9–103]. Note that the same reference number falling under different categories means that

this reference encompasses all these metrics. A number of point processes are used in the literature based on their tractability and practicality. For instance, the PPP assumption is reinforced by several experimental studies as shown in Figure 2.2. Coverage probability and ergodic capacity are extensively studied in the literature. Some authors studied average SINR, mean association area and backhaul delay but not limited to these only. The authors in [96–98], studied HO rates in multi-tier cellular networks. However, the effect of HO delay on the performance of dense cellular networks has been overlooked.

2.3 Handover Rate

Handover is the process of changing the user equipment (UE) association with mobility such that the best serving BS is always selected. One popular and simple rule for determining the best serving BS is based on the average received signal strength (RSS) level. That is, the UE changes its association if another BS provides a higher RSS than the serving BS, which may happen when the user moves away from the serving BS towards another BS. With the increasing heterogeneity of cellular networks, many other criteria are developed for selecting the best serving BS which may include load balancing, delay, and throughput metrics [104–106]. Despite of the selection rule, the UE will always change its association with mobility and the HO rate increases with the BS density. Hence, the HO cost is always an increasing function of the BS density.

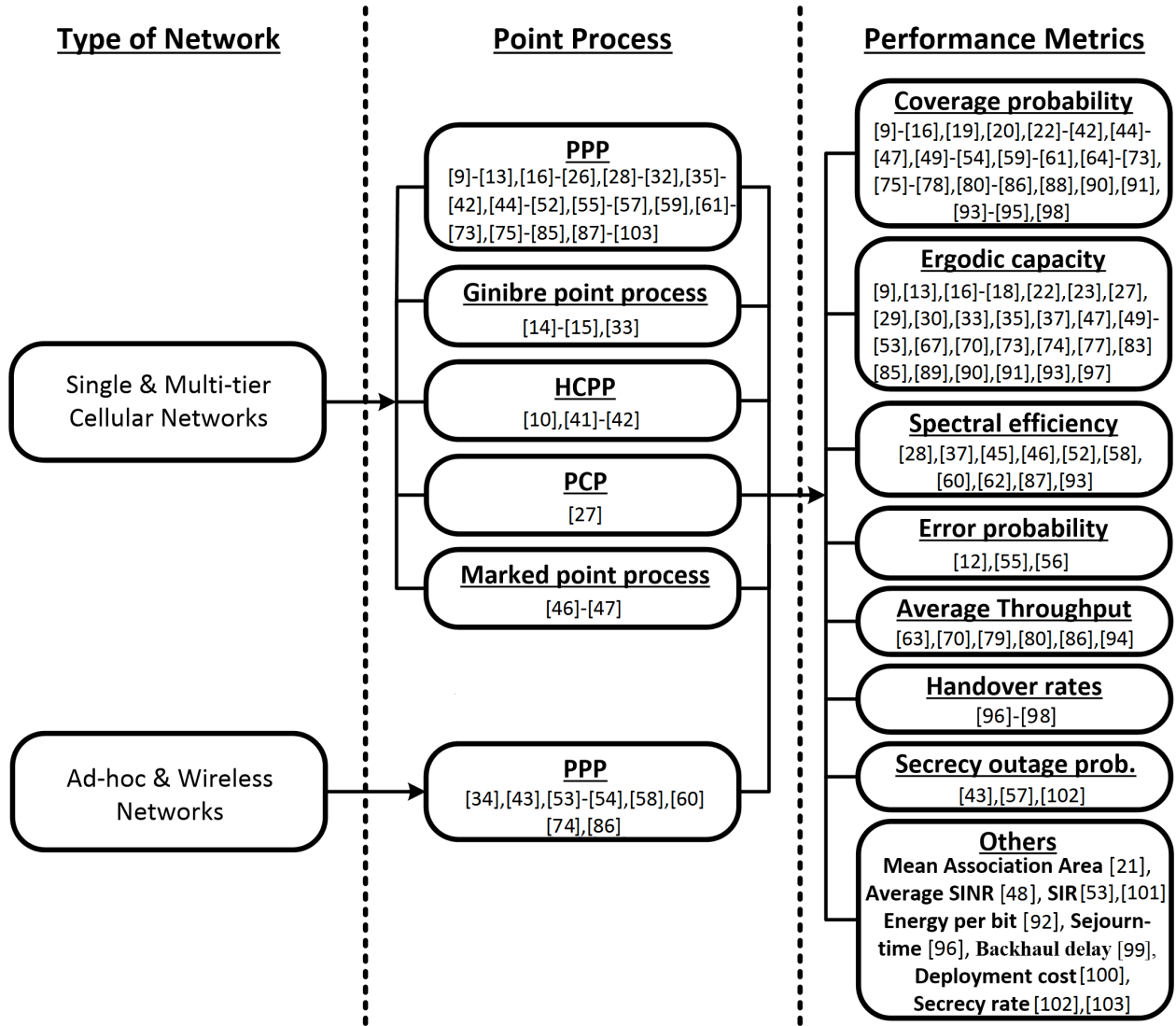


Figure 2.2: Taxonomy of detailed literature review on Stochastic Geometry

The HO process is a core element of cellular networks to support user mobility. Consequently, HO management has always been a focal research point in the context of cellular networks (see [107] for GSM/CDMA and [108, 109] for LTE systems). Modeling and improving the handover performance has been extensively addressed in the cellular network literature. For instance, the cell dwell time is characterized in [110] for the circular and

hexagonal shaped cells. An analytical model, based on application-specific signal strength tuning mechanism is presented in [111] to help optimizing the vertical HOs. HO signaling overhead reduction algorithms are proposed in [112–114] for two tier networks and in [115] for cloud-RAN based heterogeneous networks. A HO management technique, based on self-organizing maps is proposed in [116] to reduce unnecessary HOs for indoor users in two tier cellular networks. Several other techniques to reduce unnecessary HOs are studied in [117–119] for two tier and in [120] for multi-tier downlink cellular networks. HO delay for a single tier network is characterized in [121]. However, none of the aforementioned studies tackle the interplay between HO cost and user throughput as a function of the BS intensity.

For a general study on the interplay between BS intensity, handover rate, and user throughput, random BS deployment is usually considered. Such randomized BSs positions capture the diverse BS deployments that appear in different geographical locations (e.g. cities). Averaging over all possible BSs realizations leads to a general quantification, known as spatial average, on the effect of BS intensity on handover rate and user throughput. Furthermore, such randomized BS location assumption enables rigorous analytical studies for handover rate and user throughput via stochastic geometry, which is the main source of inspiration behind this work. It is shown in [10, 34] that the Poisson point process (PPP) gives a good estimate for coverage probability and ergodic rate when compared to realistic BS deployment. The Poisson cluster process (PCP) is used to study coverage probability and ergodic rate in multi-tier cellular network [27], where the clustering captures the

deployment of several small BSs in hot-traffic regions. Analytical studies for HO rate in PPP cellular networks are conducted in [96] for single-tier scenario and in [97] for multi-tier scenario. In particular, the authors in [96, 97] provide the mathematical expressions for HO rates based on PPP analysis. The work in [97] is extended to the case of PCP in [122] thus offering HO rates in PCP based network. The HO rate expressions for the recently proposed Phantom cells are studied in [123]. However, none of the aforementioned studies investigate the integrated effect of network densification (i.e. BS intensity) in terms of both the HO cost and the throughput gains. To the best of author's knowledge, this is the first study incorporating the effect of HO rate in the throughput analysis and presenting novel HO management schemes to reduce the overall HO effect on the user throughput.

2.4 Summary

In this chapter, we discussed about SG analysis and some of the extensively studied performance metrics in the literature. Furthermore, we discussed the effect of HO rate in dense cellular networks and its corresponding studies in the literature.

CHAPTER 3

SINGLE-TIER DOWNLINK CELLULAR NETWORK

In this chapter, we study the effect of HO delay on the user average rate in dense cellular network environments. In particular, we develop a mathematical paradigm, based on stochastic geometry, that incorporates the HO delay into the rate analysis. It is worth noting that the signal-to-interference-plus-noise-ratio (SINR) dependent expressions are derived based on the stationary PPP analysis. However, we show by simulation that the stationary expressions capture the SINR performance of mobile users almost exactly. This implies that averaging over all users' trajectories in all network realizations is equivalent to averaging over all users locations in all network realizations. To this end, the results manifest the prominent negative effect of HO delay on the rate at high intensities of BSs.

Hereby, we propose a flexible HO scheme denoted as *HO skipping*, which allows users to

skip associating with some of the BSs along their trajectories to reduce the HO delays. That is, a user can sacrifice being always best connected to decrease the HO delay and improve the long-term average rate. In this work, we consider a single HO skipping scheme in which a user, connected to its best serving BS, skips associating to only one subsequent best serving BS on its trajectory and must then reconnect to the following one. This pattern is repeated along the user's trajectory such that it alternates between connecting to its best serving BS and skipping the following one.

3.1 Introduction

In this chapter, we consider a single-tier downlink cellular network and derive the coverage probability and average throughput expressions for both conventional and HO skipping cases. The results show that, although BS skipping reduces the average coverage probability of mobile users, it improves their long-term average rate at high speeds and/or high network densities. The developed model can be used to decide the threshold at which BS skipping is beneficial and quantify the associated performance gains.

It is important to note that this work focuses on a single tier cellular network and a single HO skipping scheme.

3.1.1 System Model

We consider a single-tier downlink cellular network in which the BSs' locations are abstracted via a two dimensional PPP Φ of intensity λ . All BSs are assumed to transmit with the same

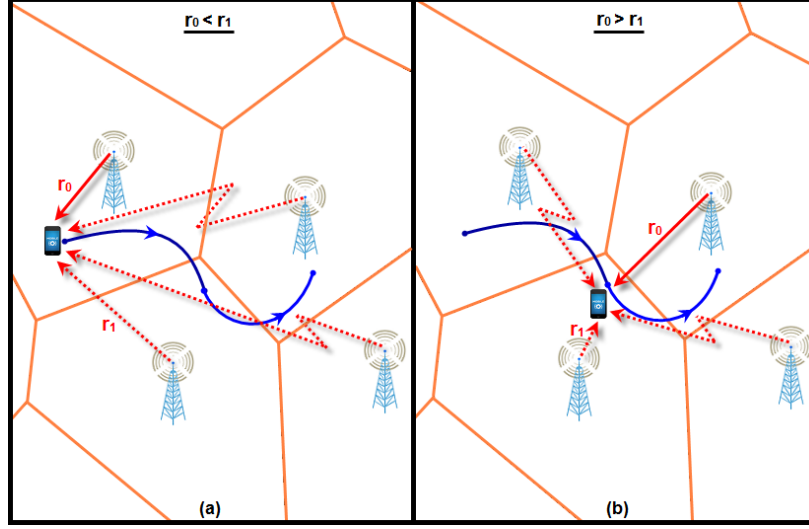


Figure 3.1: (a) represents best connected case. (b) shows the blackout case. In both cases, r_0 represents the distance between test user and its serving BS, r_1 represents the distance between test user and its first interfering BS and blue solid line represents the user trajectory.

effective isotropic radiated power (EIRP) denoted by P . A general power-law path loss model with path loss exponent $\eta > 2$ is considered. In addition to the path-loss, transmitted signals experience multi-path fading. We assume a Rayleigh fading environment such that the channel power gains have independent exponential distributions i.e. $h_i \sim \exp(1)$. The users associate according to the well-known radio signal strength (RSS) association rules. In the depicted single-tier case, the best RSS association boils down to the nearest BS association strategy. The association regions for each BS can be visualized via the Voronoi tessellation diagram shown in Figure 3.2. A list of mathematical notations used in this chapter is given in Table 3.1.

The analysis is conducted on a test mobile user¹ which is moving on an arbitrary trajectory²

¹By Slivnyak's theorem for PPP [8,9], there is no loss of generality to conduct the analysis for a test user

²The handover analysis in this work is based on the mathematical model developed in [97], which is valid for an arbitrary trajectory shape and mobility model.

Table 3.1: Mathematical Notations

Notation	Description
Φ	PPP of BSs
η	Path loss exponent
λ	BS intensity
P	Transmit power of BSs
${}_2F_1(\cdot, \cdot; \cdot; \cdot)$	Hypergeometric function
r_0	Distance between the user and serving BS
r_i	Distance between the user and i^{th} interfering BS
$H(v)$	Handover rate
\mathcal{R}	Average spectral efficiency
D_{HO}	Handover cost
d	Handover delay
\mathcal{C}	Coverage probability
AT	Average Throughput

with velocity v . We ignore HO failures due to blocking and focus on the coverage probability (defined as the probability that the SINR exceeds a certain threshold T) and the ergodic rate (defined by Shannon's capacity formula). That is, we assume that all BSs can assign a channel to the test user when this user passes within its coverage range. Furthermore, when

the test user is assigned to a certain channel from a generic BS, we assume that all other BSs across the spatial domain are reusing the same channel.

Due to the HO procedure, a delay time d is imposed on the test user, at which no useful

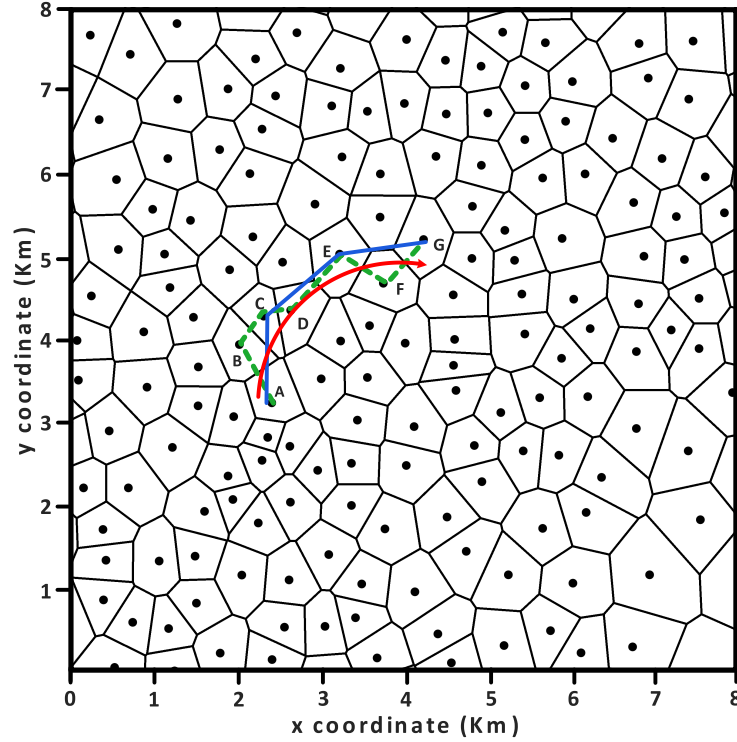


Figure 3.2: Voronoi tessellation of an actual cellular network (Macros only) in urban area with $\lambda=3$ BS per km^2 . Red solid line depicts user trajectory while green dotted and blue solid lines show conventional and skipping HOs respectively. In the conventional (skipping) scheme the test user associates to the BSs $\{A, B, C, D, E, F, G\}$ ($\{A, C, E, G\}$).

data is transmitted to it. The delay d represents the time spent in HO signaling between the serving BS, target BS, and core network elements. It is important to note that the delay d may depend on the type of BSs. For instance, the HO delay is small in macro BSs, which are microwave or optically backhauled to the core network. In contrast, the delay d may be more significant in the case of internet protocol (IP) backhauled small BSs (i.e., pico or femto) [124].

In the *conventional* HO case, the test user maintains the best connectivity throughout its trajectory. Hence, when the test user passes by a certain Voronoi cell, it connects to the BS in the center of that Voronoi cell. This implies that $Pr_0^{-\eta} > Pr_i^{-\eta}, \forall i \neq 0$ is always satisfied, where r_0 and r_i denote the distances from the test user to the serving and i^{th} interfering BSs, respectively. We propose the *skipping* HO scheme, where the test user skip associating to one BS after every HO execution. This implies that $Pr_0^{-\eta} > Pr_i^{-\eta}, \forall i \neq 0$ is satisfied for 50% of the time and $Pr_1^{-\eta} > Pr_0^{-\eta} > Pr_i^{-\eta}, \forall i \notin \{0, 1\}$ is satisfied for the rest of the time, where r_1 denotes the distance from the test user to the skipped BS when it passes within the Voronoi cell of the skipped BS. Thus, in the skipping mode, the user alternates between the blackout and best connected state along its trajectory. Here, we denote the event at which the test user is located within the Voronoi cell of a skipped BS as *blackout* event. Figure 3.1 shows the best connected and blackout events. Figure 3.2 depicts the conventional (green dotted line) and skipping (blue line) HO schemes for the red trajectory.

3.1.2 Service Distance Distribution

The first step in the analysis is to characterize the service distance in the best connected and blackout cases. Note that the service distance is random due to the irregular network topology along with user mobility. It is important to characterize the service distance as it highly affects the SINR. Particularly, when the user is best connected, the RSS association creates an interference protection of radius r_0 around the user. In the blackout case, the user

keeps its association with the same BS when it enters the Voronoi cell of another BS. Hence, the skipped BS is closer to the user than its serving BS (i.e., $r_1 < r_0$). In other words, the skipped BS is located within the radius r_0 and every other interfering BS is located outside r_0 . Note that, in the blackout case, r_1 and r_0 are correlated since $r_1 < r_0$. The distribution of serving BS in the best connected case and the joint distribution of the distances from the test user to the skipped and serving BS in the blackout case are characterized via the following lemma:

Lemma 1 *In a single tier cellular network with intensity λ , the distance distribution between a best connected user and its serving BS is given by:*

$$f_{r_0}^{(c)}(r) = 2\lambda\pi r e^{-\lambda\pi r^2}, \quad 0 \leq r \leq \infty \quad (3.1)$$

and the joint distance distribution between a user in blackout and its serving and skipped BSs is given by:

$$f_{r_0, r_1}^{(bk)}(x, y) = 4(\pi\lambda)^2 x y e^{-\pi\lambda x^2}; \quad 0 \leq y \leq x \leq \infty \quad (3.2)$$

Proof. The PDF $f_{r_0}^{(c)}(.)$ is obtained from the null probability of PPP as in [9]. The joint PDF $f_{r_0, r_1}^{(bk)}(., .)$ is obtained by writing the conditional CDF of r_0 given r_1 as $\mathbb{P}\{r_0 < x | r_1\} = 1 - e^{-\pi\lambda(x^2 - r_1^2)}$. Then, differentiating the conditional CDF of r_0 with respect to x and multiplying by the marginal PDF³ of r_1 , the joint PDF in (3.2) is obtained. ■

³Since the user is in blackout, r_1 is the distance to the closest BS and r_0 is the distance to the second nearest BS. Hence, the marginal PDF of r_1 is given by $f_{r_1}(y) = 2\lambda\pi y e^{-\lambda\pi y^2}$

The marginal and conditional service distance distributions for the blackout case are characterized by the following corollary:

Corollary 1 *The marginal PDF of the distance between the test user and its serving BS in the blackout case is given by:*

$$f_{r_0}^{(bk)}(r) = 2(\lambda\pi)^2 r^3 e^{-\lambda\pi r^2}, \quad 0 \leq r \leq \infty \quad (3.3)$$

where r_0 represents the distance between the test user and its serving BS, which is the second nearest BS in the blackout case.

The conditional (i.e., conditioning on r_0) PDF of the distance between the test user and the skipped BS in the blackout case is given by:

$$f_{r_1}^{(bk)}(r|r_0) = \frac{2r}{r_0^2}, \quad 0 \leq r \leq r_0 \leq \infty \quad (3.4)$$

Proof. The marginal PDF of r_0 is obtained by integrating (3.2) with respect to (w.r.t.) y from 0 to r_0 while the conditional PDF of r_1 is obtained by dividing (3.2) by the marginal distribution of r_0 , which is given in (3.3). ■

3.1.3 Coverage Probability

The coverage probability is defined as the probability that the test user can achieve a specified SINR threshold T . For the best connected case, the coverage probability is given by

$$\mathcal{C}_c = \mathbb{P} \left\{ \frac{Ph_0 r_0^{-\eta}}{\sum_{i \in \Phi \setminus b_0} Ph_i r_i^{-\eta} + \sigma^2} \geq T \right\}$$

where b_0 is the serving BS. In the blackout case, the coverage probability is given by

$$\mathcal{C}_{bk} = \mathbb{P} \left\{ \frac{Ph_0 r_0^{-\eta}}{Ph_1 r_1^{-\eta} + \sum_{i \in \Phi \setminus b_0, b_1} Ph_i r_i^{-\eta} + \sigma^2} \geq T \right\}$$

where b_0 and b_1 are the serving and the skipped BSs, respectively. Following [6], conditioning on r_0 and exploiting the exponential distribution of h_0 , the conditional coverage probability in the best connected case can be represented in the form of the Laplace transform (LT) of the aggregate interference as

$$\mathcal{C}_c(r_0) = e^{-\frac{T\sigma^2 r_0^\eta}{P}} \mathcal{L}_{I_r} \left(\frac{Tr_0^\eta}{P} \right) \quad (3.5)$$

where I_r is the interference from BSs located outside r_0 . Similarly, the conditional coverage probability in the blackout case can be represented as:

$$\mathcal{C}_{bk}(r_0) = e^{-\frac{T\sigma^2 r_0^\eta}{P}} \mathcal{L}_{I_1} \left(\frac{Tr_0^\eta}{P} \right) \mathcal{L}_{I_r} \left(\frac{Tr_0^\eta}{P} \right) \quad (3.6)$$

where I_1 is the interference from the skipped BS and I_r is the interference from BSs located outside r_0 . The conditional (i.e., conditioning on r_0) LTs of I_r and I_1 are characterized via the following Lemma.

Lemma 2 *The Laplace transform of I_r for the best connected and blackout cases is given by:*

$$\mathcal{L}_{I_r} \left(\frac{Tr_0^\eta}{P} \right) = \exp(-\pi\lambda r_0^2 \vartheta(T, \eta)) \quad (3.7)$$

where

$$\vartheta(T, \eta) = T^{2/\eta} \int_{T^{-2/\eta}}^{\infty} \frac{1}{1+w^{\eta/2}} dw$$

The Laplace transform of I_1 in the blackout case is given by:

$$\mathcal{L}_{I_1} \left(\frac{Tr_0^\eta}{P} \right) = \int_0^{r_0} \frac{1}{1+Tr_0^\eta r^{-\eta}} \frac{2r}{r_0^2} dr \quad (3.8)$$

Proof. See Appendix A. ■

In the special case when $\eta = 4$, which is a common path-loss exponent for outdoor environments, the LTs in Lemma 2 can be represented in a closed form as shown in the following corollary.

Corollary 2 *For the special case of $\eta = 4$, the LT in (3.7) reduces to*

$$\mathcal{L}_{I_r} \left(\frac{Tr_0^\eta}{P} \right) \Big|_{\eta=4} = \exp \left(-\pi\lambda r_0^2 \sqrt{T} \arctan \left(\sqrt{T} \right) \right) \quad (3.9)$$

and the LT in (3.8) reduces to

$$\mathcal{L}_{I_1} \left(\frac{Tr_0^\eta}{P} \right) \Big|_{\eta=4} = 1 - \sqrt{T} \arctan \left(\frac{1}{\sqrt{T}} \right) \quad (3.10)$$

Using (3.5), (3.6), and Lemma (2), the following theorem for coverage probability is obtained.

Theorem 3 *Considering a PPP cellular network with BS intensity λ in a Rayleigh fading environment, the coverage probability for the best connected and blackout users can be expressed by (3.11) and (3.12) respectively.*

$$\mathcal{C}_c = \int_0^\infty 2\pi\lambda x \exp \left(-\frac{T\sigma^2 x^\eta}{P} - \pi\lambda x^2 \left(1 + T^{2/\eta} \int_{T^{-2/\eta}}^\infty \frac{1}{1+w^{\eta/2}} dw \right) \right) dx \quad (3.11)$$

$$\mathcal{C}_{bk}^{(1)} = (2\lambda\pi)^2 \int_0^\infty y \exp \left(-Ty^\eta\sigma^2 - \lambda\pi y^2 \left(\frac{2T}{\eta-2} {}_2F_1 \left(1, 1 - \frac{2}{\eta}; 2 - \frac{2}{\eta}; -T \right) + 1 \right) \right) \int_0^y \frac{x}{1+Ty^\eta x^{-\eta}} dx dy \quad (3.12)$$

Proof. We prove the theorem by substituting the LTs from Lemma 2 and Corollary 2 in the conditional coverage probabilities in (3.5) and (3.6), then integrating over the PDF of the service distances given in Lemma 1 and Corollary 1. ■

For $\eta = 4$, (3.11) and (3.12) boil down to simpler expressions as shown below.

$$\mathcal{C}_c|_{\eta=4} = \frac{1}{1 + \sqrt{T} \arctan(\sqrt{T})} \quad (3.13)$$

$$\mathcal{C}_{bk}|_{\eta=4} = \frac{1 - \sqrt{T} \arctan(\frac{1}{\sqrt{T}})}{\left(1 + \sqrt{T} \arctan(\sqrt{T})\right)^2} \quad (3.14)$$

In the blackout case, the interference from the skipped BS (i.e., I_1) may be overwhelming to the SINR. Hence, interference management techniques (i.e. beamforming, cognitive) could be employed to improve the coverage probability⁴. In order to give insights on the gains achieved by interference management, we employ an interference cancellation technique by which the interfering signal from the skipped BS is detected, demodulated, decoded and then subtracted from the received signal [125]. In this case, the coverage probability for blackout user is given by the following theorem.

Theorem 4 *Considering a PPP cellular network with BS intensity λ in a Rayleigh fading environment, the coverage probability for blackout users with interference cancellation capabilities can be expressed as*

$$\mathcal{C}_{bk}^{(IC)} = \frac{1}{(1 + \vartheta(T, \eta))^2} \quad (3.15)$$

⁴The interference management technique can be selected based on its practical implementation feasibility in the downlink

where $\vartheta(T, \eta)$ is defined in Lemma 2. For the case of $\eta = 4$, (3.15) reduces to

$$\mathcal{C}_{bk}^{(IC)}|_{\eta=4} = \frac{1}{(1 + \sqrt{T} \arctan(\sqrt{T}))^2} \quad (3.16)$$

Proof. The theorem is obtained using the same methodology for obtaining (3.14) but eliminating I_1 from (3.6). ■

The coverage probability plots for best connected and blackout cases with and without nearest BS interference cancellation (IC) are shown in Figure 3.3. It can be observed that the simulation results (which are obtained for mobile users) are in accordance with the analysis that validates our model. The figure shows the cost of skipping in terms of coverage probability degradation. Note that the users in the BS skipping scheme alternate between the blackout and best connected cases as we allow for only one BS skipping. Hence, a user in the skipping model would spend 50% of the time with the blackout coverage and 50% of the time in best connected coverage. Figure 3.3 also shows that interference cancellation highly improves the SINR when compared to the blackout case without interference cancellation. Note that, although the expressions in Theorems 3 and 4 are obtained using stationary PPP analysis, they totally conform with the simulations done with mobile users almost exactly, which justifies the aforementioned claim in the previous section.

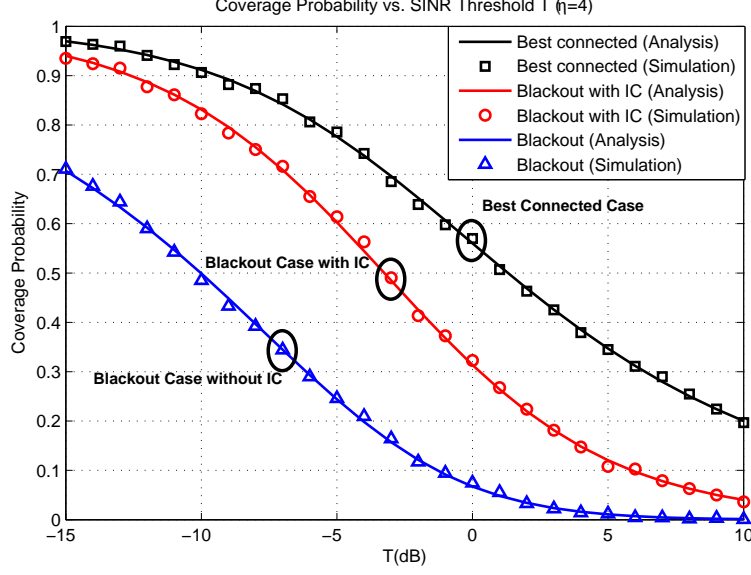


Figure 3.3: Coverage probability plots for the conventional and skipping cases at $\eta = 4$.

3.2 Single-tier Network with Coordinated Multipoint Transmission

In this section, we propose a cooperative handover management scheme that exploits both HO skipping to reduce the HO rate and BS cooperation to enhance the performance during blackout phases. The BSs cooperate by forming a network MIMO system via non-coherent coordinated multipoint (CoMP) transmission strategy [126–128]. When the user decides to skip the handover to the nearest BS, the serving BS and the target BS simultaneously transmit the user data during its transition through the skipped BS coverage area as shown in Figure 3.4. Particularly, in blackout phase, the second and third nearest BSs cooperate to serve the user in order to improve the signal-to-interference-plus-noise-ratio (SINR). Consequently, the cooperative handover management scheme simultaneously reduces HO delay

and maintains high SINR for the user along its trajectory. It is worth mentioning that the non-coherent transmission is considered in this work as it may be hard to estimate the channel state information (CSI) in the considered high mobility scenario.

Figure 3.4 shows the conventional and proposed cooperative handover schemes. In the conventional case, which we refer to as the best connected scenario, the user is always connected to the BS that provides the strongest received signal power. Hence, a handover is executed at every cell boundary crossing and the user is always associated to its nearest BS. In the proposed scheme, the user skips associating to the nearest BS at the first cell boundary crossing. The second and third nearest BSs thus cooperate to serve this user via non-coherent CoMP transmission. At the second cell boundary crossing, the user keeps its association to the nearest BS only. This pattern is repeated along the user's trajectory. Hence, on average, the user spends 50% of the time in the best connected case and 50% of the time in blackout case with BS cooperation. Let $\{r_i; i = 1, 2, 3\}$ be the set of ascending ordered distances between the user and all BSs. The user is thus served by the BS located at the distance r_1 50% of the time and is simultaneously served by the BSs located at r_2 and r_3 for rest of the time. We present our model assuming that the BSs do not have CSI as it is difficult to estimate the channel for mobility scenarios. For the sake of completeness, the non-coherent CoMP transmission is benchmarked against the coherent CoMP transmission where perfect CSI is assumed to be available.

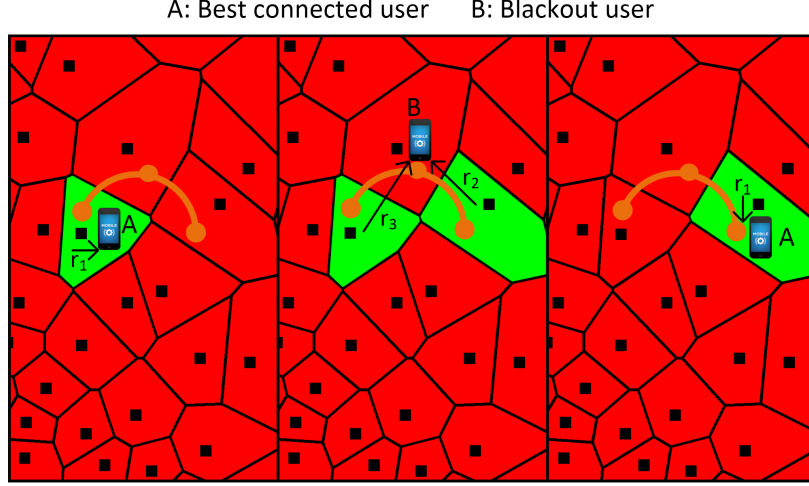


Figure 3.4: A and B represent best connected and blackout with BS cooperation users, respectively. r_i represents the distance between the user and i^{th} nearest BS. Red and green colors show interference and serving regions with BSs located at the corresponding Voronoi centers, respectively. Brown solid line represents the user trajectory.

3.2.1 Cooperative Distance Distribution

In this section, we obtain the distance distribution between the user and the serving BSs in cooperative mode. In the proposed scheme, the user is either served from the nearest BS, or the second and third nearest BSs. Hence, we first derive the joint distribution of the distances between the user to the nearest, second nearest, and third nearest BS(s), which is illustrated in the following lemma:

Lemma 3 *In a single tier cellular network with intensity λ , the joint distance distribution between a user and its skipped and serving BSs with cooperation is given by*

$$f_{r_1, r_2, r_3}^{(bk)}(x, y, z) = (2\pi\lambda)^3 x y z e^{-\pi\lambda z^2}; 0 \leq x \leq y \leq z \leq \infty \quad (3.17)$$

Proof. *By conditioning on r_3 , the joint conditional distribution of r_1 and r_2 is the order*

statistics of two i.i.d. random variables with PDF $\frac{2r}{r_3^2}$, where $0 \leq r \leq r_3$. The joint conditional distribution is given by $f_{r_1, r_2}(x, y|r_3) = \frac{8xy}{r_3^4}$, where $0 < x < y < r_3$. By following Bayes' theorem, the joint PDF $f_{r_1, r_2, r_3}^{(bk)}(., ., .)$ is obtained by multiplying the conditional joint PDF of r_1 and r_2 by the marginal PDF of r_3 . The lemma follows by performing this marginalization over r_3 , using its marginal distribution derived in eq. (2) in [129]. \blacksquare

The service distance distribution for the blackout case with BS cooperation is characterized by the following corollary:

Corollary 3 *The joint PDF of the distances between the test user and its serving/cooperating BSs in the blackout case with BS cooperation is given by:*

$$f_{r_2, r_3}^{(bk)}(y, z) = 4(\pi\lambda)^3 y^3 z e^{-\pi\lambda z^2}; \quad 0 \leq y \leq z \leq \infty \quad (3.18)$$

Proof. *The joint PDF of r_2 and r_3 is obtained by integrating (3.17) w.r.t. x from 0 to y . \blacksquare*

3.2.2 Cooperative Coverage Probability

The coverage probability for the blackout case with BS cooperation is given by:

$$\mathcal{C}_{bk}^{(2)} = \mathbb{P} \left\{ \frac{|\sqrt{P_2}g_2\|r_2\|^{-\eta/2} + \sqrt{P_3}g_3\|r_3\|^{-\eta/2}|^2}{P_1\|g_1\|^2\|r_1\|^{-\eta} + I_{r_2} + \sigma^2} > T \right\}$$

where I_{r_2} denotes the aggregate inference power in blackout with BS cooperation case. Thus, we define I_{r_2} as follows:

$$I_{r_2} = \sum_{i \in \Phi \setminus b_1, b_2, b_3} P_i \|g_i\|^2 \|r_i\|^{-\eta}$$

From [67], given that g_i s are *i.i.d.* $\mathcal{CN}(0,1)$ such that $|x_2 g_2 + x_3 g_3|^2 \sim \exp(\frac{1}{x_2^2 + x_3^2})$, we can write the conditional coverage probability for a blackout user with cooperative service as:

$$C_{bk}^{(2)}(r_2, r_3) = \exp\left(\frac{-T\sigma^2}{x_2^2 + x_3^2}\right) \mathcal{L}_{I_1}\left(\frac{T}{x_2^2 + x_3^2}\right) \mathcal{L}_{I_{r_2}}\left(\frac{T}{x_2^2 + x_3^2}\right) \quad (3.19)$$

where

$$x_i = \sqrt{P_i} \|r_i\|^{-\eta/2}, \quad I_1 = P_1 g_1 \|r_1\|^{-\eta}$$

The LTs of I_1 and I_{r_2} in blackout with BS cooperation are expressed in following lemma.

Lemma 4 *The Laplace transform of I_1 in the blackout case with BS cooperation is given by*

$$\mathcal{L}_{I_1}(s) = \int_0^{r_2} \frac{2r_1}{r_2^2(1 + sPr_1^{-\eta})} dr_1 \quad (3.20)$$

The Laplace transform of I_{r_2} can be expressed in terms of a hypergeometric function as:

$$\mathcal{L}_{I_{r_2}}(s) = \exp\left(\frac{-2\pi\lambda sPr_3^{2-\eta}}{\eta-2} {}_2F_1\left(1, 1 - \frac{2}{n}; 2 - \frac{2}{n}; -sPr_3^\eta\right)\right) \quad (3.21)$$

where

$$s = \frac{T}{P(r_2^{-\eta} + r_3^{-\eta})}$$

Proof. $\mathcal{L}_{I_1}(s)$ and $\mathcal{L}_{I_{r_2}}(s)$ are obtained by following the same procedure as done for the blackout case without BS cooperation while considering $s = \frac{T}{P(r_2^{-\eta} + r_3^{-\eta})}$. Also, we perform the integration from r_3 to ∞ while calculating the Laplace transform for I_{r_2} . ■

We evaluate the above LTs for a special case at $\eta = 4$, which is the most practical value in outdoor environment. The LTs at $\eta = 4$ are given by the following corollary.

Corollary 4 *The Laplace transforms of I_1 and I_{r_2} at $\eta = 4$ for the blackout case with BS cooperation are boiled down into much simpler expressions as shown below:*

$$\mathcal{L}_{I_1}(s) \big|_{\eta=4} = 1 - \sqrt{\frac{Tr_3^4}{r_2^4 + r_3^4}} \arctan\left(\sqrt{\frac{r_2^4 + r_3^4}{Tr_3^4}}\right) \quad (3.22)$$

$$\mathcal{L}_{I_{r_2}}(s) \big|_{\eta=4} = \exp\left(-\pi\lambda\sqrt{\frac{T}{r_2^{-4} + r_3^{-4}}} \arctan\left(\sqrt{\frac{Tr_2^4}{r_2^4 + r_3^4}}\right)\right) \quad (3.23)$$

The coverage probability for the blackout case with BS cooperation is illustrated in the following theorem.

Theorem 5 *Considering a PPP single tier downlink cellular network with BS intensity λ in a Rayleigh fading environment, the coverage probability for the blackout with BS cooperation users can be expressed by (3.25). In an interference limited environment with a special case*

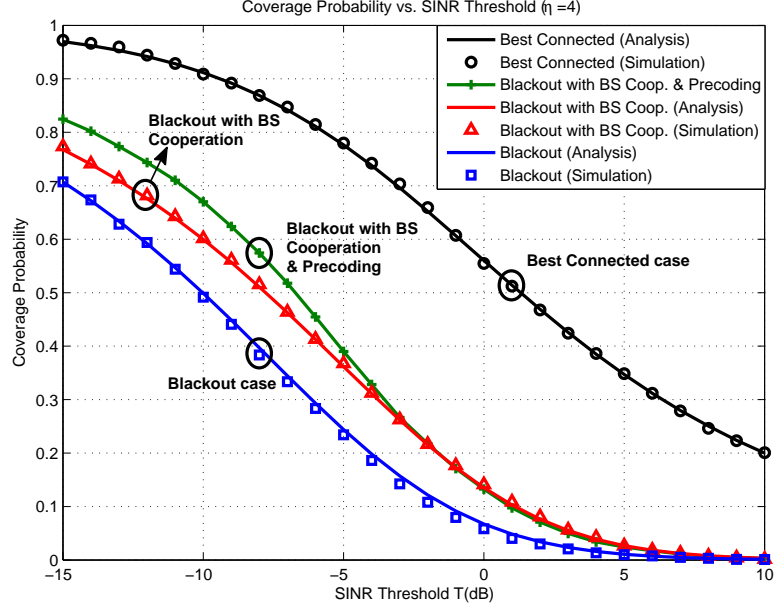


Figure 3.5: Coverage probability plots for best connected and HO skipping cases evaluated at $\eta = 4$.

at $\eta = 4$, (3.25) reduces to

$$C_{bk}^{(2)} = \int_0^\infty \int_{r_2}^\infty 4(\pi\lambda)^3 r_2^3 r_3 \left(1 - \sqrt{\frac{Tr_3^4}{r_2^4 + r_3^4}} \arctan \left(\sqrt{\frac{r_2^4 + r_3^4}{Tr_3^4}} \right) \right) \exp \left(-\pi\lambda \left(r_3^2 + \sqrt{\frac{T}{r_2^{-4} + r_3^{-4}}} \arctan \left(\sqrt{\frac{Tr_2^4}{r_2^4 + r_3^4}} \right) \right) \right) dr_3 dr_2 \quad (3.24)$$

$$C_{bk}^{(2)}|_{\eta=4} = 8(\pi\lambda)^3 \int_0^\infty \int_{r_2}^\infty r_2 r_3 \exp \left(-s\sigma^2 - \pi\lambda r_3^2 \left(1 + \frac{2sPr_3^{-\eta}}{\eta-2} {}_2F_1 \left(1, 1 - \frac{2}{\eta}; 2 - \frac{2}{\eta}; -sPr_3^\eta \right) \right) \right) \int_0^{r_2} \frac{r_1}{1 + sPr_1^{-\eta}} dr_1 dr_3 dr_2 \quad (3.25)$$

Proof. We prove the theorem by substituting the LTs of I_1 and I_{r_2} from and Lemma 4 in the conditional coverage probabilities obtained in (3.19) and integrating it over the distance distributions obtained in Corollary 1. ■

Figure 3.5 shows the coverage probabilities of the best connected vs. blackout cases with and without BS cooperation. In the blackout case, the user is connected to the second nearest BS while receiving huge interference from the nearest BS. Following the same procedure as in the previous section, we evaluate our model with nearest BS interference cancellation (IC).

Theorem 6 *In a PPP downlink cellular network with BS cooperation and IC capabilities, coverage probability in the blackout case is given by:*

$$C_{bk,IC}^{(2)} = \int_0^\infty \int_{r_2}^\infty 4(\pi\lambda)^3 r_2^3 r_3 \exp\left(-s\sigma^2 - \pi\lambda r_3^2 - \frac{2\pi\lambda s P r_3^{2-\eta}}{\eta-2} {}_2F_1\left(1, 1-\frac{2}{n}; 2-\frac{2}{n}; -s P r_3^\eta\right)\right) dr_3 dr_2 \quad (3.26)$$

Proof. We derive this relation by following the same procedure as for Theorem 5 and eliminating the LT of I_1 . ■

Figure 3.6 shows the coverage probabilities for the best connected, blackout and blackout with BS cooperation users when nearest BS IC is enabled. It can be observed that the coverage probability for the blackout case with BS cooperation and IC follows the best connected trend at low threshold values.

In Figures 3.5 and 3.6, we show by simulation that the CSI aware BS cooperation (i.e. transmission with precoding) offers marginal coverage probability gains when compared to the non-coherent BS cooperation. Particularly, the precoding offers 6% and 8% increase in coverage probability w.r.t. the non-coherent BS cooperation without and with IC, respectively. Furthermore, the gains diminish and approach zero at high SINR thresholds. It is worth mentioning that CSI aware BS cooperation coverage expressions can be derived by

following [66, Theorem 5] but with the joint service distance distribution obtained in (3.18).

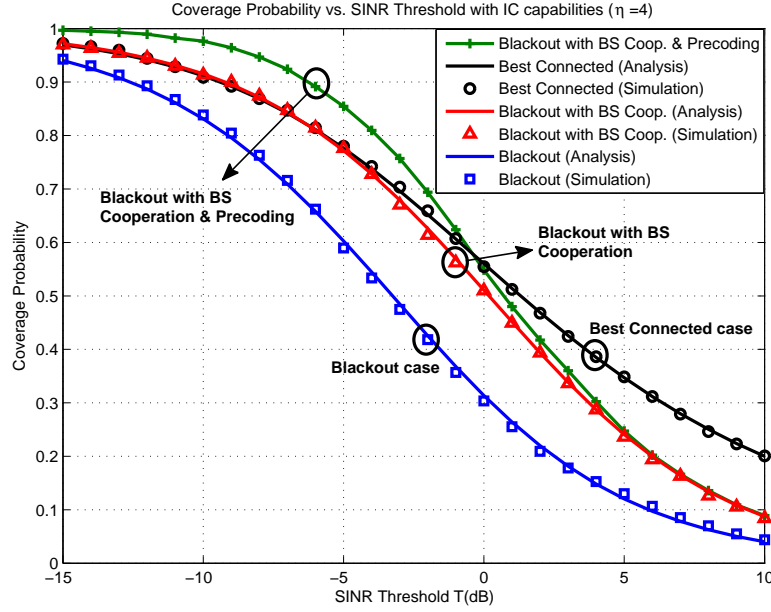


Figure 3.6: Coverage probability plots for best connected and HO skipping cases with IC evaluated at $\eta = 4$.

3.3 Handover Cost

In this section, we encompass user mobility effect and compute handover rates for both conventional and skipping schemes. The handover rates are then used to quantify the handover delay per unit time D_{HO} (i.e., time consumed in HO per time unit). D_{HO} can be expressed as a function of HO rate (HOR) and HO delay d as shown below

$$D_{HO} = \text{HOR} * d \quad (3.27)$$

Following [97], the HO rate in a single tier network can be expressed as

$$H(v) = \frac{4v}{\pi} \sqrt{\lambda} \quad (3.28)$$

Consequently, the handover delay D_{HO} for both conventional and skipping cases can be expressed as

$$D_{HO}^{(c)} = \frac{4v}{\pi} \sqrt{\lambda} d \quad (3.29)$$

$$D_{HO}^{(sk)} = \frac{2v}{\pi} \sqrt{\lambda} d \quad (3.30)$$

where $D_{HO}^{(c)}$ and $D_{HO}^{(sk)}$ are the HO cost for conventional and skipping cases respectively. Note that the handover cost for the skipping case is half of the conventional case because the user skip half of the handovers across the trajectory. Assuming HO delay of 0.7 seconds for macro BSs and 2 seconds for IP-backhauled small cells [5], we plot the handover cost in Figure 3.7.

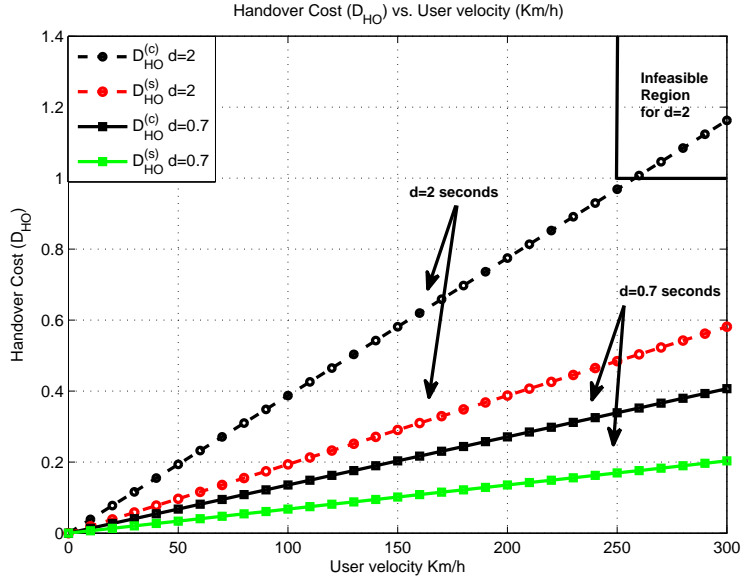


Figure 3.7: D_{HO} plots for conventional and HO skipping cases vs. user velocity (Kmph) for $\lambda = 30BS/km^2$.

3.4 Average Throughput

In this section, we derive an expression for average throughput for HO skipping case. In order to calculate the throughput, we need to omit control overhead. We assume that the control overhead consumes a fraction u_c of overall network capacity, which is 0.3 as per 3GPP Release 11 [130]. Thus, the average throughput (AT) can be expressed as

$$\text{AT} = W\mathcal{R}(1 - u_c)(1 - D_{HO}) \quad (3.31)$$

where W is the overall bandwidth of the channel and \mathcal{R} is the average spectral efficiency (i.e., nats/sec/Hz). Following [6], the average spectral efficiency can be expressed in terms of the coverage probability as

$$\mathcal{R} \stackrel{(a)}{=} \int_0^\infty \mathbb{P}\{\ln(1 + SINR) > z\} dz \quad (3.32)$$

$$\stackrel{(b)}{=} \int_0^\infty \frac{\mathbb{P}\{SINR > t\}}{t + 1} dt \quad (3.33)$$

since $\ln(1 + SINR)$ is strictly a positive random variable, thus (a) follows from the definition of expectation of a positive random variable and (b) follows by the change of variables $t = e^z - 1$ [131]. By performing the numerical evaluation for spectral efficiency in the conventional, blackout with and without cooperation case, we get the spectral efficiency in nats/sec/Hz as shown in Table 3.2.

In the HO skipping case, the user alternates between the best connected and blackout cases. Therefore, we can assume that the user spends 50% time in the best connected mode

Table 3.2: Spectral Efficiency for all cases in nats/sec/Hz

Case	Non-IC	IC
Best connected \mathcal{R}_c	1.49	-
Blackout $\mathcal{R}_{bk}^{(1)}$	0.21	0.66
Blackout (BS coop.) $\mathcal{R}_{bk}^{(2)}$	0.31	1.01

and 50% in the blackout mode with/without BS cooperation. The average spectral efficiency for the HO skipping case is given by:

$$\mathcal{R}_{sk}^{(1)} = \frac{\mathcal{R}_c + \mathcal{R}_{bk}^{(1)}}{2} \simeq 0.85 \text{ nats/sec/Hz} \quad (3.34)$$

$$\mathcal{R}_{sk}^{(2)} = \frac{\mathcal{R}_c + \mathcal{R}_{bk}^{(2)}}{2} \simeq 0.90 \text{ nats/sec/Hz} \quad (3.35)$$

where $\mathcal{R}_{sk}^{(1)}$ and $\mathcal{R}_{sk}^{(2)}$ represent the average spectral efficiency in the HO skipping case without and with BS cooperation, respectively. Similarly, the average spectral efficiency for the IC enabled HO skipping case without and with BS cooperation are found to be 1.08 nats/sec/Hz and 1.25 nats/sec/Hz, respectively.

3.5 Numerical Results

In this section, we compare the throughput performance of our developed model with the best connected and blackout cases. The simulation parameters are shown in Table 3.3. We conduct our analysis based on the nearest BS interference cancellation and consider various values for the HO delay and BS intensity.

Table 3.3: Simulation parameters

Parameter	Value	Parameter	Value
Tx Power:	1 watt	Path loss exponent η :	4
Overall Bandwidth W :	10 MHz	HO delay d :	0.7, 2 s
Control Overhead u_{conv} :	0.3	Control Overhead u_{cbk} :	0.15

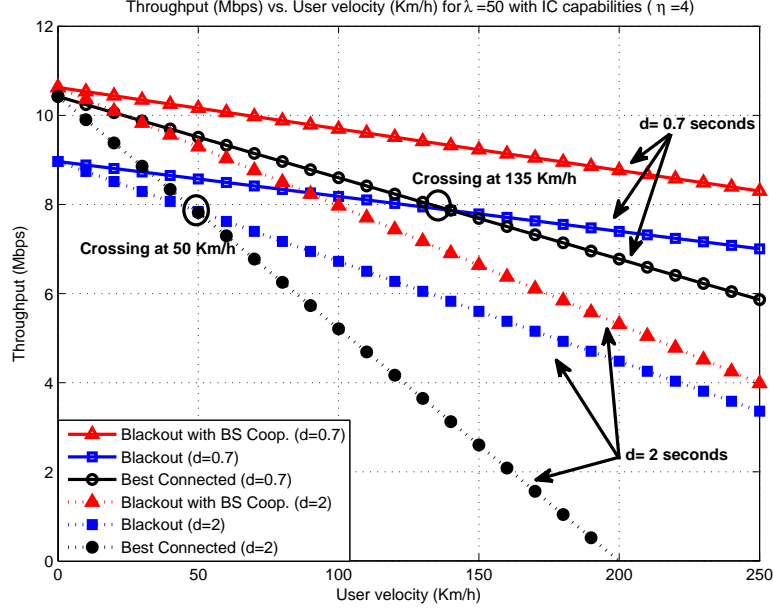


Figure 3.8: Average Throughput (Mbps) vs. user velocity (Km/h) for $\lambda = 50 BS/Km^2$

Figures 3.8 and 3.9 show performance gains in the average throughput of a blackout over conventional user. It is observed that the blackout user with BS cooperation shows considerable gains in the average throughput as compared to the conventional and blackout users without BS cooperation. For instance, the cooperative blackout user moving at the speed of 100 Km/h, in a cellular network with the BS intensity $70 BS/Km^2$ and single HO delay $d = 0.7s$, will experience performance gains of 15% and 17% as compared to the conventional and blackout cases, respectively.

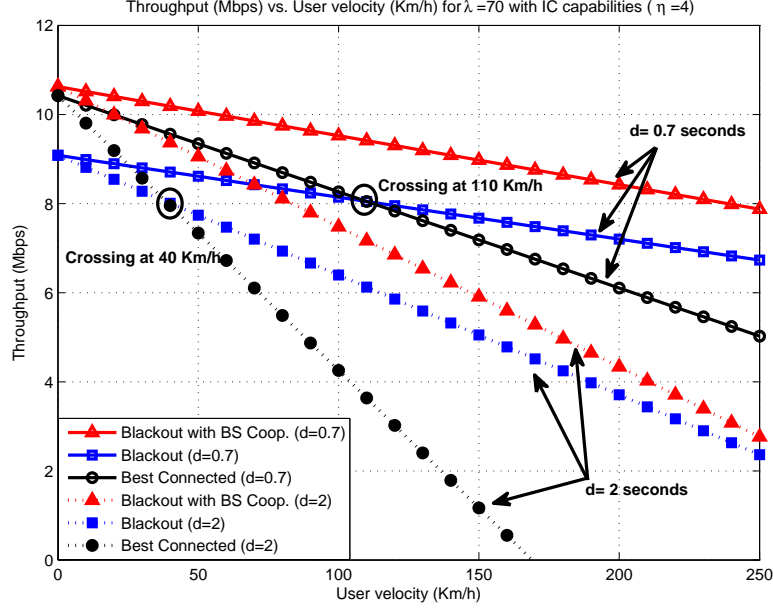


Figure 3.9: Average Throughput (Mbps) vs. user velocity (Km/h) for $\lambda = 70 \text{ BS}/\text{Km}^2$

3.6 Summary

In this chapter, we have proposed a flexible HO scheme, denoted as HO skipping scheme, for a single tier cellular network to enhance the average throughput for mobile users. We developed an analytical paradigm to model the performance of the proposed HO skipping scheme in order to study the effect of HO delay on the average throughput. The developed mathematical model is based on stochastic geometry and is validated via Monte Carlo simulations. The results manifest the negative impact of HO on the users' throughput in dense cellular networks and emphasize the potential of the proposed HO scheme to mitigate such negative HO impact. Particularly, the results show up to 56% more rate gains, which can be harvested via the proposed cooperative HO scheme when compared to the conventional HO scheme that always maintains the best BS association.

CHAPTER 4

MULTI-TIER CELLULAR NETWORKS

In this chapter, we propose a velocity-aware HO management scheme for two-tier downlink cellular network to mitigate the HO effect on the foreseen densification throughput gains. The proposed HO scheme sacrifices the best base station (BS) connectivity, by skipping HO to some BSs along the user trajectory, to maintain longer connection durations and reduce HO rates. Furthermore, the proposed scheme enables cooperative BS service and interference cancellation as discussed in Chapter 3 to compensate for skipping the best connectivity. To this end, we consider different HO skipping scenarios and develop a velocity-aware mathematical model, via stochastic geometry, to quantify the performance of the proposed HO schemes in terms of the coverage probability and user throughput. The results highlight the HO rate problem in dense cellular environments and show the importance of the proposed HO schemes. Finally, the value of BS cooperation along with handover skipping is

quantified for different user mobility profiles.

4.1 Introduction

In this chapter, we propose a simple yet effective velocity aware handover management scheme in a two-tier cellular network that is compatible with the current cellular architecture. The proposed scheme, denoted as HO skipping, bypasses association with some BSs along the user trajectory to maintain a longer service duration with serving BSs and reduce the HO rate and its associated signaling. In other words, the proposed HO skipping scheme sacrifices the best signal-to-interference-plus-noise-ratio (SINR) association to alleviate excessive HO rate and mitigate the handover effect. The proposed scheme also employs interference cancellation (IC) and cooperative BS service, via coordinated multipoint (CoMP) transmission [126–128], when the user is not associated to the BS offering the best SINR. When the user decides to skip the best SINR association, denoted as blackout phase, the user is simultaneously served by the BSs that offer the second and third best SINR associations via non-coherent transmission. It is worth mentioning that the non-coherent transmission is considered as it may be hard to estimate the channel state information (CSI) in the considered high mobility scenarios.

4.2 System Model

We consider a two-tier downlink cellular network with CoMP transmission between BSs belonging to the same or different tiers. It is assumed that the BSs belonging to the k^{th} tier have same transmit power P_k , bias factor¹ B_k , and are spatially distributed via a two-dimensional homogenous PPP Φ_k with intensity λ_k , $k \in \{1, 2\}$. The macro and femto cell tiers are denoted by $k = 1$ and $k = 2$, respectively. A power-law path-loss model with path loss exponent $\eta > 2$ is considered. For simplicity, we consider the same path loss exponents for the two tiers (i.e. $\eta_1 = \eta_2 = \eta$). Extensions to different path-loss exponents is straightforward, but comes at the expense of more involved expressions. Channel power gains are assumed to have exponential distribution with unit mean i.e. $h \sim \exp(1)$. Without loss of generality, we conduct our analysis on a test user and assume that all BSs in Φ_1 and Φ_2 are ascendingly ordered according to their distances from that user. Let R_i and r_i be the distances from the test user to the i^{th} BS in Φ_1 and Φ_2 , respectively, then the inequalities $(R_1 < R_2 < \dots)$ and $(r_1 < r_2 < \dots)$ always hold. We consider a universal frequency reuse scheme and study the performance of one frequency channel. Hence, the best received signal strength (RSS) association implies the best SINR association. A list of key mathematical notations used in this chapter is given in Table 4.1.

¹Biasing is used to manipulate user-to-BS association in order to fulfill a certain network wide objective such as traffic-offloading, load-balancing, and congestion relief [132, 133].

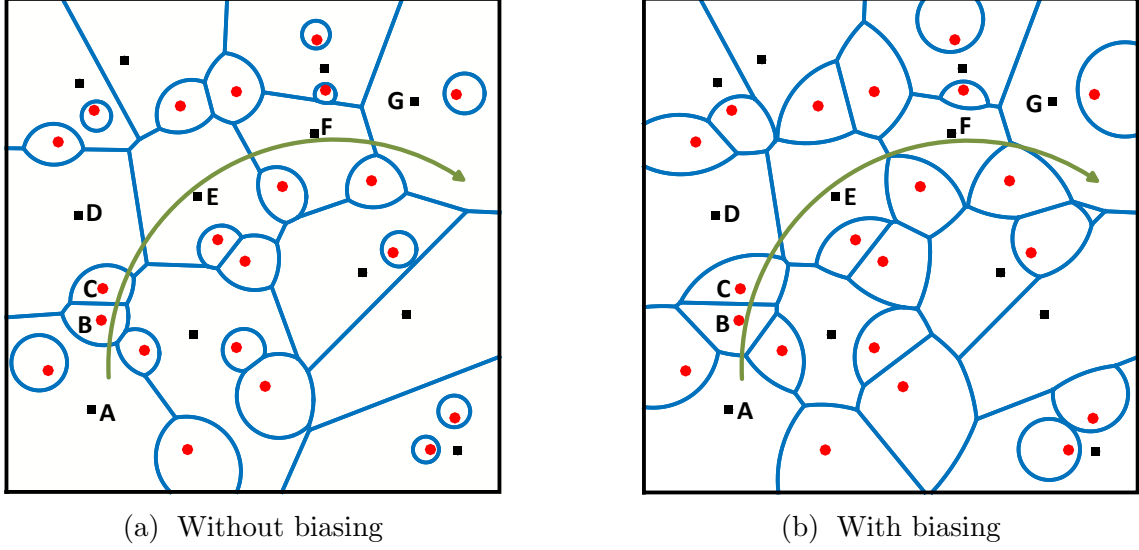


Figure 4.1: Weighted Voronoi tessellations of two tier cellular network. Green solid line represents user trajectory while black squares and red circles represent macro and femto BSs, respectively.

4.2.1 User Mobility and Handover Strategies

In the depicted system model, the association regions for the BSs can be visualized via a weighted Voronoi tessellation [134] (as shown in Figure 4.1), which is widely considered in literature (e.g. [97,135]). The conventional scheme executes a HO every time the user crosses a Voronoi cell boundary to ensure that the best SINR association is always satisfied. We assume that the test user moves with a constant velocity v on an arbitrary long trajectory that passes through all association and SINR states. The average SINR through a randomly selected user trajectory is inferred from the stationary PPP analysis. It is worth noting that a similar assumption was used in [98,135–137] for tractability. However, we incorporate user mobility in the simulations and verify the accuracy of the stationary SINR analysis for mobile users. This implies that averaging over all users' trajectories in all network realizations is equivalent to averaging over all users' locations in all network realizations.

Table 4.1: Mathematical Notations

Notation	Description
Φ_k	PPP of BSs of k^{th} tier
η	Path loss exponent
λ_k	BS intensity of k^{th} tier
P_k	Transmit power of BSs of k^{th} tier
B_k	Bias factor of k^{th} tier
R_i	Distance between the user and i^{th} macro BS
r_i	Distance between the user and i^{th} femto BS
H_{ij}	Handover rate from tier i to j
\mathcal{R}	Achievable rate per unit bandwidth
d_m	Macro to macro HO delay
d_f	Femto related HO delay
\mathcal{C}	Coverage probability
AT	Average Throughput
A_m	The probability that the macro BS provides the best SINR
A_f	The probability that the femto BS provides the best SINR

We propose multiple HO skipping strategies that show throughput gains over different user mobility profiles. Particularly, we consider four HO strategies, which represent user mobility profiles ranging from nomadic to high velocities. Mobile users maintain a list of nearby BSs based on the RSS levels and report to the core network through the serving

BS. In some cases, HO decisions are made on the radio network level based on the HO type. However, in all cases, the HOs are directed by the network entities, which have the capabilities to track the user location and velocity [138–140]. According to the employed HO strategy, the admission controller can help users skip the recommended HOs based on their velocities. BS skipping sacrifices the best SINR connectivity to reduce the handover rate and delay. In order to compensate for the degraded SINR during blackout phases, we enable BS cooperation and IC. For the IC, the interfering signal from the skipped BS is detected, demodulated, decoded and then subtracted from the received signal [125].

In this chapter, we propose the following HO strategies for the mobile users.

Best Connected Strategy (BC)

In the best connected strategy, the admission controller ensures that the biased RSS based association is always satisfied for each HO request received from the mobile station. That is, the user is connected to the nearest macro BS if $P_1 B_1 R_1^{-\eta} > P_2 B_2 r_1^{-\eta}$ is satisfied and to the nearest femto BS if $P_1 B_1 R_1^{-\eta} < P_2 B_2 r_1^{-\eta}$ is satisfied. For the user trajectory shown in Figure 4.1a, the best connected strategy enforces 6 HOs when the user moves from BS A to G through BSs {B, C, D, E, F}.

Femto Skipping Strategy (FS)

In the femto skipping strategy, we propose that the user skips some of the femto BSs along its trajectory, when $P_1 B_1 R_1^{-\eta} < P_2 B_2 r_1^{-\eta}$ is satisfied, to reduce the handover rate. In particular, the user can alternate between the best connectivity and skipping of the femto BSs along its trajectory. During the femto blackout phase, BS cooperation is enabled, which can be intra or inter-tier cooperative BS transmission depending on the relative positions of the BSs along the user trajectory. For the user trajectory shown in Figure 4.1a, the FS strategy involves 5 HOs (i.e., {C, D, E, F, G}) in moving from BS A to G. Also, the user is jointly served by the BSs {A, C} while skipping BS B.

Femto Disregard Strategy (FD)

At high mobility profiles, the cell dwell time within the femto BS coverage area may be too small. Hence, we propose the femto disregard strategy where the user skips HOs to the entire femto tier while enabling the cooperative service between the two strongest macros in blackout. This states that the user connects to the nearest macro BS if $P_1 B_1 R_1^\eta > P_2 B_2 r_1^{-\eta}$ and to the first and the second strongest macros, otherwise. For the user trajectory shown in Figure 4.1a, the FD strategy offers 4 HOs (i.e., {D, E, F, G}) and the joint transmission between the BSs {A, D} is enabled while skipping of the BSs {B, C}.

Macro Skipping Strategy (MS)

At extremely high velocities, the cell dwell time within the macro BS area may become too small. In this case, in addition to the femto disregard, the user may skip some macro BSs along its trajectory. Particularly, the user alternates between the macro best connectivity and macro blackout phases, where macro BS cooperation is enabled in the macro blackout phase. That is, the user spends 50% of the time in macro best connected mode and rest 50% in the macro blackout mode. For the user trajectory shown in Figure 4.1a, the MS strategy enforces only 2 HOs (i.e., {E, G}) and cooperation is enabled between the BSs {A, E} and {E, G} while skipping of the macro BSs D and F, respectively.

It is worth noting that the velocity ranges for each of the aforementioned skipping scheme are selected offline since they are based on the underlying BS intensity and per-BS HO delay. On the contrary, the selection of the skipped/non-skipped BSs is executed in real-time, which is facilitated by the prolonged association time offered by the proposed skipping algorithm.

4.2.2 Methodology of Analysis

We assume that no data is transmitted during HO execution and that the HO duration is dedicated for exchanging control signaling between the serving BS, target BS, and the core network. We consider different backhauling schemes that impose different HO and signaling delays [5]. In all cases, the achievable rate is calculated over the time interval over which only data can be transmitted. For each of the aforementioned HO skipping strategies, we show the imposed tradeoff between coverage probability and throughput. For the sake of an

organized presentation, we show the analysis for each HO strategy in a separate section. In the analysis of each strategy, we first derive the distance distribution between the user and its serving BS(s) as well as the Laplace transform (LT) of the aggregate interference PDF, which are then used to obtain the coverage probability and achievable rate. As discussed earlier, the coverage probabilities and achievable rates are obtained based on the stationary analysis and are verified via simulations.

4.3 Distance Analysis and Coverage Probability

In this section, we first calculate the service distance distributions for the aforementioned HO skipping cases, which are subsequently used to obtain the coverage probabilities in each case. Note that the service distance distribution for each HO skipping case is different due to different serving BS(s) in each case. For the sake of an organized presentation, we perform case by case analysis. At the end of this section, we validate the stationary analysis via simulations that account for user mobility for all HO skipping scenarios.

4.3.1 Best Connected Strategy (BC)

In the best connectivity case, the user associates with the BS that provides the highest power. Thus the user changes its association when it crosses the boundary of the neighboring cell. The always best connected case has been considerably analyzed in the literature. Here, we follow [133] and write the distribution of the distances between the user and its serving macro and femto BSs in a two tier network, which is given by the following lemma.

Lemma 5 (Distance distributions in BC case) *In a two tier cellular network, the distance distribution between the user and its serving macro BS is given by*

$$f_{R_1}^{(BC)}(R) = \frac{2\pi\lambda_1 R}{A_m^{(BC)}} \exp \left(-\pi R^2 \left(\lambda_1 + \lambda_2 \left(\frac{\beta_{21} P_2}{P_1} \right)^{2/\eta} \right) \right); \quad (4.1)$$

where $0 \leq R \leq \infty$. The distance distribution between the user and its serving femto BS can be expressed as

$$f_{r_1}^{(BC)}(r) = \frac{2\pi\lambda_2 r}{A_f^{(BC)}} \exp \left(-\pi r^2 \left(\lambda_2 + \lambda_1 \left(\frac{\beta_{12} P_1}{P_2} \right)^{2/\eta} \right) \right); \quad (4.2)$$

where $0 \leq r \leq \infty$, and $\beta_{12} = \frac{B_1}{B_2} = \frac{1}{\beta_{21}}$ while $A_m^{(BC)}$ and $A_f^{(BC)}$ are the association probabilities for macro and femto BSs, respectively.

$$A_m^{(BC)} = \frac{\lambda_1}{\lambda_1 + \lambda_2 \left(\frac{\beta_{21} P_2}{P_1} \right)^{2/\eta}}, \quad A_f^{(BC)} = \frac{\lambda_2}{\lambda_2 + \lambda_1 \left(\frac{\beta_{12} P_1}{P_2} \right)^{2/\eta}}. \quad (4.3)$$

Proof. The lemma is obtained by using the same methodology as shown in [133, Lemma 3] but considering same path loss exponent for both tiers. ■

Coverage Probability

The coverage probability is defined as the probability that the received SINR exceeds a certain threshold T . In BC case, the user associates with the macro BS with probability $A_m^{(BC)}$ and with the femto BS with probability $A_f^{(BC)}$, where the association is based on the

highest RSS. By the law of total probability, the overall coverage probability is given by

$$\mathcal{C}^{(BC)} = A_m^{(BC)} \mathcal{C}_m^{(BC)} + A_f^{(BC)} \mathcal{C}_f^{(BC)}, \quad (4.4)$$

where $\mathcal{C}_m^{(BC)}$ and $\mathcal{C}_f^{(BC)}$ are the coverage probabilities for the serving macro and femto BSs, respectively. The coverage probabilities $\mathcal{C}_m^{(BC)}$ and $\mathcal{C}_f^{(BC)}$ are given by:

$$\mathcal{C}_m^{(BC)} = \mathbb{P} \left[\frac{P_1 h R_1^{-\eta}}{I_{R(m)} + I_{r(m)} + \sigma^2} > T \right], \quad (4.5)$$

$$\mathcal{C}_f^{(BC)} = \mathbb{P} \left[\frac{P_2 h r_1^{-\eta}}{I_{R(f)} + I_{r(f)} + \sigma^2} > T \right], \quad (4.6)$$

where $I_{R(\cdot)}$ and $I_{r(\cdot)}$ are the aggregate interference powers received from the macro and femto tiers, respectively, which are defined as

$$\begin{aligned} I_{R(m)} &= \sum_{i \in \phi_1 \setminus b_1} P_1 h_i R_i^{-\eta}, & I_{r(m)} &= \sum_{i \in \phi_2} P_2 h_i r_i^{-\eta}, \\ I_{R(f)} &= \sum_{i \in \phi_1} P_1 h_i R_i^{-\eta}, & I_{r(f)} &= \sum_{i \in \phi_2 \setminus b_1} P_2 h_i r_i^{-\eta}. \end{aligned}$$

Following [6], conditioning on the distance between the user and the serving BS and exploiting the exponential distribution of h_i , the conditional coverage probabilities are given by

$$\mathcal{C}_m^{(BC)}(R_1) = \exp \left(\frac{-T R_1^\eta \sigma^2}{P_1} \right) \mathcal{L}_{I_{R(m)}} \left(\frac{T R_1^\eta}{P_1} \right) \mathcal{L}_{I_{r(m)}} \left(\frac{T R_1^\eta}{P_1} \right), \quad (4.7)$$

$$\mathcal{C}_f^{(BC)}(r_1) = \exp \left(\frac{-T r_1^\eta \sigma^2}{P_2} \right) \mathcal{L}_{I_{R(f)}} \left(\frac{T r_1^\eta}{P_2} \right) \mathcal{L}_{I_{r(f)}} \left(\frac{T r_1^\eta}{P_2} \right), \quad (4.8)$$

where $\mathcal{C}_m^{(BC)}(R_1)$ and $\mathcal{C}_f^{(BC)}(r_1)$ are the conditional coverage probabilities for macro and femto associations, respectively. The LTs of I_R and I_r for the macro and femto association cases are evaluated in the following lemma.

Lemma 6 (LTs of the interference in BC case) *The Laplace transforms of I_R and I_r in the macro association case with $s = \frac{TR_1^\eta}{P_1}$ are given by*

$$\mathcal{L}_{I_{R(m)}}(s) = \exp \left(- \frac{2\pi\lambda_1 TR_1^2}{\eta - 2} {}_2F_1 \left(1, 1 - \frac{2}{\eta}, 2 - \frac{2}{\eta}, -T \right) \right), \quad (4.9)$$

$$\mathcal{L}_{I_{r(m)}}(s) = \exp \left(- \frac{2\pi\lambda_2 TR_1^2}{\eta - 2} \left(\frac{P_2}{P_1} \right)^{2/\eta} \beta_{12}^{\eta-2/\eta} {}_2F_1 \left(1, 1 - \frac{2}{\eta}, 2 - \frac{2}{\eta}, -T\beta_{12} \right) \right), \quad (4.10)$$

The Laplace transforms of I_R and I_r in the femto association case with $s = \frac{Tr_1^\eta}{P_2}$ can be expressed as

$$\mathcal{L}_{I_{R(f)}}(s) = \exp \left(- \frac{2\pi\lambda_1 Tr_1^2}{\eta - 2} \left(\frac{P_1}{P_2} \right)^{2/\eta} \beta_{21}^{\eta-2/\eta} {}_2F_1 \left(1, 1 - \frac{2}{\eta}, 2 - \frac{2}{\eta}, -T\beta_{21} \right) \right), \quad (4.11)$$

$$\mathcal{L}_{I_{r(f)}}(s) = \exp \left(- \frac{2\pi\lambda_2 Tr_1^2}{\eta - 2} {}_2F_1 \left(1, 1 - \frac{2}{\eta}, 2 - \frac{2}{\eta}, -T \right) \right), \quad (4.12)$$

where ${}_2F_1(\cdot, \cdot, \cdot, \cdot)$ is the Gauss hypergeometric function [141].

Proof. See Appendix B. ■

In the special case when $\beta_{12} = 1$ and $\eta = 4$, which is a common path loss exponent for outdoor environments, the LTs in (4.9)-(4.12) boil down to much simpler expressions as

shown below.

$$\mathcal{L}_{I_{R(m)}}(s)|_{\eta=4} = \exp \left(-\pi \lambda_1 R_1^2 \sqrt{T} \arctan \left(\sqrt{T} \right) \right), \quad (4.13)$$

$$\mathcal{L}_{I_{r(m)}}(s)|_{\eta=4} = \exp \left(-\pi \lambda_2 R_1^2 \sqrt{\frac{TP_2}{P_1}} \arctan \left(\sqrt{T} \right) \right). \quad (4.14)$$

$$\mathcal{L}_{I_{R(f)}}(s)|_{\eta=4} = \exp \left(-\pi \lambda_1 r_1^2 \sqrt{\frac{TP_1}{P_2}} \arctan \left(\sqrt{T} \right) \right), \quad (4.15)$$

$$\mathcal{L}_{I_{r(f)}}(s)|_{\eta=4} = \exp \left(-\pi \lambda_2 r_1^2 \sqrt{T} \arctan \left(\sqrt{T} \right) \right). \quad (4.16)$$

Combining Lemmas 5 and 6, the following theorem is obtained for the coverage probability.

Theorem 7 (Coverage probabilities in BC case) *Considering two independent PPPs based two tier cellular network with BS intensity λ_i in a Rayleigh fading environment, the coverage probabilities for the macro and femto users are given by (4.17) and (4.18), respectively.*

Proof. *The theorem is proved by substituting the LTs obtained in Lemma 6 in the conditional coverage probability expressions given in (4.7) and (4.8) and then integrating over the service distance distributions provided by Lemma 5.* ■

$$\mathcal{C}_m^{(BC)} = \frac{2\pi\lambda_1}{A_m^{(BC)}} \int_0^\infty R_1 \exp \left\{ -\frac{TR_1^\eta \sigma^2}{P_1} - \pi R_1^2 \left(\lambda_1 \left(1 + \frac{2T}{\eta-2} {}_2F_1 \left(1, 1 - \frac{2}{\eta}, 2 - \frac{2}{\eta}, -T \right) \right) + \lambda_2 \left(\frac{\beta_{21}P_2}{P_1} \right)^{2/\eta} \left(1 + \frac{2T\beta_{12}^\eta}{\eta-2} {}_2F_1 \left(1, 1 - \frac{2}{\eta}, 2 - \frac{2}{\eta}, -T\beta_{12} \right) \right) \right) \right\} dR_1. \quad (4.17)$$

$$\mathcal{C}_f^{(BC)} = \frac{2\pi\lambda_2}{A_f^{(BC)}} \int_0^\infty r_1 \exp \left\{ -\frac{Tr_1^\eta \sigma^2}{P_2} - \pi r_1^2 \left(\lambda_2 \left(1 + \frac{2T}{\eta-2} {}_2F_1 \left(1, 1 - \frac{2}{\eta}, 2 - \frac{2}{\eta}, -T \right) \right) + \lambda_1 \left(\frac{\beta_{12}P_1}{P_2} \right)^{2/\eta} \left(1 + \frac{2T\beta_{21}^\eta}{\eta-2} {}_2F_1 \left(1, 1 - \frac{2}{\eta}, 2 - \frac{2}{\eta}, -T\beta_{21} \right) \right) \right) \right\} dr_1. \quad (4.18)$$

In an interference limited environment with path loss exponent $\eta = 4$ and $\beta_{12} = 1$, the coverage probabilities in Theorem 7 simplify to the following closed form expressions.

$$\mathcal{C}_m^{(FS)} = \mathcal{C}_f^{(BC)} = \frac{1}{1 + \sqrt{T} \arctan(\sqrt{T})}. \quad (4.19)$$

4.3.2 Femto Skipping Strategy (FS)

In the femto skipping case, the test user associates with the macro BS based on the highest RSS. However, the user skips some femto BS associations to reduce excessive HO rate, where the user experience blackout during femto skipping. In the blackout phase, the user is simultaneously served by the second and the third strongest BSs via non-coherent CoMP transmission. The cooperating BSs can be both macros, both femtos, or one macro and one femto. We assume that the user alternates between the femto best connected and femto blackout phases. The service distance distributions for the best connectivity associations (i.e., non-blackout) in FS scheme are similar to that of BC scheme given in (4.1) and (4.2) i.e.

$f_{R_1}^{(FS)} = f_{R_1}^{(BC)}$ and $f_{r_1}^{(FS)} = f_{r_1}^{(BC)}$. However, in the blackout case, the distance distributions are different and have to be derived for each pair of cooperating base stations (i.e. macro and macro, femto and femto, macro and femto). Furthermore, the coverage probability in the blackout case is different for each of the cooperating BSs case and the probability of each cooperation event should be calculated to obtain the total coverage probability. That said, it is cumbersome to derive the distance distributions and coverage probabilities while accounting for the cooperative BSs types via the conventional procedure used in the literature and shown in Section 4.3.1. Instead, we follow [19] and exploit the mapping theorem to develop a unified analysis for all cooperation instances by mapping the two dimensional PPPs into an equivalent one dimensional non-homogenous PPP.

Lemma 7 (Total BS intensity by mapping theorem) *The two point processes Φ_1 and Φ_2 seen from the test receiver perspective are statistically equivalent to a one dimensional non-homogeneous PPP with intensity*

$$\lambda(y) = \frac{2\pi}{\eta} \left(\lambda_1 (B_1 P_1)^{2/\eta} + \lambda_2 (B_2 P_2)^{2/\eta} \right) y^{2/\eta-1}. \quad (4.20)$$

Proof. See Appendix C. ■

Using Lemma 7, we do not need to account for the cooperating BSs types and are able to derive a unified distance distribution and coverage probability expression that accounts for all cooperation instances. This is demonstrated in the following lemma.

Lemma 8 (Distance distributions in FS case) *Let x and y be the distances between the user and the cooperating BSs. Conditioning on x , the conditional distance distribution of*

the skipped BS with distance r_1 from the user conditioned on the second nearest BS in the blackout case is given by

$$f_{r(bk)}^{(FS)}(r_1|x) = \frac{2r_1^{2/\eta-1}}{\eta x^{2/\eta}}; \quad 0 \leq r_1 \leq x \leq \infty \quad (4.21)$$

and the joint distance distribution of x and y is given by

$$f_{X,Y(bk)}^{(FS)}(x,y) = \frac{4}{\eta^2} (\pi \lambda_t)^3 x^{4/\eta-1} y^{2/\eta-1} \exp(-\pi \lambda_t y^{2/\eta}); \quad (4.22)$$

where $0 \leq x \leq y \leq \infty$ and λ_t is given by

$$\lambda_t = \lambda_1 (B_1 P_1)^{2/\eta} + \lambda_2 (B_2 P_2)^{2/\eta}. \quad (4.23)$$

Proof. See Appendix D. ■

Coverage Probability

By the law of total probability, the overall coverage probability for the FS case is given by

$$\mathcal{C}^{(FS)} = A_{m(\bar{b}k)}^{(FS)} \mathcal{C}_{m(\bar{b}k)}^{(FS)} + A_{f(\bar{b}k)}^{(FS)} \mathcal{C}_{f(\bar{b}k)}^{(FS)} + A_{bk}^{(FS)} \mathcal{C}_{bk}^{(FS)}. \quad (4.24)$$

where $\bar{b}k$ and bk represent the non-blackout and blackout phases, respectively. The coverage probabilities for the macro and femto associations in the non-blackout case are the same as the probabilities derived in (4.17) and (4.18) i.e., $\mathcal{C}_{m(\bar{b}k)}^{(FS)} = \mathcal{C}_m^{(BC)}$ and $\mathcal{C}_{f(\bar{b}k)}^{(FS)} = \mathcal{C}_f^{(BC)}$. Also, the macro association probability $A_{m(\bar{b}k)}^{(FS)}$ is the same as derived in Lemma 5. In the

blackout phase, the user skips the strongest femto BS candidate and is served by the second and the third strongest BSs via non-coherent CoMP, which changes the blackout coverage probability and results in two femto association probabilities (i.e., blackout and non-blackout associations). Since the user alternates between the femto best connected and femto blackout phases, the probabilities that the user is in femto best connected (non-blackout) and blackout phases can be expressed as $A_{f(\bar{b}k)}^{(FS)} = A_{bk}^{(FS)} = 0.5A_f^{(BC)}$. By employing the mapping theorem given in Lemma 3, we can lump the aggregate interference from both tiers and express the coverage probability in the blackout phase as

$$\mathcal{C}_{X,Y(bk)}^{(BC)} = \mathbb{P}\left[\frac{\left|h_1x^{-\frac{1}{2}} + h_2y^{-\frac{1}{2}}\right|^2}{I_{agg} + I_{r_1} + \sigma^2} > T\right], \quad (4.25)$$

where

$$I_{r_1} = \frac{h_1}{r_1}, \quad I_{agg} = \sum_{i \in \phi \setminus b_1, b_2, b_3} \frac{h_i}{z_i}, \quad (4.26)$$

where r_1 represents the distance between the user and the skipped femto BS while z_i represents the distance between the user and the interfering BSs belonging to both tiers. Since h_i 's are *i.i.d.* $\mathcal{CN}(0, 1)$, such that $|x_1h_1 + x_2h_2|^2 \sim \exp(\frac{1}{x_1^2 + x_2^2})$, we can write the conditional coverage probability (conditioned on the serving BSs) as

$$\mathcal{C}_{X,Y(bk)}^{(FS)}(x, y) = \exp\left(\frac{-T\sigma^2}{x^{-1} + y^{-1}}\right) \mathcal{L}_{I_{r_1}}\left(\frac{T}{x^{-1} + y^{-1}}\right) \mathcal{L}_{I_{agg}}\left(\frac{T}{x^{-1} + y^{-1}}\right) \quad (4.27)$$

The Laplace transforms of I_{r_1} and I_{agg} are given by the following lemma.

Lemma 9 (LTs of the interference in FS case) *The Laplace transform of I_{r_1} can be ex-*

pressed as

$$\mathcal{L}_{I_{r_1}}(s) = \int_0^x \frac{2r_1^{2/\eta-1}}{\eta x^{2/\eta} \left(1 + \frac{T}{r_1(x^{-1}+y^{-1})}\right)} dr_1. \quad (4.28)$$

The Laplace transform of I_{agg} can be expressed as

$$\mathcal{L}_{I_{agg}}(s) = \exp \left(\frac{-2\pi\lambda_t T y^{2/n-1}}{(\eta-2)(x^{-1}+y^{-1})} {}_2F_1 \left(1, 1 - \frac{2}{\eta}, 2 - \frac{2}{\eta}, \frac{-T}{x^{-1}y+1} \right) \right). \quad (4.29)$$

Proof. See Appendix E. ■

For the special case ($\eta = 4$), the LTs in (4.28) and (4.29) simplify to the expressions as given below.

$$\mathcal{L}_{I_{r_1}}(s)|_{\eta=4} = 1 - \sqrt{\frac{Ty}{x+y}} \arctan \left(\sqrt{\frac{x+y}{Ty}} \right), \quad (4.30)$$

$$\mathcal{L}_{I_{agg}}(s)|_{\eta=4} = \exp \left(-\pi\lambda_t \sqrt{\frac{T}{x^{-1}+y^{-1}}} \arctan \sqrt{\frac{Tx}{x+y}} \right), \quad (4.31)$$

Using the service distance distribution and the LTs derived in Lemma 8 and 9, the following theorem for the coverage probability is obtained.

Theorem 8 (Coverage probability in FS case) *Considering two independent PPPs based two tier downlink cellular network with BS intensity λ_i in a Rayleigh fading envi-*

ronment, the coverage probability for the blackout users in FS case is given by (4.32).

$$\mathcal{C}_{(bk)}^{(FS)} = \int_0^\infty \int_x^\infty \frac{8\pi\lambda_t^3 x^{2/\eta-1} y^{2/\eta-1}}{\eta^3} \exp \left\{ -\pi y^{2/\eta} \lambda_t - \frac{2\pi\lambda_t T y^{2/\eta-1}}{(\eta-2)(x^{-1} + y^{-1})} \right. \\ \left. {}_2F_1 \left(1, 1 - \frac{2}{\eta}, 2 - \frac{2}{\eta}, \frac{-T}{x^{-1}y + 1} \right) \right\} \int_0^x \frac{r_1^{2/\eta-1}}{1 + \frac{Tr_1^{-1}}{x^{-1}+y^{-1}}} dr_1 dy dx. \quad (4.32)$$

Proof. The theorem is obtained by substituting the LTs shown in Lemma 9 in the conditional coverage probability expression (4.27) and integrating over the distance distribution obtained in Lemma 8. ■

Interference Cancellation

In the blackout phase, the interference from the skipped BS (i.e., I_{r_1}) may be overwhelming to the SINR. Hence, interference cancellation techniques could be employed to improve the coverage probability. By considering skipped BS interference cancellation, the coverage probability for the blackout user is given by the following theorem.

Theorem 9 (Coverage probability in FS case with IC) *Considering an independent PPP based two-tier cellular network with BS intensity λ_i in a Rayleigh fading environment, the coverage probability for blackout users with interference cancellation capabilities can be expressed as*

$$\mathcal{C}_{(bk,IC)}^{(FS)} = \int_0^\infty \int_x^\infty \frac{4\pi\lambda_t^3 x^{4/\eta-1} y^{2/\eta-1}}{\eta^2} \exp \left\{ -\pi y^{2/\eta} \lambda_t - \frac{2\pi\lambda_t T y^{2/\eta-1}}{(\eta-2)(x^{-1} + y^{-1})} \right. \\ \left. {}_2F_1 \left(1, 1 - \frac{2}{\eta}, 2 - \frac{2}{\eta}, \frac{-T}{x^{-1}y + 1} \right) \right\} dy dx. \quad (4.33)$$

Proof. The theorem is obtained using the same methodology for obtaining (4.32) but with eliminated I_{r_1} from (4.27). ■

4.3.3 Femto Disregard Strategy (FD)

In FD case, the mobile user skips all femto BSs associations. Since the femto BS footprint is quite smaller than the macro BS footprint, we propose that the test user associates with the macro BSs only. More specifically, the user associates with the nearest macro BS if $P_1 B_1 R_1^\eta > P_2 B_2 r_1^{-\eta}$ is satisfied while cooperative BS service is invoked in blackout (i.e. $P_1 B_1 R_1^\eta < P_2 B_2 r_1^{-\eta}$). Since the femto tier is disregarded, only macro BS cooperation is allowed to compensate for the SINR degradation in blackout. In non-blackout case, the user associates with the macro BS offering highest RSS, thus, the distance distribution in this case is the same as in BC case given in (4.1) i.e. $f_{R_1}^{(FD)} = f_{R_1}^{(BC)}$. However, the conditional and the joint PDFs of the distances between the blackout user and its serving macros are given by the following lemma.

Lemma 10 (Distance distributions in FD case) *The conditional distribution of the distance from the skipped femto BS, conditioned on the distance from the serving macro BS, is given by*

$$f_r^{(FD)}(r_1|R_1) = \frac{2\pi\lambda_2 r_1 \exp(-\pi\lambda_2 r_1^2)}{1 - \exp(-\pi\lambda_2 R_1^2 (\frac{\beta_{21}P_2}{P_1})^{2/\eta})}, \quad (4.34)$$

where $0 \leq r_1 \leq \left(\frac{\beta_{21}P_2}{P_1}\right)^{1/\eta} R_1 \leq \infty$. The joint distance distribution between the test user and

its skipped and serving BSs in the cooperative blackout mode can be expressed as

$$f_{R_1, R_2, r_1(bk)}^{(FD)}(x, y, z) = \frac{(2\pi)^3}{A_{bk}^{(FD)}} \lambda_1^2 \lambda_2 x y z \exp(-\pi(\lambda_1 y^2 + \lambda_2 z^2)). \quad (4.35)$$

The marginal distribution of the distance between the user and its first and second strongest macro BSs in the cooperative blackout mode is given by

$$f_{R_1, R_2(bk)}^{(FD)}(x, y) = \frac{(2\pi\lambda_1)^2}{A_{bk}^{(FD)}} x y \exp(-\lambda_1 \pi y^2) \left(1 - \exp\left(-\lambda_2 \pi x^2 \left(\frac{\beta_{21} P_2}{P_1}\right)^{2/\eta}\right) \right), \quad (4.36)$$

where

$$A_{bk}^{(FD)} = A_f^{(BC)} = \frac{\lambda_2}{\lambda_2 + \lambda_1 (\beta_{12} P_1 / P_2)^{2/\eta}}. \quad (4.37)$$

Proof. The conditional distribution $f_r^{(FD)}(r_1|R_1)$ is obtained by first writing the joint distribution of r_1 and R_1 (i.e., $f_{r,R}(r_1, R_1) = (2\pi)^2 \lambda_1 \lambda_2 e^{-\pi\lambda_1 R_1^2 - \pi\lambda_2 r_1^2}$). Then dividing it by the marginal distribution of R_1 , ($r_1(\frac{\beta_{12} P_1}{P_2})^{1/\eta} < R_1 < \infty$), we obtain $f_r(r_1|R_1)$. The joint distribution $f_{R_1, R_2, r_1(bk)}^{(FD)}(., ., .)$ is obtained by first writing the conditional PDF of R_2 conditioning on R_1 as $f_{R_2}(y|R_1) = 2\pi\lambda_2 y e^{-\lambda_2 \pi(y^2 - R_1^2)}$ and calculating the joint PDF $f_{R_1, R_2}(x, y) = f(y|x)f_{R_1}(x)$. Then, multiplying by the weighted distribution of r_1 (i.e., using null probability of PPP), we get the joint distribution as given in (4.35). The marginal distance distribution between the user and its serving BSs $f_{R_1, R_2(bk)}^{(FD)}(., .)$ is obtained by integrating (4.35) with respect to r_1 , which is bounded from 0 to $R_1(\frac{\beta_{21} P_2}{P_1})^{1/\eta}$. ■

Coverage Probability

By employing the law of total probability, the overall coverage probability in the FD scheme can be written as

$$\mathcal{C}^{(FD)} = A_{bk}^{(FD)} \mathcal{C}_{m(bk)}^{(FD)} + A_{bk}^{(FD)} \mathcal{C}_{m,m(bk)}^{(FD)}. \quad (4.38)$$

The event probabilities in the above equation are the same as in BC case, given in (4.3) (i.e., $A_{bk}^{(FD)} = A_m^{(BC)}$ and $A_{bk}^{(FD)} = A_f^{(BC)}$). The coverage probability in the non-blackout case is the same as the macro association probability in BC case i.e. $\mathcal{C}_{m(bk)}^{(FD)} = \mathcal{C}_m^{(BC)}$. However, the coverage probability for the blackout case is different from the previous cases and is given by

$$\mathcal{C}_{m,m(bk)}^{(FD)} = \mathbb{P} \left[\frac{|\sqrt{P_1} h_1 R_1^{-\frac{\eta}{2}} + \sqrt{P_1} h_2 R_2^{-\frac{\eta}{2}}|^2}{I_R + I_{r_1} + I_r + \sigma^2} > T \right]. \quad (4.39)$$

where, I_R and I_r are the aggregate interference powers from the macro and femto tiers, respectively. I_{r_1} is the interference power from the strongest femto BS. Here, it is worth noting that I_R is the received aggregate interference from all macro BSs except $\{b_1, b_2\}$ and I_r is the aggregate interference power received from all femtos except $\{b_1\}$. The conditional coverage probability (conditioned on the serving BSs) for the blackout case is given by

$$\mathcal{C}_{m,m(bk)}^{(FD)}(R_1, R_2) = \exp \left(\frac{-T\sigma^2}{x_1^2 + x_2^2} \right) \mathcal{L}_{I_R} \left(\frac{T}{x_1^2 + x_2^2} \right) \mathcal{L}_{I_{r_1}} \left(\frac{T}{x_1^2 + x_2^2} \right) \mathcal{L}_{I_r} \left(\frac{T}{x_1^2 + x_2^2} \right), \quad (4.40)$$

where

$$x_i = \sqrt{P_i} R_i^{-\eta/2} \text{ and } h_i' s \text{ are i.i.d. } \mathcal{CN}(0,1).$$

Since the user is in blackout, the condition $P_2 B_2 r_1^{-\eta} > P_1 B_1 R_1^{-\eta}$ is satisfied. This implies that the first nearest femto BS must exist between 0 and $R_1 (\frac{\beta_{21} P_2}{P_1})^{1/\eta}$. Therefore, we derive the LT of I_r considering that the interfering femto BSs exist outside an interference exclusion circle with radius r_1 centered at the test receiver. The LTs of I_R , I_{r_1} and I_r in the blackout case are evaluated in the following lemma.

Lemma 11 (LTs of the interference in FD case) *The LT of the aggregate interference power received from the macro tier in the blackout phase can be characterized as*

$$\mathcal{L}_{I_R}(s) = \exp \left(\frac{-2\pi T \lambda_1 R_2^{2-\eta}}{(\eta-2)(R_1^{-\eta} + R_2^{-\eta})} {}_2F_1 \left(1, 1 - \frac{2}{\eta}, 2 - \frac{2}{\eta}, \frac{-T R_2^{-\eta}}{R_1^{-\eta} + R_2^{-\eta}} \right) \right). \quad (4.41)$$

The LT of I_{r_1} can be expressed as

$$\mathcal{L}_{I_{r_1}}(s) = \frac{2\pi \lambda_2}{1 - e^{-\lambda_2 \pi R_1^2 (\frac{\beta_{21} P_2}{P_1})^{2/\eta}}} \int_0^{R_1 (\frac{\beta_{21} P_2}{P_1})^{1/\eta}} \frac{r_1 e^{-\pi \lambda_2 r_1^2}}{\left(1 + \frac{T P_1^{-1} P_2 r_1^{-\eta}}{R_1^{-\eta} + R_2^{-\eta}} \right)} dr_1. \quad (4.42)$$

The LT of the aggregate interference power received from the entire femto tier except $\{b_1\}$ is given by

$$\mathcal{L}_{I_r}(s) = \exp \left(\frac{-2\pi \lambda_2 P_2 T r_1^{2-\eta}}{(\eta-2) P_1 (R_1^{-\eta} + R_2^{-\eta})} {}_2F_1 \left(1, 1 - \frac{2}{\eta}, 2 - \frac{2}{\eta}, \frac{-P_2 T r_1^{-\eta}}{P_1 (R_1^{-\eta} + R_2^{-\eta})} \right) \right). \quad (4.43)$$

Proof. *The LT of I_R is derived using the same procedure as shown for $\mathcal{L}_{I_{R(m)}}(s)$ in (4.9)*

but considering the macros aggregate interference from R_2 to ∞ and $s = \frac{T}{P_1(R_1^{-\eta} + R_2^{-\eta})}$. Also, the LT of I_{r_1} is derived in a similar way as of equation (3.8) but considering different s (shown above) and the conditional service distribution shown in (4.34). The LT of I_r is derived in a similar way as $\mathcal{L}_{I_R}(s)$ while taking the femto aggregate interference from r_1 to ∞ . ■

The LTs in Lemma 11 for a special case at $\eta = 4$, boil down to the closed form expressions as shown below.

$$\mathcal{L}_{I_R}(s)|_{\eta=4} = \exp \left(-\pi \lambda_1 \sqrt{\frac{T}{R_1^{-4} + R_2^{-4}}} \arctan \left(\sqrt{\frac{TR_1^4}{R_1^4 + R_2^4}} \right) \right). \quad (4.44)$$

$$\mathcal{L}_{I_r}(s)|_{\eta=4} = \exp \left(-\pi \lambda_2 \sqrt{\frac{P_2 P_1^{-1} T}{R_1^{-4} + R_2^{-4}}} \arctan \left(\sqrt{\frac{P_2 P_1^{-1} T r_1^{-4}}{R_1^4 + R_2^4}} \right) \right) \quad (4.45)$$

Using the LTs and distance distributions found in Lemmas 10 and 11, we obtain the final coverage probability for the blackout users in FD case as given in Theorem 10.

Theorem 10 (Coverage probability in FD case) *Considering two independent PPPs based two tier downlink cellular network with BS intensity λ_i in a Rayleigh fading environment, the coverage probability for the blackout case is given in (4.46).*

Proof. We obtain the coverage probability for the blackout user with cooperation by substituting the LTs found in Lemma 11 in the conditional coverage probability expression given in (4.40) and integrating it over the service distance distribution obtained in Lemma 10. ■

$$\begin{aligned}
C_{m,m(bk)}^{(FD)} &= \int_0^\infty \int_{R_1}^\infty \int_0^{R_1(\frac{\beta_{21}P_2}{P_1})^{1/\eta}} \frac{(2\pi)^3 \lambda_1^2 \lambda_2 r_1 R_1 R_2}{\left(1 + \frac{TP_2 r_1^{-\eta}}{P_1(R_1^{-\eta} + R_2^{-\eta})}\right) A_{bk}^{(FD)}} \exp\left(-\pi \lambda_2 r_1^2 - \pi \lambda_1 R_2^2 - \right. \\
&\quad \left. \frac{T\sigma^2}{P_1(R_1^{-\eta} + R_2^{-\eta})} - \frac{2\pi T}{(n-2)(R_1^{-\eta} + R_2^{-\eta})} \left\{ \lambda_1 R_2^{2-\eta} {}_2F_1\left(1, 1 - \frac{2}{\eta}, 2 - \frac{2}{\eta}, -\frac{TR_2^{-\eta}}{R_1^{-\eta} + R_2^{-\eta}}\right) + \frac{\lambda_2 P_2 r_1^{2-\eta}}{P_1} \right. \right. \\
&\quad \left. \left. {}_2F_1\left(1, 1 - \frac{2}{\eta}, 2 - \frac{2}{\eta}, \frac{-P_2 T r_1^{-\eta}}{P_1(R_1^{-\eta} + R_2^{-\eta})}\right) \right\} \right) dr_1 dR_2 dR_1. \quad (4.46)
\end{aligned}$$

$$\begin{aligned}
C_{m,m(bk,IC)}^{(FD)} &= \int_0^\infty \int_{R_1}^\infty \int_0^{R_1(\frac{\beta_{21}P_2}{P_1})^{1/\eta}} \frac{(2\pi)^3}{A_{bk}^{(FD)}} \lambda_1^2 \lambda_2 R_1 R_2 r_1 \exp\left(-\pi(\lambda_1 R_2^2 + \lambda_2 r_1^2) - \right. \\
&\quad \left. \frac{2\pi T}{(n-2)(R_1^{-\eta} + R_2^{-\eta})} \left\{ \lambda_1 R_2^{2-\eta} {}_2F_1\left(1, 1 - \frac{2}{\eta}, 2 - \frac{2}{\eta}, -\frac{TR_2^{-\eta}}{R_1^{-\eta} + R_2^{-\eta}}\right) + \frac{\lambda_2 P_2 r_1^{2-\eta}}{P_1} \right. \right. \\
&\quad \left. \left. {}_2F_1\left(1, 1 - \frac{2}{\eta}, 2 - \frac{2}{\eta}, \frac{-P_2 T r_1^{-\eta}}{P_1(R_1^{-\eta} + R_2^{-\eta})}\right) \right\} \right) dr_1 dR_2 dR_1. \quad (4.47)
\end{aligned}$$

In the blackout phase, the user associates with the two strongest macro BSs while employing interference cancellation on the strongest femto BS. For the interference cancellation case, the blackout coverage probability is given by the following theorem.

Theorem 11 (Coverage probability in FD case with IC) *Considering two independent PPPs based two tier downlink cellular network with BS intensity λ_i in a Rayleigh fading environment, the coverage probability for blackout users in FD case with IC capabilities is expressed in (4.47).*

Proof. *The theorem is obtained using the same methodology for obtaining Theorem 10 but with eliminating I_{r_1} from (4.40) and integrating over the joint distance distribution expressed in (4.35).* ■

4.3.4 Macro Skipping Strategy (MS)

In MS scheme, the test user skips all femto BSs and every other macro BSs along its trajectory. Particularly, the user in this case alternates between the macro best connected and macro blackout modes. That is, in blackout phase, the test user skips the nearest macro BS and disregards the entire tier of femto BSs. Also, the cooperative non-coherent transmission from the second and the third nearest macro BSs is only activated during macro blackout. The conditional and joint service distance distributions for the test user in the blackout phase are given by the following lemma.

Lemma 12 (Distance distributions in MS case) *The joint distance distribution between the user and its skipped and serving or cooperating BSs in the blackout mode is given by*

$$f_{R_1, R_2, R_3(bk)}^{(MS)}(x, y, z) = (2\pi\lambda_1)^3 x y z e^{-\pi\lambda_1 z^2}; 0 \leq x \leq y \leq z \leq \infty \quad (4.48)$$

The joint PDF of the distances between the test user and its serving or cooperating BSs in the blackout phase with BS cooperation is given by

$$f_{R_2, R_3(bk)}^{(MS)}(y, z) = 4(\pi\lambda)^3 y^3 z e^{-\pi\lambda z^2}; \quad 0 \leq y \leq z \leq \infty \quad (4.49)$$

The conditional (i.e., conditioning on R_2) PDF of the distance between the test user and the skipped BS in the blackout case is given by

$$f_{R(bk)}^{(MS)}(R_1|R_2) = \frac{2R_1}{R_2^2}. \quad (4.50)$$

The joint distance distribution between the user and the disregarded femto and serving macro BSs in the non-blackout mode is given by

$$f_{R_1, r_1(\bar{b}k)}^{(MS)}(x, y) = \frac{(2\pi)^2}{A_f} \lambda_1 \lambda_2 x_1 y_1 \exp(-\pi \lambda_1 x^2 - \pi \lambda_2 y^2), \quad (4.51)$$

where A_f is the probability that $P_2 B_2 r_1^{-\eta} > P_1 B_1 R_1^{-\eta}$, which is same as $A_f^{(BC)}$, given in (4.3).

The marginal distribution of the distance between the user and its serving macro BS in non-blackout mode is given by

$$f_{R_1(\bar{b}k)}^{(MS)}(x) = \frac{2\pi}{A_f} \lambda_1 x \left(\exp(-\pi \lambda_1 x^2) - \exp\left(-\pi x^2 \left(\lambda_1 + \lambda_2 \left(\frac{\beta_{21} P_2}{P_1} \right)^{2/\eta} \right) \right) \right). \quad (4.52)$$

Proof. The joint conditional distribution of R_1 and R_2 is the order statistics of two i.i.d. random variables with PDF $\frac{2R}{R_3^2}$, where $0 \leq R \leq R_3$. The joint conditional distribution is given by $f_{R_1, R_2}(x, y | R_3) = \frac{8xy}{R_3^4}$, where $0 < x < y < R_3$. By following Bayes' theorem, the joint PDF $f_{R_1, R_2, R_3(bk)}^{(MS)}(\cdot, \cdot, \cdot)$ is obtained by multiplying the conditional joint PDF of R_1 and R_2 by the marginal PDF of R_3 . The lemma follows by performing this marginalization over R_3 , using its marginal distribution derived in eq. (2) in [129]. The joint PDF of R_2 and R_3 is obtained by integrating (4.48) w.r.t. x from 0 to y . The conditional PDF is obtained by dividing the joint PDF in (4.48) by the marginal distribution in (4.49). The joint PDF $f_{R_1, r_1(\bar{b}k)}^{(MS)}(\cdot, \cdot)$ is obtained by using the null probability of independent PPPs and the marginal distribution in (4.52) is found by integrating (4.51) w.r.t. y from 0 to $x(\frac{\beta_{21} P_2}{P_1})^{1/\eta}$. ■

Coverage Probability

By the law of total probability, we can write the overall coverage probability as

$$\mathcal{C}^{(MS)} = A_{m(\bar{b}k)}^{(MS)} \mathcal{C}_{m(\bar{b}k)}^{(MS)} + A_{f(\bar{b}k)}^{(MS)} \mathcal{C}_{m'(\bar{b}k)}^{(MS)} + A_{bk}^{(MS)} \mathcal{C}_{m,m(bk)}^{(MS)}, \quad (4.53)$$

where $\mathcal{C}_{m(\bar{b}k)}^{(MS)}$ is the coverage probability for the best connected macro user while $\mathcal{C}_{m'(\bar{b}k)}^{(MS)}$ is the coverage probability for the macro user when the strongest femto candidate is disregarded (i.e., $P_2 B_2 r_1^{-\eta} > P_1 B_1 R_1^{-\eta}$). Also, $\mathcal{C}_{m,m(bk)}^{(MS)}$ is the blackout coverage probability as the user skips the nearest macro BS and associates with the second and the third strongest macro BSs. Since the test user skips every other macro BS, the user spends 50% of the time in association with the strongest macro and rest of the time in the blackout phase on average. Consequently, we assume $A_{bk}^{(MS)}$ to be 0.5. Moreover, in the non-blackout case, the user is either in best connected mode (i.e. $P_1 B_1 R_1^{-\eta} > P_2 B_1 r_1^{-\eta}$) or it disregards the strongest femto and associates with the macro BS (i.e. $P_2 B_2 r_1^{-\eta} > P_1 B_1 R_1^{-\eta}$). Thus, $A_{m(\bar{b}k)}^{(MS)}$ is considered to be $0.5 * (1 - A_{f(\bar{b}k)})$, where $A_{f(\bar{b}k)} = A_f^{(BC)}$, which is defined in (4.3). Also, $\mathcal{C}_{m(\bar{b}k)}^{(MS)}$ is the same as the best connected coverage probability for macro association as expressed in BC case (i.e., $\mathcal{C}_m^{(BC)}$). However, $\mathcal{C}_{m'(\bar{b}k)}^{(MS)}$ can be written as

$$\mathcal{C}_{m'(\bar{b}k)}^{(MS)} = \mathbb{P} \left[\frac{P_1 h_1 R_1^{-\eta}}{I_R + I_{r_1} + I_r + \sigma^2} > T \right], \quad (4.54)$$

where I_R is the aggregate interference power from the entire macro tier except $\{b_1\}$ while I_{r_1} is the interference power from the strongest femto BS which lies from 0 to $R_1(\frac{\beta_{21}P_2}{P_1})^{1/\eta}$ and I_r is the aggregate interference power received from all femtos except $\{b_1\}$. The blackout

coverage probability case can be expressed as

$$\mathcal{C}_{m,m(bk)}^{(MS)} = \mathbb{P} \left[\frac{|\sqrt{P_1}h_2R_2^{-\eta/2} + \sqrt{P_1}h_3R_3^{-\eta/2}|^2}{I_{R_1} + I_R + I_r + \sigma^2} > T \right], \quad (4.55)$$

where I_{R_1} is the received interference power from the nearest skipped macro BS while I_R is the aggregate interference power from the whole macro tier except $\{b_1, b_2, b_3\}$. Here, I_r is the aggregate interference power received from the whole femto tier, which exists from 0 to ∞ . We define I_{R_1} and I_R for the blackout case as

$$I_{R_1} = P_1 h_1 R_1^{-\eta} \quad , \quad I_R = \sum_{i \in \phi_1 \setminus \{b_1, b_2, b_3\}} P_1 h_i R_i^{-\eta}.$$

Since $h_i \sim \exp(1)$, the conditional coverage probability for the non-blackout is given by

$$\mathcal{C}_{m(bk)}^{(MS)}(R_1) = \exp \left(\frac{-T}{P_1 R_1^{-\eta}} \right) \mathcal{L}_{I_R} \left(\frac{T}{P_1 R_1^{-\eta}} \right) \mathcal{L}_{I_{r_1}} \left(\frac{T}{P_1 R_1^{-\eta}} \right) \mathcal{L}_{I_r} \left(\frac{T}{P_1 R_1^{-\eta}} \right), \quad (4.56)$$

where the LTs of I_{r_1} and I_r are the same as given in (4.42) and (4.43), respectively, with the only difference that there is no R_2 in this case as the user is connected to one macro BS only. Also, $\mathcal{L}_{I_R}(s)$ is given in (4.9). Using the conditional coverage probability expression and the service distance distribution for the best connectivity associations (i.e., non-blackout), the following theorem is obtained for the coverage probability.

Theorem 12 (Coverage probability in MS case with FD) *The coverage probability for macro association while disregarding the nearest femto BS in the non-blackout case is*

given by (4.57).

$$\begin{aligned} \mathcal{C}_{m(bk)}^{(MS)} = & \int_0^\infty \int_0^{R_1(\frac{\beta_{21}P_2}{P_1})^{1/\eta}} \frac{4\pi^2\lambda_1\lambda_2r_1R_1}{\left(1 + \frac{TP_2r_1^{-\eta}}{P_1R_1^{-\eta}}\right)A_{f(bk)}^{(MS)}} \exp\left(-\pi\lambda_2r_1^2 - \pi\lambda_1R_1^2 - \frac{2\pi T}{(\eta-2)}\left\{\frac{\lambda_2P_2T}{P_1R_1^{-\eta}}r_1^{2-\eta}.\right.\right. \\ & \left.\left._{}_2F_1\left(1, 1 - \frac{2}{\eta}, 2 - \frac{2}{\eta}, \frac{-P_2Tr_1^{-\eta}}{P_1R_1^{-\eta}}\right) + \lambda_1TR_1^2{}_2F_1\left(1, 1 - \frac{2}{\eta}, 2 - \frac{2}{\eta}, -T\right)\right\}\right)dr_1dR_1. \end{aligned} \quad (4.57)$$

Proof. The theorem is proved by substituting the LTs in the conditional coverage probability expression (4.56) and integrating over the service distance distribution found in (4.52). \blacksquare

Since h_i 's are *i.i.d.* $\mathcal{CN}(0,1)$ such that $|x_2h_2 + x_3h_3|^2 \sim \exp\left(\frac{1}{x_2^2+x_3^2}\right)$, we can write the conditional coverage probability for the blackout user as

$$\mathcal{C}_{m,m(bk)}^{(MS)}(R_2, R_3) = \exp\left(\frac{-T\sigma^2}{x_2^2 + x_3^2}\right) \mathcal{L}_{I_{R_1}}\left(\frac{T}{x_2^2 + x_3^2}\right) \mathcal{L}_{I_R}\left(\frac{T}{x_2^2 + x_3^2}\right) \mathcal{L}_{I_r}\left(\frac{T}{x_2^2 + x_3^2}\right), \quad (4.58)$$

where x_i is the same as defined in FD case. Also, note that the LT of I_r in the blackout case is different from the one expressed in FD case. Here, we consider that the femto BSs can exist anywhere from 0 to ∞ . The LTs of the I_{R_1} , I_R and I_r for the blackout mode are expressed in the lemma below.

Lemma 13 (LTs of the interference in MS case) *The LT of I_{R_1} in the blackout mode with cooperative service from the second and third strongest macro BSs is given by*

$$\mathcal{L}_{I_{R_1}}(s) = \int_0^{R_2} \frac{2R_1}{R_2^2(1 + sP_1R_1^{-\eta})} dR_1. \quad (4.59)$$

The LT of I_R in the blackout mode with BS cooperation can be expressed in terms of the

hypergeometric function as

$$\mathcal{L}_{I_R}(s) = \exp \left(\frac{-\pi \lambda_1 s P_1 R_3^{2-\eta}}{\eta - 2} {}_2F_1 \left(1, 1 - \frac{2}{\eta}, 2 - \frac{2}{\eta}, \frac{-s P_1}{R_3^\eta} \right) \right). \quad (4.60)$$

The LT of I_r in the blackout case is given by

$$\mathcal{L}_{I_r}(s) = \exp \left(-2\pi^2 \lambda_2 \frac{(s P_2)^{2/\eta}}{\eta} \csc \left(\frac{2\pi}{\eta} \right) \right). \quad (4.61)$$

Proof. The LT of I_{R_1} is obtained using the same procedure as done for I_{r_1} in (4.42) but considering $s = \frac{T}{P_1(R_2^{-\eta} + R_3^{-\eta})}$, interference region from 0 to R_2 and the conditional distribution obtained in (4.50). The LT of I_R is obtained in the similar way as $\mathcal{L}_{I_R}(s)$ for FD case but with s mentioned above and the interference boundary from R_3 to ∞ . For $\mathcal{L}_{I_r}(s)$, we follow the same procedure as of $\mathcal{L}_{I_R}(s)$ with femto interference limits from 0 to ∞ . ■

The above LTs evaluated at $\eta = 4$ are boiled down to closed form expressions as given by

$$\mathcal{L}_{I_{R_1}}(s)|_{\eta=4} = 1 - \sqrt{\frac{T}{1 + R_2^4 R_3^{-4}}} \arctan \left(\sqrt{\frac{1 + R_2^4 R_3^{-4}}{T}} \right). \quad (4.62)$$

$$\mathcal{L}_{I_R}(s)|_{\eta=4} = \exp \left(-\pi \lambda_1 \sqrt{\frac{T}{R_2^{-4} + R_3^{-4}}} \arctan \left(\sqrt{\frac{T R_2^4}{R_2^4 + R_3^4}} \right) \right). \quad (4.63)$$

$$\begin{aligned} \mathcal{C}_{m,m(bk)}^{(MS)} = & \int_0^\infty \int_{R_2}^\infty 4(\pi\lambda_1)^3 R_2^3 R_3 \int_0^{R_2} \frac{1}{1 + \frac{TR_1^{-\eta}}{R_2^{-\eta} + R_3^{-\eta}}} \frac{2R_1}{R_2^2} dR_1 \exp\left(-\pi\lambda_1 R_3^2 - \frac{\pi\lambda_1 T R_3^{2-\eta}}{(\eta-2)(R_2^{-\eta} + R_3^{-\eta})}\right) \\ & {}_2F_1\left(1, 1 - \frac{2}{\eta}, 2 - \frac{2}{\eta}, -\frac{TR_3^{-\eta}}{R_2^{-\eta} + R_3^{-\eta}}\right) - \frac{2\pi^2\lambda_2}{\eta} \left(\frac{TP_2}{R_2^{-\eta} + R_3^{-\eta}}\right)^{2/\eta} \csc\left(\frac{2\pi}{\eta}\right) dR_3 dR_2 dR_1. \end{aligned} \quad (4.65)$$

$$\mathcal{L}_{I_r}(s)|_{\eta=4} = \exp\left(-\frac{\pi^2\lambda_2}{2} \sqrt{\frac{TP_2}{P_1(R_2^{-4} + R_3^{-4})}}\right). \quad (4.64)$$

Using the service distance distribution and the LTs in Lemmas 12 and 13, we obtain the coverage probability for the MS case as shown in the following theorem.

Theorem 13 (Coverage probability in MS case) *Considering two independent PPPs based two tier downlink cellular network with BS intensity λ_i in a Rayleigh fading environment, the coverage probability for the blackout user in MS case with BS cooperation is given in (4.65).*

Proof. We obtain the coverage probability for the blackout user with cooperation by substituting the LTs found in Lemma 13 in the conditional coverage probability expression given in (4.58) and integrating it over the service distance distribution obtained in Lemma 12. \blacksquare

The coverage probability for the blackout user with interference cancellation capabilities is given by the following theorem.

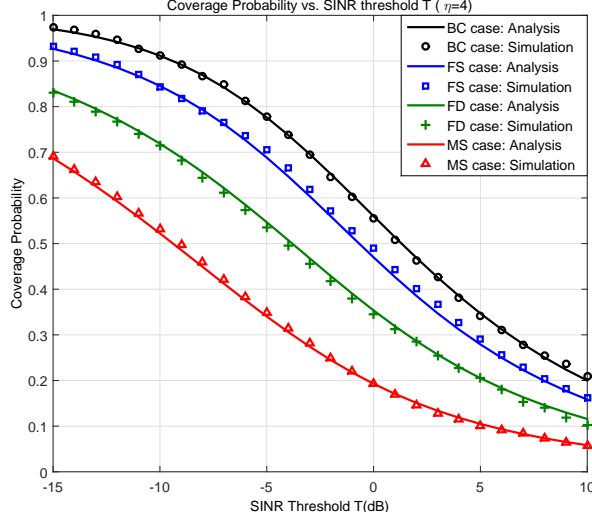
Theorem 14 (Coverage probability in MS case with IC) *Considering two independent PPPs based two tier downlink cellular network with BS intensity λ_i in a Rayleigh fading environment, the coverage probability for blackout users in the MS case with interference*

$$\mathcal{C}_{m,m(bk,IC)}^{(MS)} = \int_0^\infty \int_{R_2}^\infty 4(\pi\lambda_1)^3 R_2^3 R_3 \exp\left(-\pi\lambda_1 R_3^2 - {}_2F_1\left(1, 1 - \frac{2}{\eta}, 2 - \frac{2}{\eta}, -\frac{TR_3^{-\eta}}{R_2^{-\eta} + R_3^{-\eta}}\right)\right) \cdot \\ \frac{\pi\lambda_1 TR_3^{2-\eta}}{(\eta-2)(R_2^{-\eta} + R_3^{-\eta})} - \frac{2\pi^2\lambda_2}{\eta} \left(\frac{TP_2}{R_2^{-\eta} + R_3^{-\eta}}\right)^{2/\eta} \csc\left(\frac{2\pi}{\eta}\right) dR_3 dR_2. \quad (4.66)$$

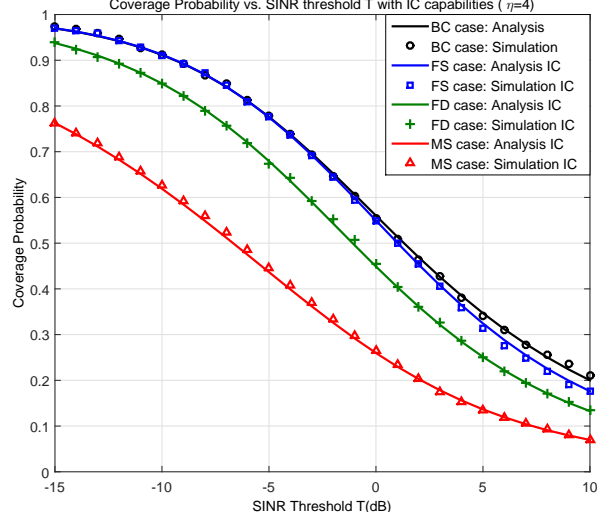
cancellation capabilities is given in (4.66).

Proof. The theorem is obtained using the same methodology for obtaining Theorem 13 but with eliminating I_{R_1} from (4.58). ■

Figures 4.2a and 4.2b show the analysis and simulations for the coverage probabilities for all of the considered HO schemes without and with nearest BS interference cancellation. While the analysis is for stationary PPPs, the simulations in Figures 4.2a and 4.2b account for user mobility. Consequently, the good match between the analysis and simulations validates our model. Figure 4.2a shows the cost of HO skipping from the coverage probability perspective. That is, sacrificing the best SINR connectivity degrades the coverage probabilities even with BS cooperation. Such coverage probability degradation can be mitigated via IC as shown in Figure 4.2b. For instance, employing BS cooperation and IC, the coverage probability for the FS scheme is almost similar to the BS scheme. Although the proposed HO schemes degrade the coverage probability, they offer tangible improvements to the average throughput due to decrease in the the HO rate as shown in the next sections.



(a) Without Interference Cancellation.



(b) With Interference Cancellation.

Figure 4.2: Coverage probability plots for all cases at $\eta = 4$, $\beta_{12} = 0$ dB, transmission power $P_1 = 1$ watt, $P_2 = 0.1P_1$ watt and BS intensities $\lambda_1 = 30$ BS/km², $\lambda_2 = 70$ BS/km².

4.4 Handover Cost

In this section, we encompass user mobility effect and compute handover rates and cost for each HO skipping scheme. We define HO cost D_{HO} as the normalized average time wasted during the execution of HOs. While handover delay is for each handoff, the handover cost averages and normalizes the handover delays over the entire user trajectory. Thus, D_{HO} is the fraction of time where no data (i.e., control only) is transmitted to the test user. Note that the HO cost is different for each HO scheme due to different employed skipping strategies. Let d_{ij} be the delay per i to j handover and H_{ij} be the number of HOs from tier i to j per unit time, then D_{HO} can be expressed as

$$D_{HO} = \sum_i^K \sum_j^K H_{ij} * d_{ij}. \quad (4.67)$$

where K is the number of network tiers, which is 2 in our case. Also, we use d_m and d_f to denote macro-to-macro HO delay and all femto related HO delays, respectively². The HO rate is defined as the number of intersections between the user trajectory and the cell boundaries per unit time. Following [97], the tier i to tier j HO rate is given by

$$H_{ij} = \begin{cases} \frac{v}{\pi} L_{ij} & \text{if } i \neq j, \\ \frac{2v}{\pi} L_{ij} & \text{if } i = j. \end{cases} \quad (4.68)$$

where v is the user velocity and L_{ij} denotes the number of Voronoi cell boundaries between a tier i and tier j BSs per unit length, which is given by

$$L_{ij} = \begin{cases} \frac{\lambda_i \lambda_j F(x_{ij})}{2(\sum_{n=1}^K \lambda_n x_{nk}^2)^{\frac{3}{2}}} + \frac{\lambda_i \lambda_j F(x_{ji})}{2(\sum_{n=1}^K \lambda_n x_{nj}^2)^{\frac{3}{2}}} & \text{if } i \neq j, \\ \frac{\lambda_i^2 F(1)}{2(\sum_{n=1}^K \lambda_n x_{nk}^2)^{\frac{3}{2}}} & \text{if } i = j. \end{cases} \quad (4.69)$$

where $x_{11} = x_{22} = 1$, $x_{12} = (\beta_{12} \frac{P_1}{P_2})^{1/\eta}$, $x_{21} = \frac{1}{x_{12}}$

$$F(x) = \frac{1}{x^2} \int_0^\pi \sqrt{(x^2 + 1) - 2x \cos(\theta)} d\theta. \quad (4.70)$$

In the BC scheme, the user experiences all types of HOs i.e. horizontal and vertical HOs.

Thus, the total HO cost in BC case is given by

$$D_{HO}^{(BC)} = H_{11}d_m + (H_{12} + H_{21} + H_{22})d_f. \quad (4.71)$$

²We assume that $d_m \leq d_f$ because macro BSs usually have high speed dedicated (e.g., fiber-optic) connectivity to the core network. On the other hand, femto BSs may reach the core network via the macro BS through additional backhaul hop or via a shared ADSL/IP connectivity.

In FS scheme, the user skips every other femto BS and associates to all macro BSs. Therefore, the HO rate from femto-to-femto and from macro-to-femto is reduced to half. Thus, we can write D_{HO} for FS case as

$$D_{HO}^{(FS)} = H_{11}d_m + \frac{H_{12} + H_{21} + H_{22}}{2}d_f. \quad (4.72)$$

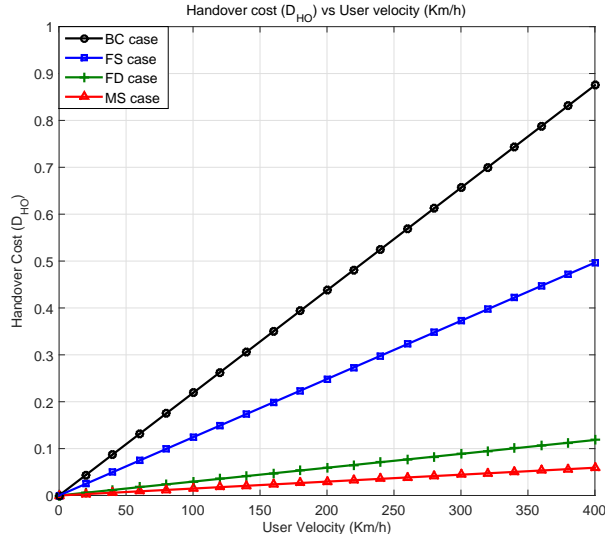
The user in the FD scheme skips all the femto BSs and associate to all macro BSs. Thus, D_{HO} can be written as

$$D_{HO}^{(FD)} = H_{11}d_m. \quad (4.73)$$

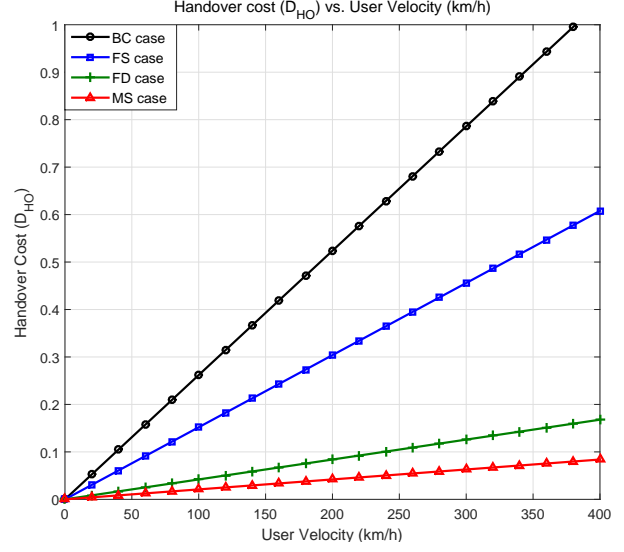
In MS case, the user disregards all femto BSs and skips every other macro BS. That is, the user spends 50% time in macro best connected phase and rest of the 50% in the macro blackout phase. Hence, we can write D_{HO} as

$$D_{HO}^{(MS)} = \frac{H_{11}}{2}d_m. \quad (4.74)$$

Figures 4.3a and 4.3b show the HO cost for each HO skipping strategy with different BS intensities. It can be observed that the HO cost increases with the increase in the user velocity and the BS intensities.



(a) $\lambda_1 = 30, \lambda_2 = 50$ BS/km².



(b) $\lambda_1 = 50, \lambda_2 = 100$ BS/km².

Figure 4.3: Handover cost vs. User velocity (km/h) with $P_1 = 1$ watt, $P_2 = 0.1P_1$ watt, $\beta_{12} = 0$ dB, $d_m = 0.35$ s, $d_f = 2d_m$.

4.5 User Throughput

In this section, we derive an expression for the user throughput, which is applicable to all HO skipping cases. In order to calculate the throughput, we need to omit the HO execution period. Thus the average throughput (AT) can be expressed as

$$AT = WR(1 - D_{HO}). \quad (4.75)$$

where W is the overall bandwidth of the channel and \mathcal{R} is the achievable rate per unit bandwidth (i.e., nats/sec/Hz), which can be expressed as

$$\mathcal{R} = \ln(1 + T)\mathbb{P}[SINR > T]. \quad (4.76)$$

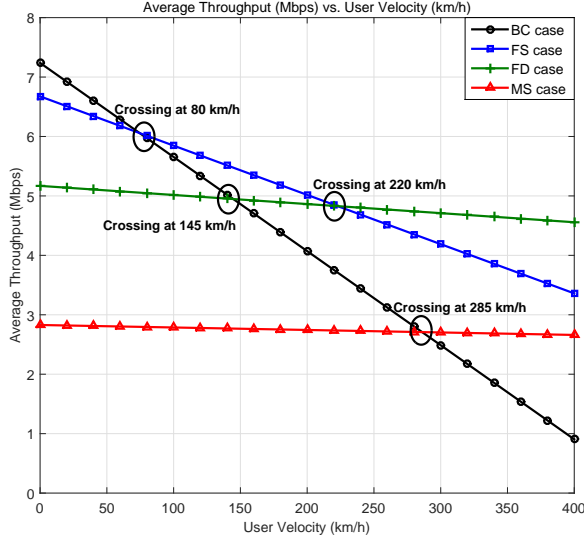
By performing the numerical evaluation for achievable rate per unit bandwidth in each case, we get \mathcal{R} in nats/sec/Hz as shown in Table 4.2.

Table 4.2: Achievable rate for all cases in nats/sec/Hz ($T = 6$ dB, $\beta_{12} = 0$ dB)

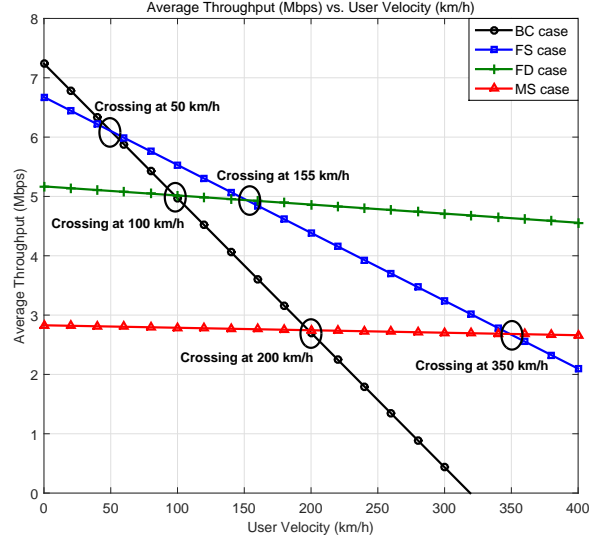
Case	Non-IC	IC
Best Connected $\mathcal{R}^{(BC)}$	0.50	-
Femto Skipping $\mathcal{R}^{(FS)}$	0.40	0.46
Femto Disregard $\mathcal{R}^{(FD)}$	0.29	0.36
Macro Skipping $\mathcal{R}^{(MS)}$	0.15	0.20

4.5.1 Design Insights

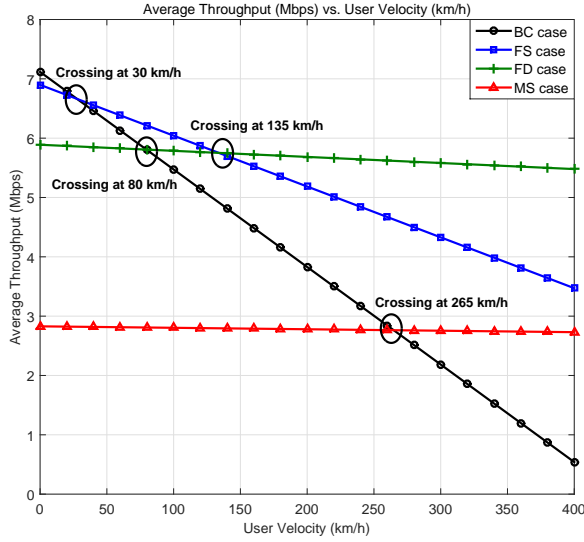
We first study the negative impact of HO on the user's average throughput and highlight the velocity ranges over which the proposed HO schemes outperform the legacy best connected HO strategy. Figure 4.4 shows a linear decay in the user throughput with velocity, which can be mitigated by the proposed HO skipping schemes. Similar performance behavior can be observed for highest SINR association in Figures 4.4a and 4.4b as well as for biased SINR association in Figures 4.4c and 4.4d. Nevertheless, the gains provided by the proposed HO schemes are higher and occur at lower speeds for the case of biased association. This is because small cell edge users intrinsically experience blackout due to biasing, since the interfering macro BS signal is higher than the intended small BS signal. In all cases, the effective velocity ranges for each HO strategy is determined by the intersection points between the average throughput curves. For instance, once the user velocity exceeds 100 km/h, the femto skipping (FS) strategy provides more than 11% gains in the average throughput without biasing and 20% gains with biasing as compared to the best connected associations. Furthermore, the proposed adaptive HO skipping results show up to 77% gains in the average



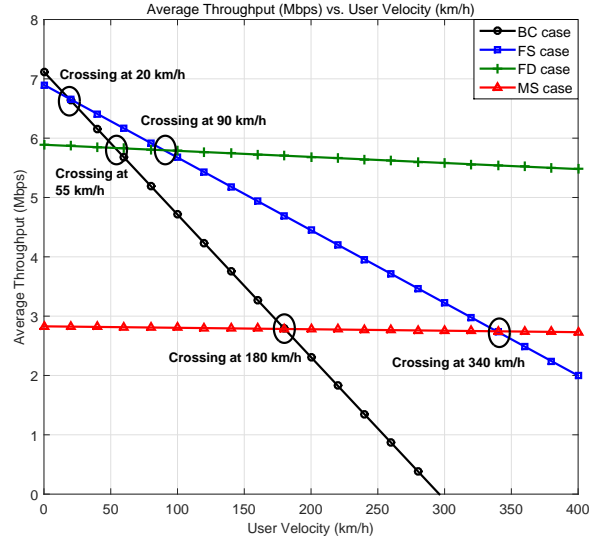
(a) $\beta_{21} = 0$ dB, $d_m = 0.35$ s, $d_f = 2d_m$.



(b) $\beta_{21} = 0$ dB, $d_m = 0.35$ s, $d_f = 3d_m$.



(c) $\beta_{21} = 6$ dB, $d_m = 0.35$ s, $d_f = 2d_m$.



(d) $\beta_{21} = 6$ dB, $d_m = 0.35$ s, $d_f = 3d_m$.

Figure 4.4: Average Throughput (Mbps) vs. User velocity (km/h) with $W = 10$ MHz, $P_1 = 1$ watt, $P_2 = 0.1P_1$ watt, $\lambda_1 = 30$ BS/km², $\lambda_2 = 70$ BS/km², $T = 6$ dB.

throughput as compared to the best connected association for the user velocity ranging from 80 km/h to 200 km/h. However, it is worth noting that the cases FS and FD show gains in the average throughput at medium and high velocity ranges, respectively. Also, we can observe that the skipping of macros in a two tier network outperforms the RSS based association at

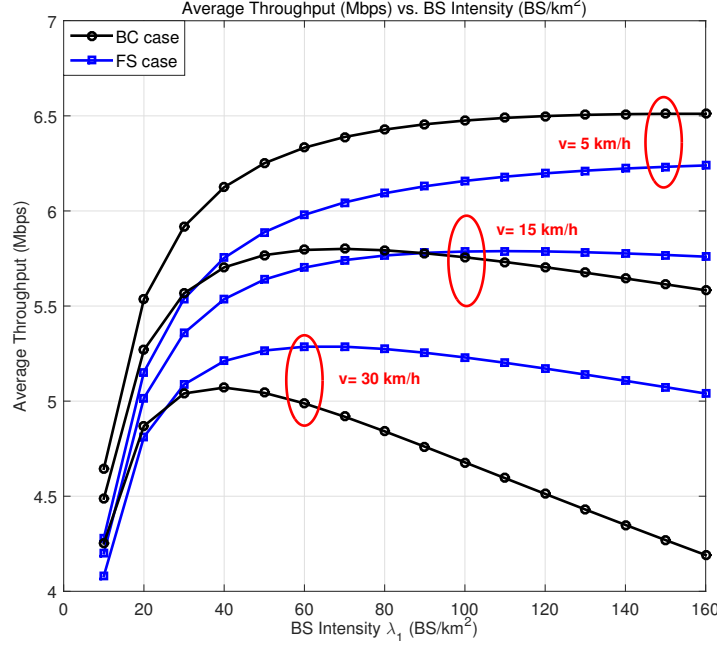


Figure 4.5: Average throughput per user vs. BS intensity with $P_1 = 1$ watt, $P_2 = 0.1P_1$ watt, $\lambda_2 = 2\lambda_1$, $\lambda_u = 10$ user/km², $T = 6$ dB, $\beta_{21} = 0$ dB, $d_m = 0.7$ s, $d_f = 3d_m$.

very high user velocities.

To see the overall gain of network densification, we consider its positive and negative impacts on user throughput. From one side, increasing the BS intensity decreases the number of users associated to each BS, which increases the share each user gets from the BS resources. From the other side, increasing the BS intensity aggravates the handover cost. This tradeoff is highlighted in Figure 4.5 by plotting the average throughput versus the BS intensity. The results in Figure 4.5 are obtained by assuming stationary users modeled via a homogeneous PPP of intensity λ_u , utilizing the model in [35, Corollary 2] to evaluate the average number of users served by each BS, and [135, Equation 12] to calculate the average throughput per user assuming equal sharing among the users (including the test mobile user) for the resources in each BS. The figure shows that there is a turning point at which the handover

cost dominates the performance such that densification degrades the user throughput. The figure also highlights the potential of FS HO strategy to extend the densification gain to higher BS intensities and user velocities. The FS HO scheme is particularly selected for the comparison in Figure 4.5 because it outperforms the other schemes at the considered low user velocity (cf. Figure 4.4).

4.6 Summary

This chapter discusses user velocity aware HO skipping schemes for two tier cellular network to enhance the average rate for mobile users. We develop an analytical paradigm to model the performance of the proposed cooperative HO skipping schemes in order to study the effect of HO delay on the user rate. The developed mathematical model is based on stochastic geometry and is validated via Monte Carlo simulations. The results manifest the negative impact of HO on the users' rate in dense cellular networks and emphasize the potential of the proposed HO schemes to mitigate such negative HO impact. Particularly, the results show up to 77% more rate gains, which can be harvested via the proposed HO schemes when compared to the conventional HO scheme that always maintains the best RSS association. For future work, we will extend our study towards location aware HO skipping. Thus, we will propose HO skipping based on user trajectory, which will maximize the gains while meeting the quality of service requirements.

CHAPTER 5

TOPOLOGY AWARE HANDOVER MANAGEMENT

In this chapter, we exploit topology awareness and user trajectory estimation to propose smart HO skipping schemes in single and two tier downlink cellular networks. The proposed schemes account for the location of the trajectory within the cells and/or the cell-size to take the HO skipping decision. The average performance of the proposed schemes is quantified via extensive simulations considering random BS deployments. More specifically, we consider two network scenarios, namely, a single-tier cellular network abstracted by PPP and a two tier cellular network abstracted by PPP macro BSs overlaid with PCP small BSs. Then we study the impact of HO delay on user throughput in the two network scenarios and show the gains and effectiveness of the proposed schemes by Monte Carlo simulations. The results manifest the HO problem of the always best connectivity scheme at high speeds in dense cellular environments where the cell dwell time approaches HO

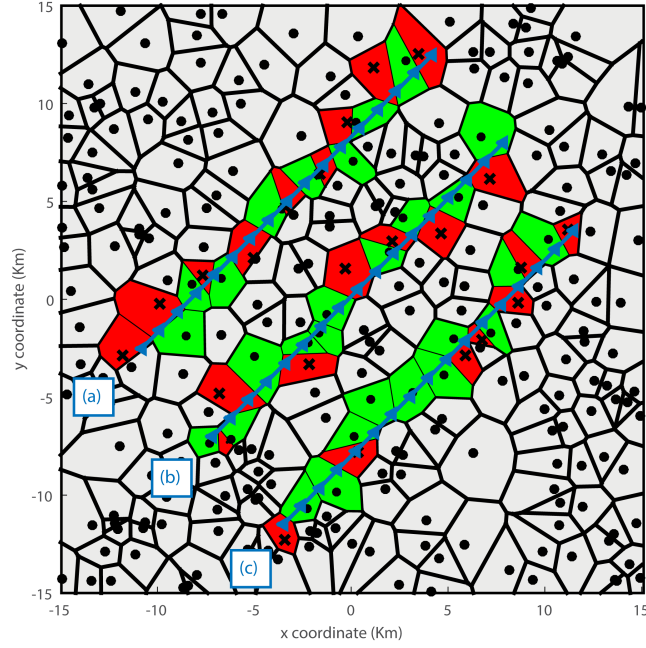


Figure 5.1: Voronoi tessellation of a PPP based single tier cellular network with black circles representing the BSs' locations in 30 km x 30 km grid. (a), (b), and (c) represent alternating, user location aware, and cell-size aware HO skipping schemes, respectively. Blue line represents user trajectory while green and red colors denote serving (circles) and skipped (cross) BSs' coverage areas, respectively.

delay. The user throughput via the proposed skipping schemes outperforms the always best connected scheme at velocities starting from 30 km/h. Particularly, for BSs intensity of 50 BS/km², the proposed schemes show up to 8% more rate gains with respect to (w.r.t.) best connectivity and 23% w.r.t. alternating skipping over the user velocity of 100 km/h, which is the average monorail speed in downtown. More gains are expected at higher BSs intensities, particularly in ultra-dense networks [3]. Finally, several insights into the design of HO skipping and the effective range of velocities for each of the proposed skipping schemes are presented.

HO skipping reduces the frequency at which the HO process is performed by sacrificing some of the best BS connectivity associations. Hence, maintaining longer service durations with the serving BSs and reducing HO delay. For instance, in an RSS based association scheme with universal frequency reuse, HO skipping sacrifices some best signal-to-noise-plus-interference-ratio (SINR) associations along the trajectory. When the user skips the HO to the BS providing the strongest signal, denoted as blackout (BK) phase, the interference from the skipped BS may be overwhelming to the SINR. To improve the SINR during blackout, nearest BS interference cancellation (IC) [125] and non-coherent cooperative BS service via coordinated multipoint (CoMP) transmission [126–128] can be exploited to improve the SINR during blackout.¹ In the cooperative BS service, the user can be jointly served by the serving BS and the next target BS. In addition to IC and CoMP, the performance of the skipping scheme can be further improved by reducing the blackout durations along the users trajectories via smart skipping schemes. Different from the topology agnostic (i.e. alternating skipping) approach proposed in Chapter 3 & 4, this chapter focuses on the following three novel variants of HO skipping. Note that all of the following skipping schemes assume that the trajectory within the target BS footprint is known via some trajectory estimation techniques available in the literature.

Location-Aware HO Skipping

The location aware HO skipping scheme accounts for the shortest distance between the user trajectory and the target BS to decide the HO skipping. That is, the HO skips associating

¹Non-coherent CoMP is used as channel state information is hard to predict at high velocities.

to the target BS if and only if the minimum distance along the user trajectory and the target BS exceeds a pre-defined threshold L . The threshold L can be designed such that the user skips the BSs in which the trajectory passes through the cell edge only. The location aware HO skipping scheme is illustrated in Figure 5.1(scheme b).

Cell-Size Aware HO Skipping

Cell-size aware HO skipping scheme allows users to skip HOs to target BSs that have a footprint (i.e. service area) less than a pre-defined threshold s . Since the cell dwell time depends of the BS footprint size, size aware skipping scheme aims at avoiding large blackout durations. Hence, it allows users to skip small sized cells and associate with large cells. The cell-size aware HO skipping scheme is illustrated in Figure 5.1(scheme c). Note that it is implicitly assumed that the service areas of all BSs are known to the network, which can be inferred from several network planning tools used by cellular operators such as Aircom Asset [142] and Mentum Planet [143]. Such tools take antenna characteristics, BS configuration, terrain and clutter information into account to predict cell-sizes.

Hybrid HO Skipping

Neither the location aware skipping nor the size aware skipping alone accurately reflects the true cell dwell time. Hence, combining both schemes gives a better inference about the cell dwell time, which can improve the HO skipping decisions and performance. Consequently, the hybrid HO skipping scheme combines both location awareness and cell-size awareness to decide which BS to skip. That is, it takes user location and cell area into account while

making the decision for HO.

The challenging aspect of HO skipping is estimating user trajectory, which is highly critical. In some cases, the user trajectory estimation is straight forward i.e. users riding monorails in downtowns. For other cases, it may be complex and several studies including [144, 145] are conducted in the literature on the estimation of mobile user trajectory. Once the cell size information and the user trajectory are known, HO skipping can be triggered based on pre-defined user location and cell size thresholds. Such thresholds are computed offline based on the desired network objective. However, it is worth noting that any error in the estimation of user trajectory may diminish the performance gains shown in this in the results section.

5.1 Handover Skipping in Single Tier Networks

In this section, we consider a single tier downlink cellular network, where the BSs' locations are modeled via a two-dimensional homogenous PPP Φ of intensity λ . It is assumed that all BSs transmit with the same power P . A general path loss model with path loss exponent $\eta > 2$ is assumed. Without loss of generality, we focus on a test mobile user and index all BSs with an ascending order according to their instantaneous distances from the test user. By Slivnyak-Mecke theorem for the PPP [146], the performance of any other user in the network is equivalent to the performance of the test user. Defining R_k as the distance from the test user to the k^{th} BS, then the inequalities ($R_1 < R_2 < R_3 < \dots$) always hold. Channel

Table 5.1: Simulation parameters for PPP based cellular network

Parameter	Value	Parameter	Value
Overall Bandwidth W :	10 MHz	Path loss exponent η :	4
BS intensity λ :	50 BS/km ²	HO delay d :	1 s
Size Threshold s :	$1.28/\lambda$ km ²	Location Threshold L :	$2.3/\lambda$ km
Hybrid Thresholds s, L :	$0.38/\lambda$ km ² , $1.8/\lambda$ km	Tx Power P :	1 watt

gains are assumed to have *i.i.d.* Rayleigh distributions with unit variance i.e. $h \sim \exp(1)$. We consider a universal frequency reuse scheme and study the performance of one frequency channel. We consider user mobility with constant velocity v over an arbitrary long trajectory and assume that a HO is triggered when the user enters the Voronoi cell of the target BS. This implies that $PR_1^{-\eta} > PR_i^{-\eta}$, $\forall i > 1$ is always satisfied. We first analyze the coverage probability for all HO skipping cases and then evaluate the HO cost and average throughput with the simulation parameters shown in Table 5.1.

5.1.1 Coverage Probability

The coverage probability is defined as the probability that the SINR received by the test user exceeds a certain threshold T . The coverage probability for the best connected case is given by

$$\mathcal{C}_{BC} = \mathbb{P} \left\{ \frac{Ph_1R_1^{-\eta}}{\sum_{i \in \Phi \setminus b_1} Ph_iR_i^{-\eta} + \sigma^2} > T \right\} \quad (5.1)$$

where the nearest BS, denoted as b_1 , is removed from the interfering BSs in (5.1) because the serving BS do not contribute to the aggregate interference.

In the blackout case, the test user is not served from the nearest BS due to HO skipping.

Instead, the test user maintains the association with the serving BS (which is not the nearest anymore) or handovers the connection to the next target BS depending on their relative distances during blackout. If CoMP is enabled, then the test user is simultaneously served by both the serving and the next target BSs during the blackout phase. Let R_s and R_t denote the distances from the test user to the serving BS (denoted as b_s) and next target BS (denoted as b_t) during the blackout phase, respectively. Then the coverage probabilities for the blackout case with IC capabilities without and with BS cooperation are given by $\mathcal{C}_{BK(IC)}^{(1)}$ and $\mathcal{C}_{BK(IC)}^{(2)}$, respectively.

$$\mathcal{C}_{BK(IC)}^{(1)} = \mathbb{P} \left\{ \frac{Ph_x \min(R_s, R_t)^{-\eta}}{\sum_{i \in \Phi \setminus \{b_1, b_x\}} Ph_i R_i^{-\eta} + \sigma^2} > T \right\} \quad (5.2)$$

where the subscript $x = s$ if $R_s < R_t$ and $x = t$ otherwise.

$$\mathcal{C}_{BK(IC)}^{(2)} = \mathbb{P} \left\{ \frac{|\sqrt{P}g_x R_s^{-\eta/2} + \sqrt{P}g_t R_t^{-\eta/2}|^2}{\sum_{i \in \Phi \setminus \{b_1, b_s, b_t\}} Ph_i R_i^{-\eta} + \sigma^2} > T \right\} \quad (5.3)$$

where g_x and g_t are zero-mean and unit-variance complex Gaussian channels to reflect the non-coherent CoMP transmission. Note that b_1 in (5.2) and (5.3) is the skipped BS whose signal power is eliminated from the aggregate interference by virtue of IC.

The coverage probability for the best connected scenario given in equation (5.1) is mathematically characterized in [9]. Furthermore, the coverage probability for the HO skipping (i.e. blackout) scenarios given in (5.2) and (5.3) are characterized in equations (3.15) and (3.26), respectively. However, it is highly difficult to conduct tractable analysis for the proposed HO skipping schemes due to the random shape of the Voronoi cell and the ran-

dom location and orientation of the trajectory within the Voronoi cell. Therefore, we show the coverage probabilities for the best connected and HO skipping cases based on Monte Carlo simulations. The simulations in this chapter follow Chapter 3 & 4, where both the mathematical analysis and the simulations are used and validated.

Figures 5.2 and 5.3 show the coverage probability plots for the best connected and HO skipping cases without and with BS cooperation, respectively. As expected, sacrificing the always best connectivity reduces the average coverage probability over the user trajectory. Nevertheless, employing a smart skipping scheme via location and size awareness can mitigate such coverage probability reduction. Furthermore, comparing the results in Figures 5.2 and 5.3 quantifies the contribution of BS cooperation to the coverage probability. Note that the hybrid scheme shown in Figures 5.2 and 5.3 uses more relaxed size and distance constraints than the locations and size aware schemes as shown in Table 5.1. Hence, it is able to have more HO skips with comparable coverage probability to the locations and size aware schemes. Note that the coverage probabilities shown in Figures 5.2 and 5.3 reflect the negative impact only of the HO skipping. The next section incorporates the HO cost into the analysis in order to fairly assess HO skipping.

5.1.2 Handover Cost

This section evaluates the HO cost for the best connected and HO skipping cases. The HO cost \mathcal{D} is defined in terms of the normalized HO delay, which is given by

$$\mathcal{D} = \min(\mathcal{H}_t \times d, 1) \quad (5.4)$$

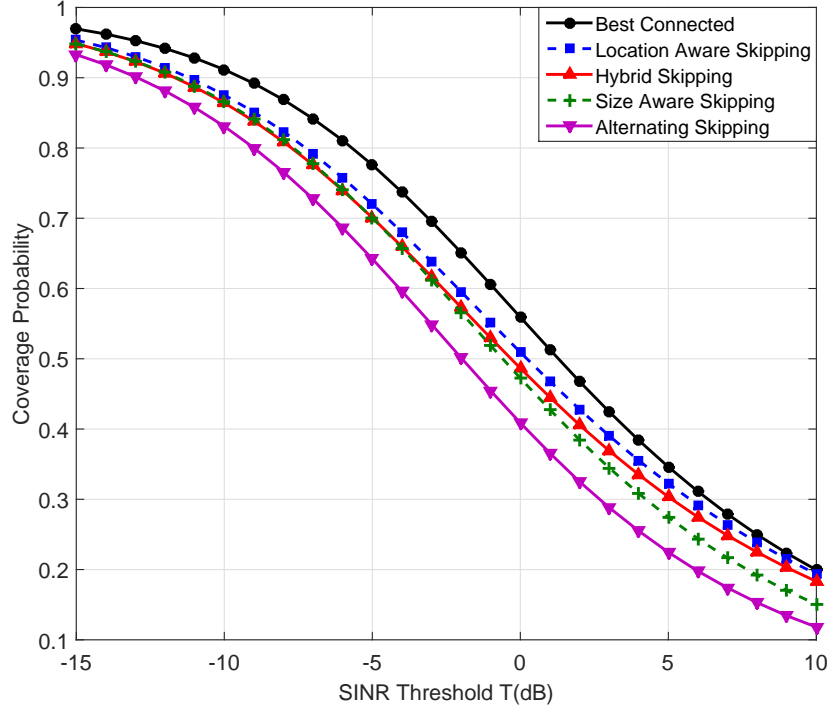


Figure 5.2: Coverage probability vs. SINR threshold for best connected and HO skipping cases.

where \mathcal{H}_t is the handover rate per unit time and d is the delay in seconds per handover. Hence, the handover cost \mathcal{D} is a unit-less quantity used to quantify the fraction of time wasted without useful data transmission along the user trajectory, which is due to handover signaling and radio link switching between serving and target BSs. Note that if $\mathcal{H}_t \times d \geq 1$, this means that the cell dwell time is less than the handover delay. Hence, the entire time is wasted in handover signaling without useful data transmission and \mathcal{D} is set to one.

The HO rate for a PPP based single tier network is characterized in [97] for a generic trajectory and mobility model as

$$\mathcal{H}_t = \frac{4v}{\pi} \sqrt{\lambda} \quad (5.5)$$

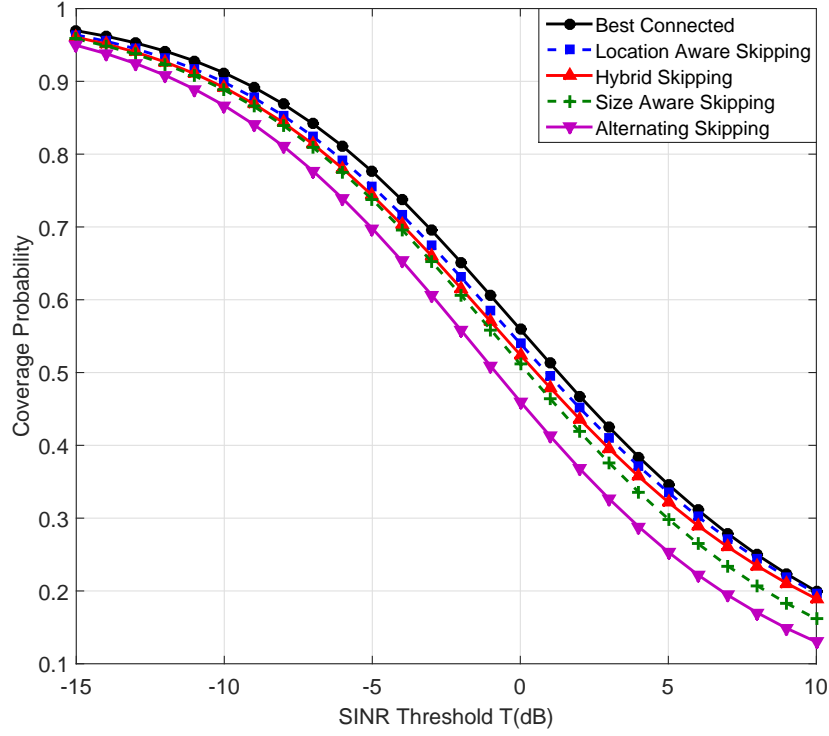


Figure 5.3: Coverage probability vs. SINR threshold for best connected and HO skipping cases with CoMP transmission.

In order to calculate the HO rate via simulations, we first calculate the number of HOs per unit length and then multiply it with the user velocity. The number of handover per unit length is calculated by dividing the number of handovers by the trajectory length. Thus, \mathcal{D} can be expressed as

$$\mathcal{D} = \mathcal{H}_l \times v \times d \quad (5.6)$$

where \mathcal{H}_l is the number of HOs per unit length.

Fig 5.4 depicts the HO cost for the best connected and HO skipping schemes. Since the HO cost depends on the number of HOs, the best connectivity association shows significant

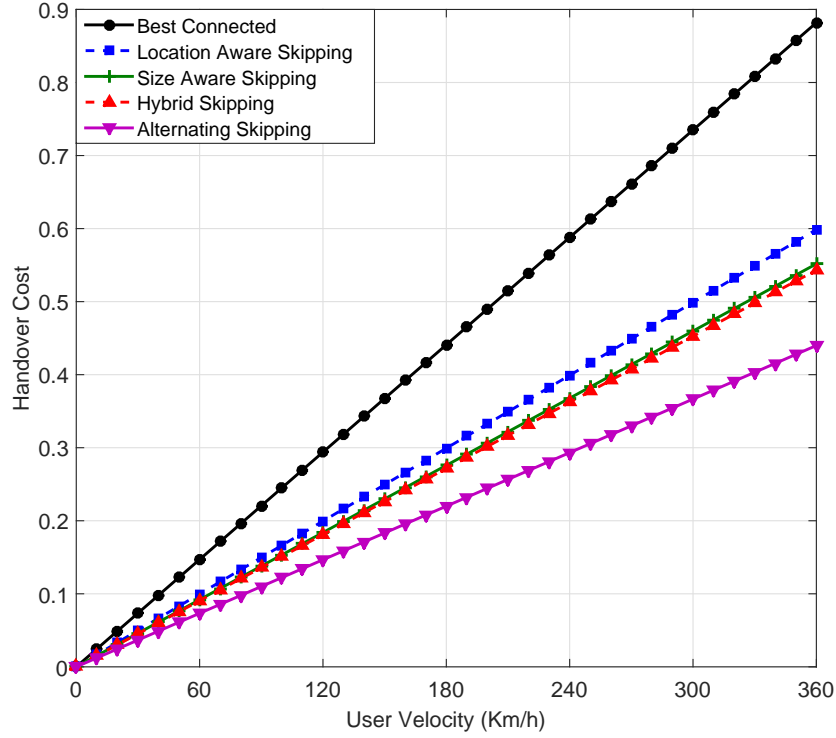


Figure 5.4: Handover cost for conventional and HO skipping cases.

HO cost as compared to the HO skipping strategies. The alternating HO skipping shows the minimal handover cost as it results in the maximum number of HO skips. However, the alternating skipping is topology agnostic and can have inefficient skipping decisions. Such inefficient decisions can be reduced via location and size awareness on the expense of having higher HO cost (cf. Fig 5.4) but better coverage probability (cf. Figures 5.2 and 5.3). While Figures 5.2 and 5.3 focus on the negative impact of the skipping schemes, Fig 5.4 focuses on their positive impact. In the next section, the integrated effect (i.e. both the negative and positive) of the skipping schemes are assessed in the context of user throughput.

5.1.3 Average Throughput

Average throughput is a key performance indicator (KPI) for the cellular operators, which can be used to show the interplay between HO cost and capacity gain imposed by network densification. In this section, we quantify the effect of HO rate, and the impact of each of HO skipping schemes, on the average user throughput. The average throughput, denoted as \mathcal{T} , is defined as:

$$\mathcal{T} = W\mathcal{R}(1 - \mathcal{D}). \quad (5.7)$$

where W denotes the overall bandwidth and \mathcal{R} represents the ergodic spectral efficiency, which is defined by Shannon capacity formula as

$$\mathcal{R} = \mathbb{E}(\ln(1 + \text{SINR})) \quad (5.8)$$

Table 5.2 shows the spectral efficiencies for the best connected and HO skipping cases with and without IC capabilities, which are obtained via simulations using the definition in (5.8). The spectral efficiencies given in Table 5.2 are used to obtain throughput plots via (5.7) as shown in Figure 5.5. The figure clearly shows the HO cost impact on the user throughput when the velocity increases. The figure also shows that the negative impact of the HO could be relieved using the skipping schemes. Particularly, the location aware HO skipping outperforms all other schemes at low velocities i.e. 30 km/h. With the proper adjustment of the hybrid skipping scheme, it outperforms the best connected association at 45 km/h

Table 5.2: Spectral Efficiency for all cases in nats/sec/Hz

Scenario	Non-IC	IC
Best connected (\mathcal{R}_{BC})	1.49	-
Location Aware (\mathcal{R}_{LA})	1.40	1.45
Hybrid (\mathcal{R}_{HB})	1.36	1.42
Size Aware (\mathcal{R}_{SA})	1.21	1.28
Alternating (\mathcal{R}_{AL})	1.02	1.11

and the location aware scheme at 135 km/h. Note that the slope of the hybrid curve is tunable through the cell-size threshold s and the minimum distance threshold L . Size aware HO skipping is the least effective compared to the location aware and hybrid schemes, even though it shows considerable gains as compared to the topology agnostic (i.e. alternating HO skipping) scheme. Note that the size aware scheme is easier to implement than the location aware and hybrid schemes as it does not require complete information about the user trajectory in the target cell. Finally, the alternating HO skipping becomes comparable in performance with other schemes at very high user velocity (beyond 280 km/h) because the HO cost is significant and requires high number of skips to be mitigated. Since the individual HO skipping schemes show gains over different velocity ranges, a dynamic switching among these techniques will maximize the benefit of HO skipping.

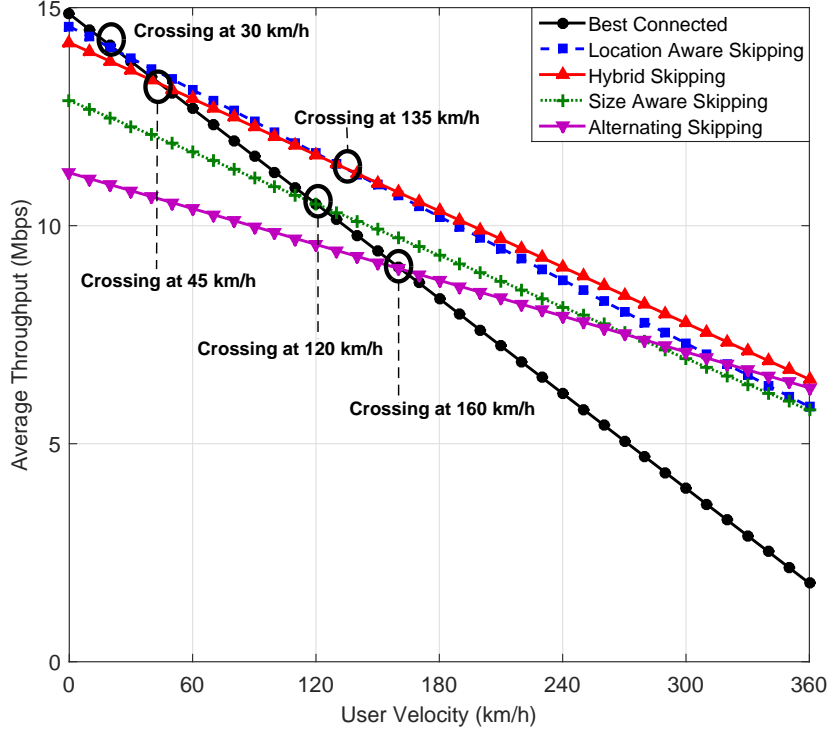


Figure 5.5: Average throughput vs. user velocity for conventional and HO skipping cases.

5.2 Handover Skipping in Two Tier Networks

Current cellular networks are evolving towards a multi-tier architecture in which the macro BSs are overlaid with small BSs to cover traffic hotspots. Since hotspots are usually concentrated around popular/social regions, the small BSs are better modeled via a PCP [27]. The PCP is generated from a parent PPP in which each point in the parent PPP is replaced by multiple cluster points. The distribution of the cluster points around each parent point location determines the type of the PCP. In this work, we consider the Matérn cluster process in which the parent points are generated via a homogenous PPP with intensity λ_p while the daughter points are uniformly distributed within a ball of radius r , where the number of daughter points in each cluster follows poisson distribution with

intensity λ_c . The parent points represent the macro BSs of tier-1 and the daughter points represent small BSs of tier-2 as shown in Figure 5.6. The total intensity of the BSs in the network becomes $\lambda' = \lambda_p \lambda_c + \lambda_p$. It is assumed that the BSs belonging to the i^{th} tier have same transmit power P_i , $i \in \{1, 2\}$ and unity bias factor. A power-law path-loss model with path loss exponent $\eta_i > 2$ is considered. Channel gains are assumed to have *i.i.d.* Rayleigh distributions. Due to the different powers used by the macro and small BSs, the coverage regions in Figure 5.6 are represented via a weighted Voronoi tessellation [134].

For the considered two-tier network, we follow the same methodology in Section 5.1 and study the users throughput to characterize the HO cost and assess the skipping solutions. We conduct our study on a test user moving with velocity v and assume an RSS based association such that the HO is triggered when the user enters the Voronoi cell of the target BS. Motivated by its superior performance when compared to all skipping schemes, this section focuses on the location aware skipping. Particularly, we compare the location aware skipping scheme for different distance thresholds to the always best connected strategy.

To assess the user throughput, we first evaluate the coverage probabilities, spectral efficiencies, and HO costs. Then the average throughput is calculated as in (5.7). Table 5.3 shows the spectral efficiencies for the best connected and location aware HO skipping schemes with distance threshold $L = 0.77/\lambda'$, $2.56/\lambda'$. Figure 5.7 shows the average throughput plots for the best connected and location aware HO skipping cases. It is observed that the location aware HO skipping scheme in a PCP based cellular network outperforms the best connected

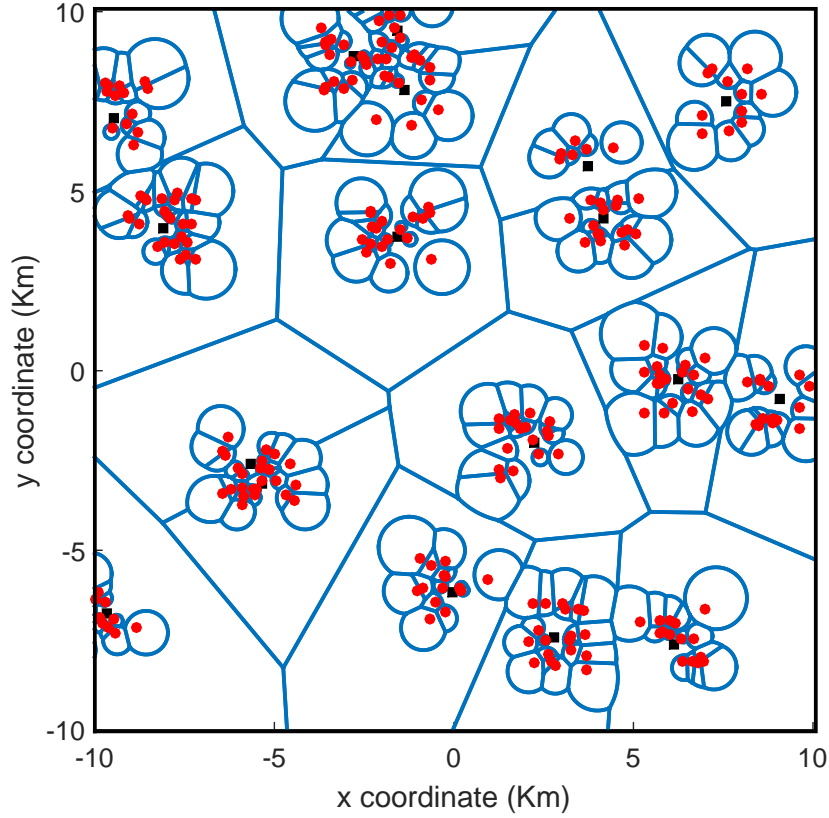


Figure 5.6: Weighted Voronoi tessellation of two tier PCP based downlink cellular network with $\lambda_p = 0.04$ BS/km², $\lambda_c = 1$ BS/km², $P_1 = 1$ watt, $P_2 = 0.5P_1$ watt, $r = 2$ km. Black squares represent macro BSs while red circles denote femto BSs.

association once the user exceeds 40 km/h. The results show up to 47% throughput gains, which can be harvested through proposed smart handover strategy. From Figure 5.7, it is observed that the location awareness with less threshold outperforms location awareness with higher distance threshold once the user exceeds 210 km/h. This is because decreasing the distance threshold L relaxes the skipping constraint and increases the number of skips, which compensates for the excessive HO cost that happens at high mobility. It is worth noting that the considered clustering scheme in this chapter is used for illustrative purposes only, in which similar results and insights apply to other clustering schemes.

Table 5.3: Spectral Efficiency for PCP Network in nats/sec/Hz

Scenario	Non-IC	IC
Best connected (\mathcal{R}_{BC})	1.26	-
Location Aware $L = 2.56/\lambda'$ (\mathcal{R}_{LA})	1.18	1.22
Location Aware $L = 0.77/\lambda'$ (\mathcal{R}_{LA})	1.01	1.08

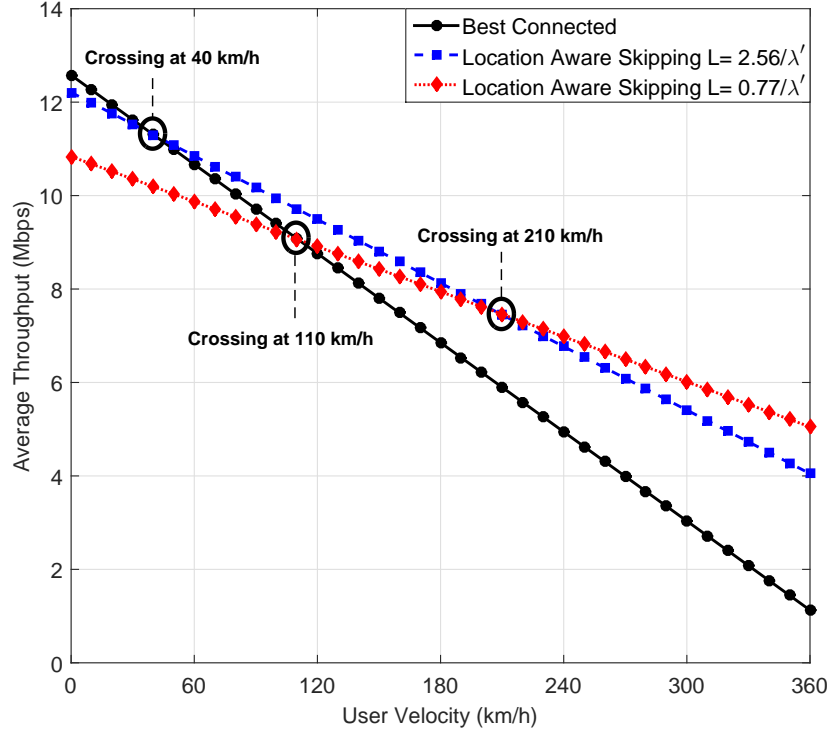


Figure 5.7: Average throughput vs. user velocity for PCP based two tier network with $P_1 = 1$ watt, $P_2 = 0.1$ watt, $\lambda_p = 4$ BS/km², $\lambda_c = 12$ BS/km², $d = 1$ s, $r = 0.6$ km, $\eta_1 = \eta_2 = 4$

5.3 Summary

This chapter sheds light on the negative impact of cellular network densification due to the imposed excessive handover rate. Particularly, the chapter studies the average throughput decay with user velocity in dense cellular environments. To this end, the chapter proposes simple yet effective HO management schemes via topology aware HO skipping. The proposed

schemes take user location and/or cell-size into account to make HO decisions, thus avoiding unnecessary HOs along the user trajectory. The effectiveness of the proposed schemes are validated in two network scenarios, namely, a PPP single tier cellular network and PCP two tier cellular network. When compared to the conventional best RSS based connected strategy, the proposed skipping models show up to 47% gains in the average throughput over the user velocity ranging from 30 km/h to 240 km/h at BS intensity of 50 BS/km². Higher gains are expected at higher BSs intensities.

CHAPTER 6

TWO TIER UPLINK CELLULAR NETWORKS

This chapter studies the mobility aware user-to-BS association policies, within a stochastic geometry framework, in two tier uplink cellular networks with fractional channel inversion power control. Particularly, we model the base stations' (BSs) locations using the widely accepted poisson point process (PPP) and obtain the coverage probability and handover (HO) cost expressions for the coupled and decoupled uplink and downlink associations. To this end, we compute the network throughput for the mobile users and study the merits and demerits of each association strategy.

6.1 Introduction

Heterogeneity and spectrum sharing are fundamentals of the current and future cellular networks. In heterogenous and interference limited networks, efficient user to BS association is

crucial to maximally utilize the deployed small BSs. For instance, downlink range expansion, that sacrifices the best received signal strength is proposed in [147] to avoid overloading macro BSs while under-utilizing the small BSs. The best serving BS from the uplink and downlink perspective may be different, which motivated the concept of downlink uplink decoupled (DUDe) association. The authors in [148] studied DUDe architecture where the users see the heterogeneous network as a homogeneous single tier network in the uplink to guarantee the nearest BS association in the uplink while keeping the conventional received signal strength (RSS) association in the downlink. This decoupled association policy increases the percentage of users achieving the desired average throughput but does not guarantee the gains in the overall network level performance metrics. Furthermore, the performance gains might be different for mobile users experiencing handovers (HO) along their trajectories. Therefore, a thorough study incorporating user mobility is required to benchmark the performance of different association scenarios.

Performance analysis in uplink cellular networks is a focal research point in the context of cellular network. Therefore, the uplink cellular networks are extensively studied in the literature. For instance, the authors in [29] characterized the uplink coverage probability expression for a single tier network with the fractional channel inversion power control. Joint uplink-downlink rate coverage is studied in [30] for optimally coupled and decoupled multi-tier cellular networks. The authors in [149] studied the uplink spectral efficiency in two tier cellular network with minimum path-loss BS association. However, none of the aforementioned studies considered user mobility in the rate analysis. And, the mobility-

aware uplink analysis still entails to be presented to have a sheer uplink analysis. To the best of our knowledge, no such study exists on the uplink analysis which incorporates the HO effect in to the rate analysis for uplink-downlink coupled¹ and decoupled associations.

This chapter utilizes the tools from stochastic geometry to characterize the uplink coverage probability and network throughput expressions in two tier coupled (conventional RSS) and decoupled cellular architectures with fractional channel inversion power control. The performance gains highlight the significance of each association strategy in different practical scenarios. For instance, the DUDe offers more rate gains as compared to RSS in case of stationary users. However, the RSS outperforms the DUDe, if user mobility and its corresponding HO delay is considered in the analysis.

6.2 System Model

We consider two tier cellular network where the BSs belonging to each tier are modeled via an independent homogenous poisson point process (PPP) Φ_k with intensity λ_k and transmission power P_k , where $k \in \{1, 2\}$. We denote macro and femto BSs by $k = 1$ and $k = 2$, respectively. A power-law path-loss model with path-loss exponent $\eta_k > 2$ is considered. For simplicity, we consider same path loss exponents for both tiers. However, the extension with different path-loss exponents is straight forward, but comes at the expense of more involved expressions. Channel gains are assumed to have Rayleigh distribution with unit power i.e. $h \sim \exp(1)$. Mobile users u are distributed via a homogeneous PPP Ψ with intensity λ_u . It

¹In the coupled architecture, the uplink association follows the downlink association, which is based on the maximum RSS in the downlink.

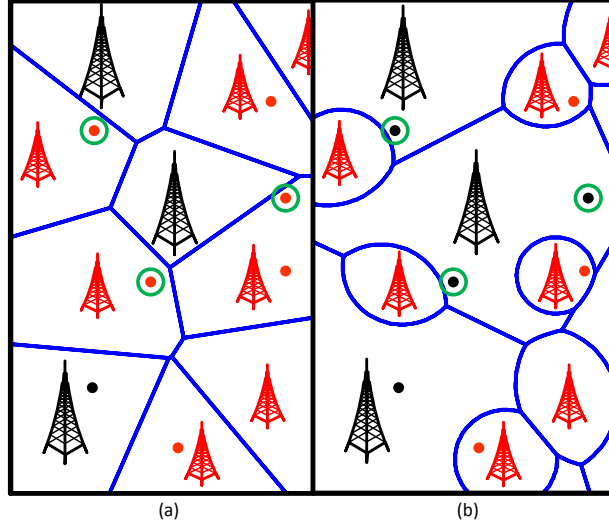


Figure 6.1: User-to-BS associations for (a) DUDe and (b) RSS based policies modeled via weighted Voronoi tessellation. Macro and femto BSs/users are represented by black and red colors, respectively. Green circles show the disparity in user-to-BS associations in RSS and DUDe architecture.

is assumed that there is at most one active user in each BS's service area that transmits over a fixed frequency channel to guarantee that there is no intra-cell interference. Mobile users transmit with the fractional power control of the form $P_u x^{\eta\epsilon}$, where P_u is the power limiting parameter and $\epsilon \in \{0, 1\}$ is the power control factor (PCF). The cell boundaries in each association scenario can be visualized via a weighted Voronoi tessellation (cf. Figure 6.1). Let $u_0 \in \tilde{\Psi}$ be a randomly selected active user, then the uplink user-to-BS association policies in the RSS and DUDe architectures are defined by $b_r = \arg \max_{b \in \Phi} P_k \|u_0 - b\|^{-\eta}$ and $b_d = \arg \min_{b \in \Phi} \|u_0 - b\|$, respectively, where $\|\cdot\|$ denotes the Euclidean norm.

6.3 Stationary Analysis

In this section, we characterize the user transmission power distribution, service distance distribution, and coverage probability based on the stationary PPP analysis. However, we incorporate user mobility in the simulations and verify the accuracy of the stationary coverage analysis. This implies that averaging over all users' trajectories in all network realizations is equivalent to averaging over all users' locations in all network realizations. The user transmission power distribution is given by the following lemma.

Lemma 14 (Transmission Power Distribution) *The distribution of the power P_i transmitted by the i^{th} user at the distance $r_i \in \Phi$ from the test BS is given by*

$$f_{P_i}(z|r_i) = \frac{2\pi\lambda_t z^{\frac{2}{\epsilon\eta}-1} e^{-\pi\lambda_t \left(\frac{z}{P_u}\right)^{2/\eta}}}{\epsilon\eta P_u^{2/\epsilon\eta} \gamma(1, -\pi\lambda_t r^2)}; \quad 0 \leq z \leq P_u r_i^{\epsilon\eta} \quad (6.1)$$

where $\gamma(a, b) = \int_0^b t^{a-1} e^{-t} dt$ is the lower incomplete gamma function and λ_t is the total intensity given by

$$\lambda_t = \begin{cases} \lambda_1 P_1^{2/\eta} + \lambda_2 P_2^{2/\eta}, & \text{for RSS} \\ \Lambda, & \text{for DUDe} \end{cases}$$

Proof. We evaluate the truncated power distribution $f_{P_i}(z|r_i)$ using the service distance distribution $f_r(x) = 2\pi\lambda_t x e^{-\pi\lambda_t x^2}$, evaluated using the null probability of PPP and the transmit power of a generic user equipment given by $P = P_u x^{\epsilon\eta}$. The total intensity in the DUDe architecture is calculated by the fact that the test user sees the heterogeneous network as a homogenous network with intensity $\Lambda = \lambda_1 + \lambda_2$. For the total intensity in the RSS architec-

ture, we exploit the mapping theorem [8, Theorem 2.34] and follow Lemma 7 and map the two dimensional PPPs into an equivalent one dimensional non-homogenous PPP with the resultant intensity $\lambda_t = \lambda_1 P_1^{2/\eta} + \lambda_2 P_2^{2/\eta}$. ■

Despite that Φ_k are two independent PPPs, the users point process Ψ is not a PPP. However, for tractability, we follow [150] and approximate the aggregate interference seen at the test BS with the interference seen from a non-homogeneous PPP with the intensity function $\lambda(x) = \lambda(1 - e^{-\pi\lambda x^2})$. In order to capture the interference received from the active users only, we take tier association load factors into account. The reason is, there might exist some BSs, which are not serving any users. Thus considering interference from inactive users lying under the footprints of such BSs would overestimate the aggregate interference. Finally, the resultant interference field seen from the test BS perspective can be modeled as a non-homogeneous PPP with the intensity function $\lambda(x) = \rho\lambda(1 - e^{-\pi\rho\lambda x^2})$, where ρ is the tier load factor, which is the probability of having user-to-BS association in a particular tier.

Lemma 15 (User Intensity Function) *Let $\tilde{\Psi} \in \mathbb{R}^+$ be a PPP with the intensity function $\tilde{\lambda}(w)$, which is given by*

$$\tilde{\lambda}(w) = \frac{2\pi^{1-\epsilon}\lambda'_t P_u^{2/\eta}}{\eta w^{1-\frac{2}{\eta}}\lambda_t^\epsilon} \int_0^{\pi\lambda_t(P_u w)^{\frac{2}{\eta(1-\epsilon)}}} y^\epsilon e^{-y} \frac{\gamma\left(1, \pi^{1-\epsilon}\lambda'_t(P_u w)^{2/\eta}\left(\frac{y}{\lambda_t}\right)^\epsilon\right)}{\gamma\left(1, (\pi\lambda_t)^{1-\epsilon}(P_u w)^{2/\eta}y^\epsilon\right)} dy \quad (6.2)$$

where λ'_t is the total intensity weighted by the individual tier load factors and given by

$$\lambda'_t = \begin{cases} \rho_1\lambda_1 P_1^{2/\eta} + \rho_2\lambda_2 P_2^{2/\eta}, & \text{for RSS} \\ \rho\Lambda, & \text{for DUDe} \end{cases}$$

Proof. The lemma is followed by using the Mapping theorem with the mapping function given by $w_i = \|x_i\|^\eta$ and the Displacement theorem [8, Theorem 2.33] with the PDF given by (6.1). Thus the resulting intensity after mapping and displacement can be obtained as

$$\tilde{\lambda}(w) = \int_0^\infty \zeta(r, w) \lambda(r) dr \quad (6.3)$$

where $\zeta(r, w)$ is the displacement kernel given by

$$\zeta(r, w) = \frac{r}{w^2} f_{P_i} \left(\frac{r}{w}, r^{1/\eta} \right) \quad (6.4)$$

The load factors ρ , ρ_1 , and ρ_2 are obtained by first writing the probability of having n number of users in a cell with cell size A given by $P_A(n) = \frac{(\lambda_u A)^n}{n!} e^{-\lambda_u A}$, solving it for $n \neq 0$ and then integrating it over the distribution of A , given in [151, equations 2, 10, & 11, resp.]. ■

Corollary 5 (Intensity Function with Full Load) For the special case of fully loaded network ($\rho = \rho_1 = \rho_2 = 1$), the intensity function $\tilde{\lambda}(w)$ boils down to a simpler expression given by

$$\tilde{\lambda}(w) = \frac{2(\pi\lambda_t)^{1-\epsilon} P_u^{2/\eta}}{\eta w^{1-\frac{2}{\eta}}} \gamma \left(1 + \epsilon, \pi\lambda_t (P_u w)^{\frac{2}{\eta(1-\epsilon)}} \right) \quad (6.5)$$

6.3.1 Coverage Probability

In this section, we obtain the uplink coverage probability expression in the RSS and DUDe association scenarios. The coverage probability with the fractional power control can be

represented as

$$\mathcal{C} = \mathbb{P} \left[\frac{P_u h r^{\eta(\epsilon-1)}}{I_{agg} + \sigma^2} > T \right]. \quad (6.6)$$

where $I_{agg} = \sum_{w_i \in \phi} h_i w_i^{-1}$ is the aggregate interference seen from the active users followed by the mapping theorem and σ^2 is the noise power. We exploit the exponential distribution of h and the service distance distribution to write the general coverage probability expression, which is valid for both RSS and DUDe association scenarios. However, the disparity comes in the total intensity (i.e. λ_t) and its corresponding functions.

Theorem 15 (Coverage Probability) *The uplink coverage probability in the DUDe and RSS associations based two tier cellular networks with fractional channel inversion power control is given by (6.7).*

$$\mathcal{C} = 2\pi\lambda_t \int_0^\infty r \exp \left(-\pi\lambda_t r^2 - \int_{\mathbf{1}\{\epsilon=1\}}^\infty \frac{2\pi^{1-\epsilon} \lambda'_t P_u^{2/\eta}}{\eta w^{1-\frac{2}{\eta}} \lambda_t^\epsilon \left(1 + \frac{P_u w}{T r^{\eta(1-\epsilon)}}\right)} \int_0^{\pi\lambda_t (P_u w)^{\frac{2}{\eta(1-\epsilon)}}} y^\epsilon e^{-y} \cdot \frac{\gamma \left(1, \pi^{1-\epsilon} \lambda'_t (P_u w)^{2/\eta} \left(\frac{y}{\lambda_t}\right)^\epsilon\right)}{\gamma \left(1, (\pi\lambda_t)^{1-\epsilon} (P_u w)^{2/\eta} y^\epsilon\right)} dy dw \right) dr. \quad (6.7)$$

Proof. *The coverage probability expression is obtained by first writing the conditional coverage probability conditioned on the serving BS distance and then applying the probability generating functional (PGFL) for PPP [8] with the intensity function given in (6.2) and integrating it over the service distance distribution given by $f_r(x) = 2\pi\lambda_t x e^{-\pi\lambda_t x^2}$. ■*

Corollary 6 (Coverage Prob. with Full Load) *The uplink coverage probability in a fully loaded network can be expressed in the terms of Gauss hypergeometric function*

${}_2F_1(\cdot, \cdot, \cdot, \cdot)$ as

$$\mathcal{C} = \exp \left(-2P_u^{2/\eta} T {}_2F_1 \left(1, 1 - \frac{2}{\eta}, 2 - \frac{2}{\eta}, -\frac{T}{P_u} \right) \right) \quad (6.8)$$

For the special case at $\eta = 4$ and full channel inversion power control $\epsilon = 1$, the uplink coverage probability in a fully loaded network boils down to a simpler expression given by

$$\mathcal{C} = \exp \left(-\sqrt{T} \arctan \left(\sqrt{\frac{T}{P_u}} \right) \right) \quad (6.9)$$

6.3.2 Network Throughput

In this section, we characterize the network throughput per unit area ($1 \times 1 \text{ km}^2$) for stationary users. We focus on the application throughput, which requires the elimination of the HO delay incurred during HOs execution. Thus the network throughput per unit area is given by

$$\mathcal{NT} = \rho_L W \mathcal{R}. \quad (6.10)$$

where ρ_L is the load factor ($\rho_L = \rho_1 \lambda_1 + \rho_2 \lambda_2$ for RSS and $\rho_L = \rho \Lambda$ for DUDe), W is the overall bandwidth of the channel, and \mathcal{R} is the achievable rate per unit bandwidth (i.e., nats/sec/Hz), which can be expressed as a function of coverage probability given by $\mathcal{R} = \ln(1 + T^*) \mathbb{P}[SINR > T^*]$, where T^* is the optimum value of the coverage threshold that maximizes the achievable rate, which is found numerically and is mathematically expressed as $T^* = \arg \max_T \mathcal{R}(T)$. Figures 6.2a and 6.2b show the achievable rate \mathcal{R} in RSS and DUDe

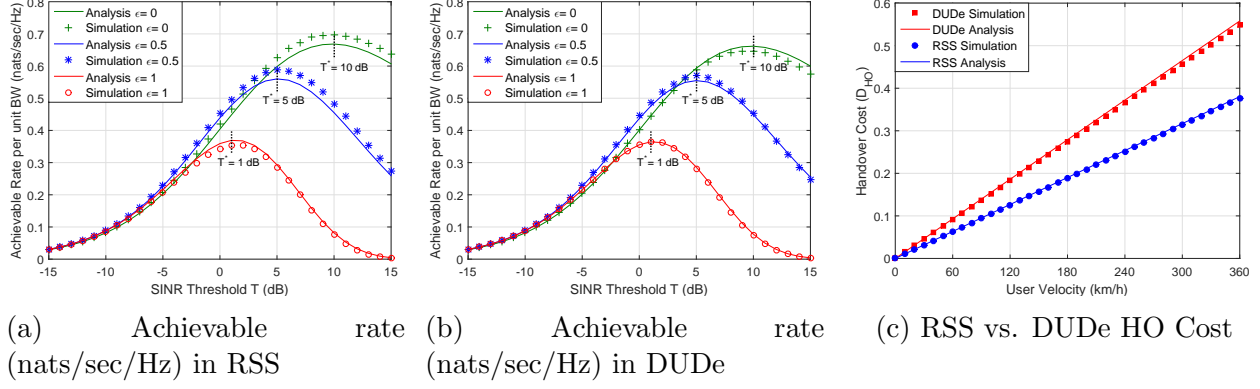


Figure 6.2: Achievable rate per unit bandwidth (nats/sec/Hz) and HO cost in RSS and DUDe architectures

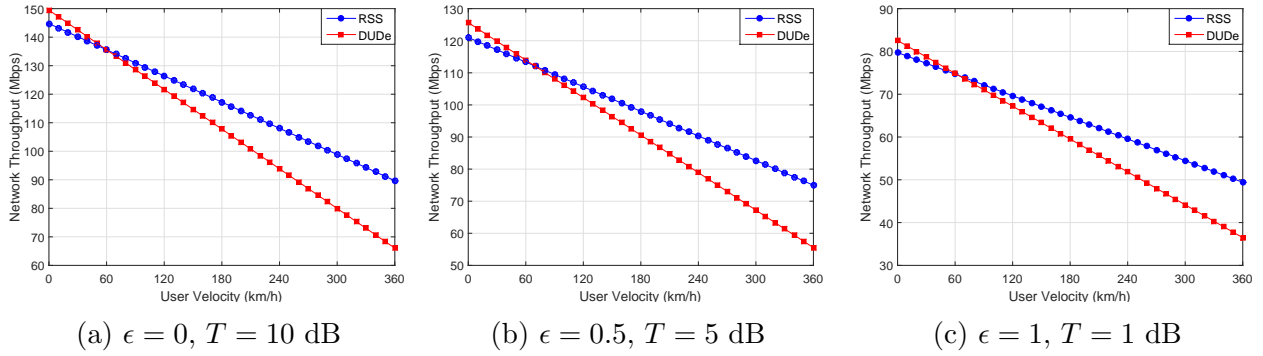


Figure 6.3: Network Throughput (Mbps) per unit area plots with RSS and DUDe associations

association scenarios, respectively, with the simulation parameters given in Table 6.1. It is noticed that the simulation results conform with the mathematical analysis.

6.4 User Mobility Analysis

In this section, we incorporate user mobility and handover rates in the network rate analysis. We perform our analysis on mobile users moving with velocity v along arbitrary long trajectories. It is assumed that a HO is performed when the user crosses the Voronoi cell boundary. While the cell boundaries are defined according to the association rule (c.f. Fig-

Table 6.1: Simulation parameters

Parameter	Value	Parameter	Value
Macros Power P_1 :	10 watt	Femtos Power P_2 :	$P_1/6$ watt
Macros intensity λ_1 :	3 BS/km ²	Femtos intensity λ_2 :	15 BS/km ²
Users intensity λ_u :	50 BS/km ²	PCF ϵ :	0, 0.5, 1
User Power factor P_u :	1	Path-loss exponent η :	4
Channel BW W :	10 MHz	HO delay d :	0.7 s

ure 6.1). By assuming all active users moving with the same velocity, we can write the network throughput as

$$\mathcal{NT}^{(m)} = \rho_L W \mathcal{R} (1 - D_{HO}). \quad (6.11)$$

where D_{HO} is the time wasted in HO per unit time. It is a function of overall HO rate \mathcal{H} and delay per HO d and is given by

$$D_{HO} = \mathcal{H} * d. \quad (6.12)$$

HO rates with RSS association policy are given in equation 4.68 for multi-tier PPP based cellular networks. In the RSS architecture, the overall HO rate \mathcal{H} is obtained by the summation of all inter and intra tier HOs. While the uplink and downlink HOs are performed simultaneously. In decoupled architecture, the user may perform downlink HO followed by the uplink HO. Thus the overall HO rate in this case would be the summation of the downlink and uplink HOs per unit time. Since, in DUDe, the uplink association is based on the user-to-BS distance, we can substitute $P_1 = P_2$ in (4.68) to obtain the uplink HO rate in

the decoupled architecture. Here, we assume that the useful data transmission in the DUDe architecture gets disrupted with each downlink and uplink HO, which are either executed simultaneously or one followed by another. Based on the said assumption, the total HO rate in DUDe architecture is given by

$$\mathcal{H}^{DUDe} = \mathcal{H}^{DL} + \mathcal{H}^{UL} - H_{11}^{UL} - H_{22}^{DL} \quad (6.13)$$

where (6.13) is followed by the fact that for each macro-macro uplink HO, downlink HO is triggered at the same instance. Similarly, femto-femto uplink HO is triggered with each femto-femto downlink HO. Therefore, H_{11}^{UL} and H_{22}^{DL} are eliminated from the overall HO rate to avoid duplicity in the HO count. Figure 6.2c shows the HO cost in the RSS and DUDe association scenarios using the parameters given in Table 6.1. From the Figure 6.2c, it is observed that the mathematical analysis conforms with the monte-carlo simulations. Moreover, it is worth noting that the DUDe association shows high HO cost as compared to the conventional RSS association. While the cost increases with the increase in the user velocity.

6.5 Design Insights

From the Figure 6.3, it is observed that the RSS association outperforms the DUDe association once the user exceeds 60 km/h and shows higher performance gains at higher user velocity. Particularly, the RSS association policy offers up to 35% gains in the network throughput as compared to the DUDe association. The user-velocity aware dynamic switch

between the two association schemes will help to achieve the desired capacity improvements foreseen through heterogeneity.

6.6 Summary

In this chapter, we exploit stochastic geometry tools to analyze the effect of user mobility in the uplink rate analysis with different user-to-BS association scenarios. The developed mathematical model is validated via Monte Carlo simulations. The analysis and the simulation results clearly reflect the significance of the conventional RSS association over DUDe in the uplink due to minimal HO cost at high user velocity.

CHAPTER 7

CONCLUSIONS & FUTURE WORK

This work exploits the tools from stochastic geometry to investigate the effect of HO rate on the user throughput in downlink and uplink cellular networks. In order to mitigate the HO effect in downlink cellular network, several HO skipping techniques are proposed, which outperform the conventional best connectivity association at certain velocities. With proposed HO skipping schemes, we can achieve up to 77% rate gains as compared to the best connected association. For uplink cellular networks, we consider different user-to-BS association scenarios and study the HO effect on the network throughput. The mathematical expressions are obtained using stochastic geometry framework and are validated by monte-carlo simulations.

Since the future networks involve more heterogeneity and disparity in BSs transmit power, the future work may include the extension from two tier to k -tier networks. Since traffic management and efficient resource handling has always been a major concern of cellular operators, future work may also consider BS congestion into account while making HO

decisions.

Appendices

A. Proof of Lemma 2

The Laplace transform of I_r is given by

$$\begin{aligned}\mathcal{L}_{I_r}(s) &= \mathbb{E}\{e^{-sI_r}\} \\ &= \mathbb{E}\left\{e^{-s\sum_{i\in\phi\setminus b_0,b_1} P_i h_i R_i^{-\eta}}\right\}\end{aligned}\tag{7.1}$$

Due to the independence between fading and BSs location, we get:

$$\begin{aligned}\mathcal{L}_{I_r}(s) &= \mathbb{E}_\phi\left\{\prod_{i\in\phi\setminus b_0,b_1} \mathbb{E}_{h_i}\{e^{-sP_i h_i R_i^{-\eta}}\}\right\} \\ &= \mathbb{E}_\phi\left\{\prod_{i\in\phi\setminus b_0,b_1} \mathcal{L}_{h_i}(sP_i R_i^{-\eta})\right\}\end{aligned}\tag{7.2}$$

But since $h_i \sim \exp(1)$, we can write

$$\mathcal{L}_{I_r}(s) = \mathbb{E}_\phi\left\{\prod_{i\in\phi\setminus b_0,b_1} \frac{1}{1 + sP_i R_i^{-\eta}}\right\}\tag{7.3}$$

Assuming $P_i = P, \forall i$ and using probability generating functional (PGFL) for PPP [146], we

get

$$\begin{aligned}
\mathcal{L}_{I_r}(s) &= \exp \left(-2\pi\lambda \int_{r_0}^{\infty} \left(1 - \frac{1}{1 + sPv^{-\eta}}\right) v dv \right) \\
&= \exp \left(-2\pi\lambda \int_{r_0}^{\infty} \frac{1}{\frac{1}{Tr_0^\eta v^{-\eta}} + 1} v dv \right)
\end{aligned} \tag{7.4}$$

By change of variables $w = \left(\frac{v}{T^{1/\eta} r_0} \right)^2$ and substituting $s = \frac{Tr_0^\eta}{P}$, we get

$$\begin{aligned}
\mathcal{L}_{I_r} \left(\frac{Tr_0^\eta}{P} \right) &= \exp \left(-\pi\lambda r_0^2 T^{2/\eta} \int_{T^{-2/\eta}}^{\infty} \frac{1}{1 + w^{\eta/2}} dw \right) \\
&= \exp \left(-\pi\lambda r_0^2 \vartheta(T, \eta) \right)
\end{aligned} \tag{7.5}$$

where

$$\vartheta(T, \eta) = T^{2/\eta} \int_{T^{-2/\eta}}^{\infty} \frac{1}{1 + w^{\eta/2}} dw \tag{7.6}$$

Laplace transform of I_1 can be expressed as

$$\begin{aligned}
\mathcal{L}_{I_1}(s) &= \mathbb{E} \{ e^{-sI_1} \} \\
&= \mathbb{E} \{ e^{-sPhr_1^{-\eta}} \} \\
&= \mathbb{E}_{r_1} \{ \mathbb{E}_h [e^{-sPhr_1^{-\eta}}] \} \\
&= \mathbb{E}_{r_1} \{ \mathcal{L}_h(sPr_1^{-\eta}) \}
\end{aligned} \tag{7.7}$$

But since $h \sim \exp(1)$, we get

$$\begin{aligned}\mathcal{L}_{I_1}(s) &= \mathbb{E}_{r_1} \left\{ \frac{1}{1 + sPr^{-\eta}} \right\} \\ &= \int_0^{r_0} \frac{1}{1 + sPr^{-\eta}} f_{r_1}(r) dr\end{aligned}\tag{7.8}$$

Using conditional distribution of r_1 obtained in corollary 1, we get

$$\mathcal{L}_{I_1} \left(\frac{Tr_0^\eta}{P} \right) = \int_0^{r_0} \frac{1}{1 + Tr_0^\eta r^{-\eta}} \frac{2r}{r_0^2} dr\tag{7.9}$$

B. Proof of Lemma 6

The Laplace transform of I_R can be expressed as

$$\mathcal{L}_{I_R(m)}(s) = \mathbb{E}[e^{-sI_R}] = \mathbb{E}[e^{-s \sum_{i \in \phi_1 \setminus b_1} P_1 h_i R_i^{-\eta}}].\tag{7.10}$$

Due to the independence between fading coefficients and BSs locations, we get

$$\begin{aligned}\mathcal{L}_{I_R(m)}(s) &= \mathbb{E}_\phi \left\{ \prod_{i \in \phi_1 \setminus b_1} \mathbb{E}_{h_i} \{ e^{-sP_1 h_i R_i^{-\eta}} \} \right\} \\ &= \mathbb{E}_\phi \left\{ \prod_{i \in \phi_1 \setminus b_1} \mathcal{L}_{h_i}(sP_1 R_i^{-\eta}) \right\}.\end{aligned}\tag{7.11}$$

However, since $h_i \sim \exp(1)$, we can write

$$\mathcal{L}_{I_R(m)}(s) = \mathbb{E}_\phi \left\{ \prod_{i \in \phi_1 \setminus b_1} \frac{1}{1 + sP_1 R_i^{-\eta}} \right\}.\tag{7.12}$$

Using the probability generating functional (PGFL) for PPP [146] yields

$$\mathcal{L}_{I_R(m)}(s) = \exp \left(-2\pi\lambda_1 \int_{R_1}^{\infty} \left(1 - \frac{1}{1 + sP_1 v^{-\eta}}\right) v dv \right). \quad (7.13)$$

Now, invoke the change of variables $w = (sP_1)^{-1/\eta}v$ and set $s = \frac{TR_1^\eta}{P_1}$ to get

$$\begin{aligned} \mathcal{L}_{I_R(m)}(s) &= \exp \left(-2\pi\lambda_1 R_1^2 T^{2/\eta} \int_{T^{-1/\eta}}^{\infty} \frac{w}{1 + w^\eta} dw \right), \\ &= \exp \left(-\frac{2\pi\lambda_1 T R_1^2}{\eta - 2} {}_2F_1\left(1, 1 - \frac{2}{\eta}, 2 - \frac{2}{\eta}, -T\right) \right). \end{aligned} \quad (7.14)$$

The LT of I_r can be written as

$$\mathcal{L}_{I_r(m)}(s) = \mathbb{E} \left\{ e^{-s \sum_{i \in \phi_2} P_2 h_i r_i^{-\eta}} \right\}. \quad (7.15)$$

Following the same procedure utilized for $\mathcal{L}_{I_R(m)}(s)$ above and considering the interference region of femto BSs from $R_1(\frac{\beta_{21}P_2}{P_1})^{1/\eta}$ to ∞ , we get the following expression for $\mathcal{L}_{I_r(m)}(s)$

$$\mathcal{L}_{I_r(m)}(s) = \exp \left(\frac{-2\pi\lambda_2 T R_1^2}{\eta - 2} \left(\frac{\beta_{21}P_2}{P_1}\right)^{2/\eta} \beta_{12}^\eta {}_2F_1\left(1, 1 - \frac{2}{\eta}, 2 - \frac{2}{\eta}, -T\beta_{12}\right) \right). \quad (7.16)$$

Similarly, the LTs $\mathcal{L}_{I_{R(f)}}(s)$ and $\mathcal{L}_{I_{r(f)}}(s)$ in the femto association can be obtained using the macro interference region from $r_1(\frac{\beta_{12}P_1}{P_2})^{1/\eta}$ to ∞ and femto interference from $r_1 \rightarrow \infty$.

C. Proof of Lemma 7

First, we write intensity measure of the points inside a ball \mathbf{B} of radius r as $\Lambda(\mathbf{B}) = \pi\lambda r^2$ and the intensity function, which is given by $\lambda(x) = 2\pi\lambda r$. Then, using mapping theorem, we can write the intensity measure on a line from 0 to y as $\Lambda([0, y]) = \pi\lambda(PBy)^{2/\eta}$ and the

intensity function $\lambda(y) = \frac{2}{\eta}\pi\lambda(PB)^{2/\eta}y^{2/\eta-1}$. Now, using the superposition of point processes (eq. 5.19 in [146]), we can express the total intensity as

$$\lambda(y) = \frac{2\pi}{\eta} \left(\lambda_1 (B_1 P_1)^{2/\eta} + \lambda_2 (B_2 P_2)^{2/\eta} \right) y^{2/\eta-1}. \quad (7.17)$$

D. Proof of Lemma 8

The conditional distance distribution of r_1 conditioned on the second strongest BS distance x given in (4.21) is obtained as follows

$$f_r(r_1|x) = \frac{\lambda(r_1)}{\int_0^x \lambda(z)dz} = \frac{2r_1^{2/\eta-1}}{\eta x^{2/\eta}}. \quad (7.18)$$

Using the null probability of PPP and employing mapping theorem, we can express the service distance distribution in a single tier network as

$$f_Y(y) = \frac{d}{dy} (1 - e^{-\pi\lambda(PBy)^{2/\eta}}) \quad (7.19)$$

$$= \frac{2}{\eta} \pi \lambda (PB)^{2/\eta} y^{2/\eta-1} e^{-\pi\lambda(PB)^{2/\eta} y^{2/\eta}}. \quad (7.20)$$

Following (7.20) and using the total intensity measure, we can write the PDF of r_1 (i.e., distance between the user and the strongest femto BS) in a two tier network as

$$f_{r_1}(r) = \frac{2}{\eta} \pi \lambda_t r^{2/\eta-1} \exp(-\pi r^{2/\eta} \lambda_t), \quad (7.21)$$

where $\lambda_t = \lambda_1(B_1 P_1)^{2/\eta} + \lambda_2(B_2 P_2)^{2/\eta}$. We can write the conditional distance distribution of

the third strongest BS conditioning on r_1 as

$$P[x_2 < y|r_1] = 1 - \exp\left(\int_{r_1}^y \frac{2\pi\lambda_t}{\eta} r^{2/\eta-1} dr\right) - \exp\left(\int_{r_1}^y \frac{2\pi\lambda_t r^{2/\eta-1}}{\eta} dr\right) \int_{r_1}^y \frac{2\pi\lambda_t r^{2/\eta-1}}{\eta/1!} dr. \quad (7.22)$$

By differentiating the above equation w.r.t. y , we get

$$f(y|r_1) = \frac{2}{\eta} (\pi\lambda_t)^2 y^{2/\eta-1} (y^{2/\eta} - r_1^{2/\eta}) e^{-\pi\lambda_t(y^{2/\eta} - r_1^{2/\eta})}. \quad (7.23)$$

The conditional distance distribution of the second strongest BS conditioning on r_1 can be calculated as

$$f_{x_1}(x|r_1) = \frac{\lambda(x)}{\int_{r_1}^y \lambda(z) dz} = \frac{2x^{2/\eta-1}}{\eta(y^{2/\eta} - r_1^{2/\eta})}. \quad (7.24)$$

The product of (7.23) and (7.24) yields the joint conditional distribution given by

$$f_{x_1, x_2}(x, y|r_1) = \left(\frac{2}{\eta} \pi\lambda_t\right)^2 (xy)^{2/\eta-1} \exp(-\pi\lambda_t(y^{2/\eta} - r_1^{2/\eta})). \quad (7.25)$$

Using the law of conditional probability (i.e. $f(a, b|c) = \frac{f(a, b, c)}{f(c)}$), we get the joint distribution

$f_{x_1, x_2, r}(x, y, r_1)$ as

$$f_{x_1, x_2, r}(x, y, r_1) = \left(\frac{2}{\eta} \pi\lambda_t\right)^3 (xyr_1)^{2/\eta-1} \exp(-\pi\lambda_t y^{2/\eta}). \quad (7.26)$$

By integrating the above distribution w.r.t. r_1 , from $0 \rightarrow x$, we get $f_{x_1, x_2}(x, y)$ as

$$f_{x_1, x_2}(x, y) = \frac{4}{\eta^2} (\pi \lambda_t)^3 x^{4/\eta-1} y^{2/\eta-1} \exp(-\pi \lambda_t y^{2/\eta}). \quad (7.27)$$

E. Proof of Lemma 9

The LT of I_{r_1} can be expressed as

$$\mathcal{L}_{I_{r_1}}(s) = \mathbb{E}[e^{-s I_{r_1}}] = \mathbb{E}[e^{-s \frac{h_1}{r_1}}], \quad (7.28)$$

Since $h \sim \exp(1)$, we can write $\mathcal{L}_{I_{r_1}}(s)$ as

$$\mathcal{L}_{I_{r_1}}(s) = \mathbb{E}\left[\frac{1}{1 + s/r_1}\right] = \int_0^x \frac{1}{1 + s/r_1} f(r_1) dr_1, \quad (7.29)$$

Using (4.21) obtained in Lemma 8 and substituting $s = \frac{T}{x^{-1}+y^{-1}}$, we can express $\mathcal{L}_{I_{r_1}}(s)$ as

$$\mathcal{L}_{I_{r_1}}(s) = \int_0^x \frac{2r_1^{2/\eta-1}}{\eta x^{2/\eta} \left(1 + \frac{T}{r_1(x^{-1}+y^{-1})}\right)} dr_1. \quad (7.30)$$

Similarly, the LT of I_{agg} can be written as

$$\mathcal{L}_{I_{agg}}(s) = \mathbb{E}\left\{e^{-s \sum_{i \in \phi \setminus b_1} h_i/u_i}\right\}. \quad (7.31)$$

Due to the independence of the fading coefficients and the BSs locations, the exponential fading distribution $h_i \sim \exp(1)$, and applying the we obtain PGFL for PPP, we get

$$\mathcal{L}_{I_{agg}}(s) = \exp\left(-\frac{2\pi\lambda_t}{\eta} \int_y^\infty \frac{z^{2/\eta-1}}{1 + z/s} dz\right). \quad (7.32)$$

Finally, setting $s = \frac{T}{x^{-1}+y^{-1}}$ and after some simplification, we obtain

$$\mathcal{L}_{I_{agg}}(s) = \exp \left(\frac{-2\pi\lambda_t T y^{2/n-1}}{(\eta-2)(x^{-1}+y^{-1})} {}_2F_1 \left(1, 1 - \frac{2}{\eta}, 2 - \frac{2}{\eta}, \frac{-T}{x^{-1}y+1} \right) \right). \quad (7.33)$$

REFERENCES

- [1] B. Romanous, N. Bitar, A. Imran, and H. Refai, “Network densification: Challenges and opportunities in enabling 5G,” in *20th International Workshop on Computer Aided Modelling and Design of Communication Links and Networks (CAMAD)*, 2015, pp. 129–134.
- [2] X. Ge, S. Tu, G. Mao, C.-X. Wang, and T. Han, “5G Ultra-Dense cellular networks,” *IEEE Wireless Communications*, vol. 23, no. 1, pp. 72–79, 2016.
- [3] H. Zhang, Y. Dong, J. Cheng, M. Hossain, V. Leung *et al.*, “Fronthauling for 5G LTE-U ultra dense cloud small cell networks,” *IEEE Wireless Communications*, *Accepted*, 2016.
- [4] K. Dimou, M. Wang, Y. Yang, M. Kazmi, A. Larmo, J. Pettersson, W. Muller, and Y. Timmer, “Handover within 3GPP LTE: Design principles and performance,” in *2009 IEEE 70th Vehicular Technology Conference Fall (VTC 2009-Fall)*, Sept 2009, pp. 1–5.
- [5] T. Mahmoodi and S. Seetharaman, “On using a sdn-based control plane in 5G mobile networks,” in *Wireless World Research Forum meeting*, vol. 32.

- [6] H. ElSawy, E. Hossain, and M. Haenggi, “Stochastic geometry for modeling, analysis, and design of multi-tier and cognitive cellular wireless networks: A survey,” *IEEE Communications Surveys & Tutorials*, vol. 15, no. 3, pp. 996–1019, 2013.
- [7] H. ElSawy, A. S. Salem, M.-S. Alouini, and M. Z. Win, “Modeling and analysis of cellular networks using stochastic geometry: A tutorial,” *IEEE Commun. Surveys Tuts.*, vol. 19, no. 1, pp. 167–203, 2017.
- [8] M. Haenggi, *Stochastic geometry for wireless networks*. Cambridge University Press, 2012.
- [9] J. G. Andrews, F. Baccelli, and R. K. Ganti, “A tractable approach to coverage and rate in cellular networks,” *IEEE Transactions on Communications*, vol. 59, no. 11, pp. 3122–3134, 2011.
- [10] A. Guo and M. Haenggi, “Spatial stochastic models and metrics for the structure of base stations in cellular networks,” *IEEE Transactions on Wireless Communications*, vol. 12, no. 11, pp. 5800–5812, 2013.
- [11] B. Blaszczyzyn, M. K. Karray, and H. P. Keeler, “Using poisson processes to model lattice cellular networks,” in *IEEE INFOCOM Proceedings*. IEEE, 2013, pp. 773–781.
- [12] M. Di Renzo and W. Lu, “The equivalent-in-distribution (eid)-based approach: On the analysis of cellular networks using stochastic geometry,” *IEEE Communications Letters*, vol. 18, no. 5, pp. 761–764, 2014.

- [13] M. Di Renzo and P. Guan, “Stochastic geometry modeling of coverage and rate of cellular networks using the gil-pelaez inversion theorem,” *IEEE Communications Letters*, vol. 18, no. 9, pp. 1575–1578, 2014.
- [14] N. Deng, W. Zhou, and M. Haenggi, “The ginibre point process as a model for wireless networks with repulsion,” *IEEE Transactions on Wireless Communications*, vol. 14, no. 1, pp. 107–121, 2015.
- [15] Miyoshi, Naoto and Shirai, Tomoyuki, “A cellular network model with ginibre configured base stations,” *Advances in Applied Probability*, vol. 46, no. 3, pp. 832–845, 2014.
- [16] H. S. Dhillon, R. K. Ganti, F. Baccelli, and J. G. Andrews, “Coverage and ergodic rate in k-tier downlink heterogeneous cellular networks,” in *Communication, Control, and Computing (Allerton), 2011 49th Annual Allerton Conference on*. IEEE, 2011, pp. 1627–1632.
- [17] H. S. Dhillon and J. G. Andrews, “Downlink rate distribution in heterogeneous cellular networks under generalized cell selection,” *Wireless Communications Letters, IEEE*, vol. 3, no. 1, pp. 42–45, 2014.
- [18] M. Di Renzo, A. Guidotti, and G. E. Corazza, “Average rate of downlink heterogeneous cellular networks over generalized fading channels: A stochastic geometry approach,” *Communications, IEEE Transactions on*, vol. 61, no. 7, pp. 3050–3071, 2013.

- [19] P. Madhusudhanan, J. G. Restrepo, Y. Liu, T. X. Brown, and K. R. Baker, “Downlink performance analysis for a generalized shotgun cellular system,” *IEEE Trans. Wireless Commun.*, vol. 13, no. 12, pp. 6684–6696, 2014.
- [20] W. C. Cheung, T. Q. Quek, and M. Kountouris, “Throughput optimization, spectrum allocation, and access control in two-tier femtocell networks,” *IEEE Journal on Selected Areas in Communications*, vol. 30, no. 3, pp. 561–574, 2012.
- [21] S. Singh, F. Baccelli, and J. G. Andrews, “On association cells in random heterogeneous networks,” *IEEE Wireless Communications Letters*, vol. 3, no. 1, pp. 70–73, 2014.
- [22] R. W. Heath, M. Kountouris, and T. Bai, “Modeling heterogeneous network interference using poisson point processes,” *IEEE Transactions on Signal Processing*, vol. 61, no. 16, pp. 4114–4126, 2013.
- [23] T. Bai, R. Vaze, and R. W. Heath, “Analysis of blockage effects on urban cellular networks,” *IEEE Transactions on Wireless Communications*, vol. 13, no. 9, pp. 5070–5083, 2014.
- [24] T. Bai and R. W. Heath, “Location-specific coverage in heterogeneous networks,” *IEEE Signal Processing Letters*, vol. 20, no. 9, pp. 873–876, 2013.
- [25] B. Yu, L. Yang, H. Ishii, and S. Mukherjee, “Dynamic tdd support in macrocell-assisted small cell architecture,” *IEEE Journal on Selected Areas in Communications*, vol. 33, no. 6, pp. 1201–1213, 2015.

- [26] S. Mukherjee, “Distribution of downlink sinr in heterogeneous cellular networks,” *IEEE Journal on Selected Areas in Communications*, vol. 30, no. 3, pp. 575–585, 2012.
- [27] Y. J. Chun, M. O. Hasna, and A. Ghrayeb, “Modeling heterogeneous cellular networks interference using poisson cluster processes,” *IEEE Journal on Selected Areas in Communications*, vol. 33, no. 10, pp. 2182–2195, 2015.
- [28] H. ElSawy and E. Hossain, “On stochastic geometry modeling of cellular uplink transmission with truncated channel inversion power control,” *IEEE Transactions on Wireless Communications*, vol. 13, no. 8, pp. 4454–4469, 2014.
- [29] T. D. Novlan, H. S. Dhillon, and J. G. Andrews, “Analytical modeling of uplink cellular networks,” *IEEE Transactions on Wireless Communications*, vol. 12, no. 6, pp. 2669–2679, 2013.
- [30] S. Singh, X. Zhang, and J. Andrews, “Joint rate and SINR coverage analysis for decoupled uplink-downlink biased cell associations in HetNets,” *IEEE Trans. Wireless Commun.*, vol. 14, no. 10, pp. 5360–5373, 2015.
- [31] H. Y. Lee, Y. J. Sang, and K. S. Kim, “On the uplink sir distributions in heterogeneous cellular networks,” *IEEE Communications Letters*, vol. 18, no. 12, pp. 2145–2148, 2014.
- [32] Z. Zeinalpour-Yazdi and S. Jalali, “Outage analysis of uplink two-tier networks,” *IEEE Transactions on Communications*, vol. 62, no. 9, pp. 3351–3362, 2014.
- [33] T. Kobayashi and N. Miyoshi, “Uplink cellular network models with ginibre deployed base stations,” in *26th International Teletraffic Congress (ITC)*. IEEE, 2014, pp. 1–7.

- [34] S. Singh, H. S. Dhillon, and J. G. Andrews, “Offloading in heterogeneous networks: Modeling, analysis, and design insights,” *IEEE Transactions on Wireless Communications*, vol. 12, no. 5, pp. 2484–2497, 2013.
- [35] S. Singh and J. G. Andrews, “Joint resource partitioning and offloading in heterogeneous cellular networks,” *IEEE Transactions on Wireless Communications*, vol. 13, no. 2, pp. 888–901, 2014.
- [36] H. S. Dhillon, R. K. Ganti, and J. G. Andrews, “Load-aware modeling and analysis of heterogeneous cellular networks,” *IEEE Transactions on Wireless Communications*, vol. 12, no. 4, pp. 1666–1677, 2013.
- [37] M. Mirahsan, R. Schoenen, and H. Yanikomeroglu, “Hethetnets: Heterogeneous traffic distribution in heterogeneous wireless cellular networks,” *IEEE Journal on Selected Areas in Communications*, vol. 33, no. 10, pp. 2252–2265, 2015.
- [38] Y. Lin, W. Bao, W. Yu, and B. Liang, “Optimizing user association and spectrum allocation in hetnets: a utility perspective,” *IEEE Journal on Selected Areas in Communications*, vol. 33, no. 6, pp. 1025–1039, 2015.
- [39] R. K. Ganti and M. Haenggi, “Spatial analysis of opportunistic downlink relaying in a two-hop cellular system,” *IEEE Transactions on Communications*, vol. 60, no. 5, pp. 1443–1450, 2012.
- [40] W. Lu and M. Di Renzo, “Performance evaluation of relay-aided cellular networks by using stochastic geometry,” in *IEEE 19th International Workshop on Computer Aided*

- Modeling and Design of Communication Links and Networks (CAMAD)*. IEEE, 2014, pp. 265–269.
- [41] H. ElSawy and E. Hossain, “Two-tier hetnets with cognitive femtocells: Downlink performance modeling and analysis in a multichannel environment,” *IEEE Transactions on Mobile Computing*, vol. 13, no. 3, pp. 649–663, 2014.
- [42] H. ElSawy, E. Hossain, and D. I. Kim, “Hetnets with cognitive small cells: user offloading and distributed channel access techniques,” *IEEE Communications Magazine*, vol. 51, no. 6, pp. 28–36, 2013.
- [43] H. Alves, C. H. de Lima, P. H. Nardelli, R. D. Souza, and M. Latva-aho, “On the secrecy of interference-limited networks under composite fading channels,” *IEEE Signal Processing Letters*, vol. 22, no. 9, pp. 1306–1310, 2015.
- [44] H. ElSawy and E. Hossain, “Channel assignment and opportunistic spectrum access in two-tier cellular networks with cognitive small cells,” in *IEEE Global Communications Conference (GLOBECOM)*. IEEE, 2013, pp. 4477–4482.
- [45] Y. S. Soh, T. Q. Quek, M. Kountouris, and G. Caire, “Cognitive hybrid division duplex for two-tier femtocell networks,” *IEEE Transactions on Wireless Communications*, vol. 12, no. 10, pp. 4852–4865, 2013.
- [46] C. H. De Lima, M. Bennis, and M. Latva-aho, “Coordination mechanisms for self-organizing femtocells in two-tier coexistence scenarios,” *IEEE Transactions on Wireless Communications*, vol. 11, no. 6, pp. 2212–2223, 2012.

- [47] C. H. de Lima, M. Bennis, and M. Latva-aho, “Statistical analysis of self-organizing networks with biased cell association and interference avoidance,” *IEEE Transactions on Vehicular Technology*, vol. 62, no. 5, pp. 1950–1961, 2013.
- [48] T. K. Thuc, E. Hossain, and H. Tabassum, “Downlink power control in two-tier cellular networks with energy-harvesting small cells as stochastic games,” *IEEE Transactions on Communications*, vol. 63, no. 12, pp. 5267–5282, 2015.
- [49] P. Semasinghe, E. Hossain, and K. Zhu, “An evolutionary game for distributed resource allocation in self-organizing small cells,” *IEEE Transactions on Mobile Computing*, vol. 14, no. 2, pp. 274–287, 2015.
- [50] R. Tanbourgi, H. S. Dhillon, and F. K. Jondral, “Analysis of joint transmit–receive diversity in downlink mimo heterogeneous cellular networks,” *IEEE Transactions on Wireless Communications*, vol. 14, no. 12, pp. 6695–6709, 2015.
- [51] A. K. Gupta, H. S. Dhillon, S. Vishwanath, and J. G. Andrews, “Downlink multi-antenna heterogeneous cellular network with load balancing,” *IEEE Transactions on Communications*, vol. 62, no. 11, pp. 4052–4067, 2014.
- [52] H. S. Dhillon, M. Kountouris, and J. G. Andrews, “Downlink MIMO HetNets: modeling, ordering results and performance analysis,” *IEEE Transactions on Wireless Communications*, vol. 12, no. 10, pp. 5208–5222, 2013.

- [53] R. Tanbourgi, H. S. Dhillon, J. G. Andrews, and F. K. Jondral, “Effect of spatial interference correlation on the performance of maximum ratio combining,” *IEEE Transactions on Wireless Communications*, vol. 13, no. 6, pp. 3307–3316, 2014.
- [54] Tanbourgi, Ralph and Dhillon, Harpreet S and Andrews, Jeffrey G and Jondral, Friedrich K, “Dual-branch MRC receivers under spatial interference correlation and nakagami fading,” *IEEE Transactions on Communications*, vol. 62, no. 6, pp. 1830–1844, 2014.
- [55] M. Di Renzo and P. Guan, “A mathematical framework to the computation of the error probability of downlink mimo cellular networks by using stochastic geometry,” *IEEE Transactions on Communications*, vol. 62, no. 8, pp. 2860–2879, 2014.
- [56] M. Di Renzo and W. Lu, “Stochastic geometry modeling and performance evaluation of MIMO cellular networks using the equivalent-in-distribution (EiD)-based approach,” *IEEE Transactions on Communications*, vol. 63, no. 3, pp. 977–996, 2015.
- [57] G. Geraci, S. Singh, J. G. Andrews, J. Yuan, and I. B. Collings, “Secrecy rates in broadcast channels with confidential messages and external eavesdroppers,” *Wireless Communications, IEEE Transactions on*, vol. 13, no. 5, pp. 2931–2943, 2014.
- [58] S. Govindasamy, D. W. Bliss, and D. H. Staelin, “Asymptotic spectral efficiency of the uplink in spatially distributed wireless networks with multi-antenna base stations,” *IEEE Transactions on Communications*, vol. 61, no. 7, pp. 100–112, 2013.

- [59] J. Zhang and J. G. Andrews, “Distributed antenna systems with randomness,” *IEEE Transactions on Wireless Communications*, vol. 7, no. 9, pp. 3636–3646, 2008.
- [60] C. Li, J. Zhang, and K. Letaief, “Performance analysis of SDMA in multicell wireless networks,” in *IEEE Global Communications Conference (GLOBECOM)*. IEEE, 2013, pp. 3867–3872.
- [61] N. Lee, D. Morales-Jimenez, A. Lozano, and R. W. Heath, “Spectral efficiency of dynamic coordinated beamforming: A stochastic geometry approach,” *IEEE Transactions on Wireless Communications*, vol. 14, no. 1, pp. 230–241, 2015.
- [62] Y. Lin and W. Yu, “Downlink spectral efficiency of distributed antenna systems under a stochastic model,” *IEEE Transactions on Wireless Communications*, vol. 13, no. 12, pp. 6891–6902, 2014.
- [63] A. Adhikary, H. S. Dhillon, and G. Caire, “Massive-MIMO meets hetnet: Interference coordination through spatial blanking,” *IEEE Journal on Selected Areas in Communications*, vol. 33, no. 6, pp. 1171–1186, 2015.
- [64] G. Nigam, P. Minero, and M. Haenggi, “Spatiotemporal cooperation in heterogeneous cellular networks,” *IEEE Journal on Selected Areas in Communications*, vol. 33, no. 6, pp. 1253–1265, 2015.
- [65] X. Zhang and M. Haenggi, “A stochastic geometry analysis of inter-cell interference coordination and intra-cell diversity,” *IEEE Transactions on Wireless Communications*, vol. 13, no. 12, pp. 6655–6669, 2014.

- [66] G. Nigam, P. Minero, and M. Haenggi, “Coordinated multipoint joint transmission in heterogeneous networks,” *IEEE Transactions on Communications*, vol. 62, no. 11, pp. 4134–4146, 2014.
- [67] A. H. Sakr and E. Hossain, “Location-aware cross-tier coordinated multipoint transmission in two-tier cellular networks,” *Wireless Communications, IEEE Transactions on*, vol. 13, no. 11, pp. 6311–6325, 2014.
- [68] F. Baccelli and A. Giovanidis, “A stochastic geometry framework for analyzing pairwise-cooperative cellular networks,” *IEEE Transactions on Wireless Communications*, vol. 14, no. 2, pp. 794–808, 2015.
- [69] M. Wildemeersch, T. Q. Quek, M. Kountouris, A. Rabbachin, and C. H. Slump, “Successive interference cancellation in heterogeneous networks,” *IEEE Transactions on Communications*, vol. 62, no. 12, pp. 4440–4453, 2014.
- [70] T. M. Nguyen, Y. Jeong, T. Q. Quek, W. P. Tay, and H. Shin, “Interference alignment in a poisson field of mimo femtocells,” *IEEE Transactions on Wireless Communications*, vol. 12, no. 6, pp. 2633–2645, 2013.
- [71] C. Li, J. Zhang, M. Haenggi, and K. B. Letaief, “User-centric intercell interference nulling for downlink small cell networks,” *IEEE Transactions on Communications*, vol. 63, no. 4, pp. 1419–1431, 2015.

- [72] R. Tanbourgi, S. Singh, J. G. Andrews, and F. K. Jondral, “A tractable model for non-coherent joint-transmission base station cooperation,” *IEEE Transactions on Wireless Communications*, vol. 13, no. 9, pp. 4959–4973, 2014.
- [73] S. Akoum and R. W. Heath, “Interference coordination: Random clustering and adaptive limited feedback,” *IEEE Transactions on Signal Processing*, vol. 61, no. 7, pp. 1822–1834, 2013.
- [74] Huang, Kaibin and Andrews, Jeffrey G and Guo, Dongning and Heath Jr, Robert W and Berry, Randall A, “Spatial interference cancellation for multiantenna mobile ad hoc networks,” *IEEE Transactions on information Theory*, vol. 58, no. 3, pp. 1660–1676, 2012.
- [75] H. S. Dhillon, Y. Li, P. Nuggehalli, Z. Pi, and J. G. Andrews, “Fundamentals of heterogeneous cellular networks with energy harvesting,” *IEEE Transactions on Wireless Communications*, vol. 13, no. 5, pp. 2782–2797, 2014.
- [76] A. H. Sakr and E. Hossain, “Analysis of-tier uplink cellular networks with ambient RF energy harvesting,” *IEEE Journal on Selected Areas in Communications*, vol. 33, no. 10, pp. 2226–2238, 2015.
- [77] Sakr, Ahmed Hamdi and Hossain, Ekram, “Cognitive and energy harvesting-based D2D communication in cellular networks: Stochastic geometry modeling and analysis,” *IEEE Transactions on Communications*, vol. 63, no. 5, pp. 1867–1880, 2015.

- [78] Y. S. Soh, T. Q. Quek, M. Kountouris, and H. Shin, “Energy efficient heterogeneous cellular networks,” *IEEE Journal on Selected Areas in Communications*, vol. 31, no. 5, pp. 840–850, 2013.
- [79] M. Wildemeersch, T. Q. Quek, C. H. Slump, and A. Rabbachin, “Cognitive small cell networks: Energy efficiency and trade-offs,” *IEEE Transactions on Communications*, vol. 61, no. 9, pp. 4016–4029, 2013.
- [80] C. Li, J. Zhang, and K. Letaief, “Throughput and energy efficiency analysis of small cell networks with multi-antenna base stations,” *IEEE Transactions on Wireless Communications*, vol. 13, no. 5, pp. 2505–2517, 2014.
- [81] D. Cao, S. Zhou, and Z. Niu, “Optimal combination of base station densities for energy-efficient two-tier heterogeneous cellular networks,” *IEEE Transactions on Wireless Communications*, vol. 12, no. 9, pp. 4350–4362, 2013.
- [82] Cao, Dongxu and Zhou, Sheng and Niu, Zhisheng, “Improving the energy efficiency of two-tier heterogeneous cellular networks through partial spectrum reuse,” *IEEE Transactions on Wireless Communications*, vol. 12, no. 8, pp. 4129–4141, 2013.
- [83] M. Di Renzo, “Stochastic geometry modeling and analysis of multi-tier millimeter wave cellular networks,” *IEEE Transactions on Wireless Communications*, vol. 14, no. 9, pp. 5038–5057, 2015.

- [84] S. Singh, M. N. Kulkarni, A. Ghosh, and J. G. Andrews, “Tractable model for rate in self-backhauled millimeter wave cellular networks,” *IEEE Journal on Selected Areas in Communications*, vol. 33, no. 10, pp. 2196–2211, 2015.
- [85] T. Bai and R. W. Heath, “Coverage and rate analysis for millimeter-wave cellular networks,” *IEEE Transactions on Wireless Communications*, vol. 14, no. 2, pp. 1100–1114, 2015.
- [86] J. Lee and T. Q. Quek, “Hybrid full-/half-duplex system analysis in heterogeneous wireless networks,” *IEEE Transactions on Wireless Communications*, vol. 14, no. 5, pp. 2883–2895, 2015.
- [87] Alves, Hirley and de Lima, Carlos HM and Nardelli, Pedro and Demo Souza, Richard and Latva-aho, Matti, “On the average spectral efficiency of interference-limited full-duplex networks,” in *9th International Conference on Cognitive Radio Oriented Wireless Networks and Communications (CROWNCOM)*. IEEE, 2014, pp. 550–554.
- [88] N. Deng, W. Zhou, and M. Haenggi, “Heterogeneous cellular network models with dependence,” *IEEE Journal on Selected Areas in Communications*, vol. 33, no. 10, pp. 2167–2181, 2015.
- [89] M. Di Renzo, “A stochastic geometry approach to the rate of downlink cellular networks over correlated log-normal shadowing,” in *IEEE 78th Vehicular Technology Conference (VTC Fall)*. IEEE, 2013, pp. 1–5.

- [90] H. ElSawy, E. Hossain, and M.-S. Alouini, “Analytical modeling of mode selection and power control for underlay D2D communication in cellular networks,” *IEEE Transactions on Communications*, vol. 62, no. 11, pp. 4147–4161, 2014.
- [91] X. Lin, J. G. Andrews, and A. Ghosh, “Spectrum sharing for device-to-device communication in cellular networks,” *IEEE Transactions on Wireless Communications*, vol. 13, no. 12, pp. 6727–6740, 2014.
- [92] H. S. Dhillon, H. C. Huang, H. Viswanathan, and R. A. Valenzuela, “Power-efficient system design for cellular-based machine-to-machine communications,” *IEEE Transactions on Wireless Communications*, vol. 12, no. 11, pp. 5740–5753, 2013.
- [93] M. Peng, Y. Li, T. Q. Quek, and C. Wang, “Device-to-device underlaid cellular networks under rician fading channels,” *IEEE Transactions on Wireless Communications*, vol. 13, no. 8, pp. 4247–4259, 2014.
- [94] H. Sun, M. Wildemeersch, M. Sheng, and T. Q. Quek, “D2D enhanced heterogeneous cellular networks with dynamic tdd,” *IEEE Transactions on Wireless Communications*, vol. 14, no. 8, pp. 4204–4218, 2015.
- [95] M. G. Khoshkholgh, Y. Zhang, K.-C. Chen, K. G. Shin, and S. Gjessing, “Connectivity of cognitive device-to-device communications underlying cellular networks,” *IEEE Journal on Selected Areas in Communications*, vol. 33, no. 1, pp. 81–99, 2015.

- [96] X. Lin, R. K. Ganti, P. J. Fleming, and J. G. Andrews, “Towards understanding the fundamentals of mobility in cellular networks,” *IEEE Transactions on Wireless Communications*, vol. 12, no. 4, pp. 1686–1698, 2013.
- [97] W. Bao and B. Liang, “Stochastic geometric analysis of user mobility in heterogeneous wireless networks,” *IEEE Journal on Selected Areas in Communications*, vol. 33, no. 10, pp. 2212–2225, 2015.
- [98] S. Sadr and R. S. Adve, “Handoff rate and coverage analysis in multi-tier heterogeneous networks,” *IEEE Transactions on Wireless Communications*, vol. 14, no. 5, pp. 2626–2638, 2015.
- [99] D. C. Chen, T. Q. Quek, and M. Kountouris, “Backhauling in heterogeneous cellular networks: Modeling and tradeoffs,” *IEEE Transactions on Wireless Communications*, vol. 14, no. 6, pp. 3194–3206, 2015.
- [100] V. Suryaprakash, P. Rost, and G. Fettweis, “Are heterogeneous cloud-based radio access networks cost effective?” *IEEE Journal on Selected Areas in Communications*, vol. 33, no. 10, pp. 2239–2251, 2015.
- [101] N. Lee, R. W. Heath, D. Morales-Jimenez, and A. Lozano, “Base station cooperation with dynamic clustering in super-dense cloud-ran,” in *IEEE Globecom Workshops (GC Wkshps)*. IEEE, 2013, pp. 784–788.

- [102] G. Geraci, H. S. Dhillon, J. G. Andrews, J. Yuan, and I. B. Collings, “Physical layer security in downlink multi-antenna cellular networks,” *IEEE Transactions on Communications*, vol. 62, no. 6, pp. 2006–2021, 2014.
- [103] H. Wang, X. Zhou, and M. C. Reed, “Physical layer security in cellular networks: A stochastic geometry approach,” *IEEE Transactions on Wireless Communications*, vol. 12, no. 6, pp. 2776–2787, 2013.
- [104] H. Kim, G. De Veciana, X. Yang, and M. Venkatachalam, “Distributed-optimal user association and cell load balancing in wireless networks,” *IEEE/ACM Trans. Networking*, vol. 20, no. 1, pp. 177–190, 2012.
- [105] A. K. Gupta, H. S. Dhillon, S. Vishwanath, and J. G. Andrews, “Downlink coverage probability in mimo hetnets with flexible cell selection,” in *IEEE Global Communications Conference (GLOBECOM)*. IEEE, 2014, pp. 1534–1539.
- [106] H. ElSawy, E. Hossain, and S. Camorlinga, “Traffic offloading techniques in two-tier femtocell networks,” in *2013 IEEE International Conf. on Commun. (ICC)*. IEEE, 2013, pp. 6086–6090.
- [107] G. P. Pollini, “Trends in handover design,” *IEEE Commun. Mag.*, vol. 34, no. 3, pp. 82–90, 1996.
- [108] R. Trestian, O. Ormond, and G.-M. Muntean, “Game theory-based network selection: Solutions and challenges,” *IEEE Commun. Surveys Tuts.*, vol. 14, no. 4, pp. 1212–1231, 2012.

- [109] G. Gódor, Z. Jakó, Á. Knapp, and S. Imre, “A survey of handover management in LTE-based multi-tier femtocell networks: Requirements, challenges and solutions,” *Computer Networks*, vol. 76, pp. 17–41, 2015.
- [110] D. Hong and S. S. Rappaport, “Traffic model and performance analysis for cellular mobile radio telephone systems with prioritized and nonprioritized handoff procedures,” *IEEE Trans. Veh. Technol.*, vol. 35, no. 3, pp. 77–92, 1986.
- [111] A. H. Zahran, B. Liang, and A. Saleh, “Signal threshold adaptation for vertical handoff in heterogeneous wireless networks,” *Mobile Networks and Applications*, vol. 11, no. 4, pp. 625–640, 2006.
- [112] H. Zhang, W. Ma, W. Li, W. Zheng, X. Wen, and C. Jiang, “Signalling cost evaluation of handover management schemes in LTE-advanced femtocell,” in *73rd IEEE Vehicular Technology Conference (VTC Spring)*. IEEE, 2011, pp. 1–5.
- [113] H. Zhang, W. Zheng, X. Wen, and C. Jiang, “Signalling overhead evaluation of henb mobility enhanced schemes in 3GPP LTE-Advanced,” in *IEEE 73rd Vehicular Technology Conference (VTC Spring)*. IEEE, 2011, pp. 1–5.
- [114] M. Z. Chowdhury and Y. M. Jang, “Handover management in high-dense femtocellular networks,” *EURASIP Journal on Wireless Communications and Networking*, no. 1, pp. 1–21, 2013.

- [115] H. Zhang, C. Jiang, J. Cheng, and V. C. Leung, "Cooperative interference mitigation and handover management for heterogeneous cloud small cell networks," *IEEE Wireless Communications*, vol. 22, no. 3, pp. 92–99, 2015.
- [116] N. Sinclair, D. Harle, I. A. Glover, and R. C. Atkinson, "A kernel methods approach to reducing handover occurrences within LTE," in *18th European Wireless Conference*. VDE, 2012, pp. 1–8.
- [117] H. Zhang, X. Wen, B. Wang, W. Zheng, and Y. Sun, "A novel handover mechanism between femtocell and macrocell for LTE based networks," in *Second International Conference on Communication Software and Networks (ICCSN'10)*. IEEE, 2010, pp. 228–231.
- [118] W. Zheng, H. Zhang, X. Chu, and X. Wen, "Mobility robustness optimization in self-organizing LTE femtocell networks," *EURASIP Journal on Wireless Communications and Networking*, no. 1, p. 1, 2013.
- [119] P.-Y. Kong and A. Sluzek, "Average packet delay analysis for a mobile user in a two-tier heterogeneous cellular network," *IEEE Systems Journal*, no. 99, 2015.
- [120] H. Zhang, C. Jiang, R. Q. Hu, and Y. Qian, "Self-organization in disaster-resilient heterogeneous small cell networks," *IEEE Network*, vol. 30, no. 2, pp. 116–121, 2016.
- [121] S. Ulukus and G. P. Pollini, "Handover delay in cellular wireless systems," in *IEEE International Conf. on Commun. (ICC)*. IEEE, 1998.

- [122] W. Bao and B. Liang, “Handoff rate analysis in heterogeneous wireless networks with poisson and poisson cluster patterns,” in *Proceedings of the 16th ACM International Symposium on Mobile Ad Hoc Networking and Computing*. ACM, 2015, pp. 77–86.
- [123] C.-H. Lee and Z.-S. Syu, “Handover analysis of macro-assisted small cell networks,” in *IEEE International Conf. on Internet of Things(iThings), Green Computing and Commun. (GreenCom), and Cyber, Physical and Social Computing(CPSCoM)*. IEEE, 2014, pp. 604–609.
- [124] J. Andrews, H. Claussen, M. Dohler, S. Rangan, and M. Reed, “Femtocells: Past, present, and future,” *IEEE J. Sel. Areas Commun.*, vol. 30, no. 3, pp. 497–508, April 2012.
- [125] J. Horng, G. Vannucci, and J. Zhang, “Down-link interference cancellation for high-data-rate channels in advanced digital wireless networks,” Nov. 7 2002, uS Patent App. 10/289,712”.
- [126] 3GPP TR 36.819 v11.0.0, “Coordinated multi-point operation for LTE,” 3GPP TSG RAN WG1, Tech. Rep., Sept. 2011.
- [127] A. Davydov, G. Morozov, I. Bolotin, and A. Papathanassiou, “Evaluation of joint transmission CoMP in C-RAN based LTE-A hetnets with large coordination areas,” in *IEEE Globecom Workshops (GC Wkshps)*. IEEE, 2013, pp. 801–806.
- [128] B. Cheng, X. Mi, X. Xu, Z. Xu, X. Xu, and M. Zhao, “A real-time implementation of CoMP transmission based on cloud-RAN infrastructure,” in *International Wireless*

- Communications and Mobile Computing Conference (IWCMC)*, Aug 2014, pp. 1033–1038.
- [129] M. Haenggi, “On distances in uniformly random networks,” *IEEE Trans. Inform. Theory*, vol. 51, no. 10, pp. 3584–3586, 2005.
- [130] C. Hoymann, D. Larsson, H. Koorapaty, and J.-F. Cheng, “A Lean carrier for LTE,” *IEEE Commun. Mag.*, vol. 51, no. 2, pp. 74–80, 2013.
- [131] H. Ibrahim, H. Elsayy, U. T. Nguyen, and M.-S. Alouini, “Modeling virtualized downlink cellular networks with ultra-dense small cells,” in *IEEE International Conf. on Commun. (ICC)*, 2015, pp. 5360–5366.
- [132] S. Parkvall, A. Furuskar, and E. Dahlman, “Evolution of LTE toward IMT-advanced,” *IEEE Communications Magazine*, vol. 49, no. 2, pp. 84–91, 2011.
- [133] H.-S. Jo, Y. J. Sang, P. Xia, and J. G. Andrews, “Heterogeneous cellular networks with flexible cell association: A comprehensive downlink sinr analysis,” *IEEE Trans. Wireless Commun.*, vol. 11, no. 10, pp. 3484–3495, 2012.
- [134] P. F. Ash and E. D. Bolker, “Generalized dirichlet tessellations,” *Geometriae Dedicata*, vol. 20, no. 2, pp. 209–243, 1986.
- [135] H. Ibrahim, H. Elsayy, U. T. Nguyen, and M.-S. Alouini, “Mobility-aware modeling and analysis of dense cellular networks with C-plane/U-plane split architecture,” *IEEE Trans. Commun.*, vol. 64, no. 11, pp. 4879–4894, 2016.

- [136] G. Zhang, T. Q. Quek, A. Huang, and H. Shan, “Delay and reliability tradeoffs in heterogeneous cellular networks,” *IEEE Trans. Wireless Commun.*, pp. 1101–1113, 2016.
- [137] X. Ge, J. Ye, Y. Yang, and Q. Li, “User mobility evaluation for 5G small cell networks based on individual mobility model,” *IEEE J. Sel. Areas Commun.*, vol. 34, no. 3, pp. 528–541, 2016.
- [138] M. Thorpe, M. Kottkamp, A. Rössler, and J. Schütz, “LTE location based services technology introduction,” *Rohde & Schwarz*, 2013, available at http://cdn.rohde-schwarz.com/pws/dl_downloads/dl_common_library/dl_brochures_and_datasheets/pdf_1/LTE_LBS_White_Paper.pdf.
- [139] Y.-u. Chung and D. Cho, “Velocity estimation using adaptive array antennas,” in *IEEE Vehicular Technology Conference*, vol. 4. IEEE; 1999, 2001, pp. 2565–2569.
- [140] A. Merwaday, I. Güvenç, W. Saad, A. Mehbodniya, and F. Adachi, “Sojourn time-based velocity estimation in small cell poisson networks,” *IEEE Communications Letters*, vol. 20, no. 2, pp. 340–343, 2016.
- [141] M. Abramowitz and I. A. Stegun, *Handbook of Mathematical Functions, Tenth printing*. Dover Publications, 1972.
- [142] <http://www.teoco.com/products/planning-optimization/asset-radio-planning>.
- [143] <http://www.infovista.com/products/Mentum-Planet>.

- [144] R. H. Milocco and S. Boumerdassi, “Estimation and prediction for tracking trajectories in cellular networks using the recursive prediction error method,” in *IEEE International Symposium on a World of Wireless Mobile and Multimedia Networks (WoWMoM)*. IEEE, 2010, pp. 1–7.
- [145] I. Leontiadis, A. Lima, H. Kwak, R. Stanojevic, D. Wetherall, and K. Papagiannaki, “From cells to streets: Estimating mobile paths with cellular-side data,” in *Proceedings of the 10th ACM International on Conference on emerging Networking Experiments and Technologies*. ACM, 2014, pp. 121–132.
- [146] S. N. Chiu, D. Stoyan, W. S. Kendall, and J. Mecke, *Stochastic geometry and its applications*. John Wiley & Sons, 2013.
- [147] 3GPP TSG-RAN WG1 R1-083813, “Range expansion for efficient support of heterogeneous networks,” *Europe, Qualcomm*, 2008.
- [148] H. Elshaer, F. Boccardi, M. Dohler, and R. Irmer, “Downlink and uplink decoupling: A disruptive architectural design for 5g networks,” in *Global Communications Conference (GLOBECOM), 2014 IEEE*. IEEE, 2014, pp. 1798–1803.
- [149] K. Smiljkovic, H. Elshaer, P. Popovski, F. Boccardi, M. Dohler, L. Gavrilovska, and R. Irmer, “Capacity analysis of decoupled downlink and uplink access in 5G heterogeneous systems,” *arXiv preprint arXiv:1410.7270*, 2014.
- [150] J. G. Andrews, A. K. Gupta, and H. S. Dhillon, “A primer on cellular network analysis using stochastic geometry,” *arXiv preprint arXiv:1604.03183*, 2016.

- [151] D. Cao, S. Zhou, and Z. Niu, “Optimal base station density for energy-efficient heterogeneous cellular networks,” in *IEEE International Conf. on Commun. (ICC)*. IEEE, 2012, pp. 4379–4383.

Vita

Rabe Arshad received B.Sc. degree in electrical engineering from the University of Engineering & Technology (UET) Lahore, Pakistan in 2010. Right after the graduation, he joined Mobilink, a multi-national cellular operator, as Radio Frequency Planning Engineer and served for four years till 2015. During his stay in Mobilink, he received Masters degree in Project Management from Shaheed Zulfiqar Ali Bhutto Institute of Science and Technology (SZABIST), Pakistan in 2014. He started his M.Sc degree in electrical engineering at the Department of Electrical Engineering, King Fahd University of Petroleum and Minerals (KFUPM), Saudi Arabia, in 2015. During his stay at KFUPM, he had associated with King Abdullah University of Science and Technology (KAUST), Saudi Arabia, as a visiting student and worked on KFUPM-KAUST joint research initiative. His research interests include stochastic geometry, handover management, point process theory and heterogeneous wireless networks.